

Los Alamos National Laboratory is operated by the University of California for the United States Department of Energy under contract W-7405-ENG-36.

TITLE: FROM GROUND STATE TO FISSION FRAGMENTS: A COMPLEX, MULTI-DIMENSIONAL MULTI-PATH PROBLEM

AUTHOR(S): P. Möller, T-2 Sole Source Contractor  
J. R. Nix, T-2  
W. J. Swiatecki, Lawrence Berkeley Laboratory

SUBMITTED TO: The Specialists' Meeting on Physics and Engineering of Fission, Kyoto University Research Reactor Inst., Kumatori-cho, Osaka, Japan, January 7, 1992

#### DISCLAIMER

This report was prepared as an account of work sponsored by an agency of the United States Government. Neither the United States Government nor any agency thereof, nor any of their employees, makes any warranty, express or implied, or assumes any legal liability or responsibility for the accuracy, completeness, or usefulness of any information, apparatus, product, or process disclosed, or represents that its use would not infringe privately owned rights. Reference herein to any specific commercial product, process, or service by trade name, trademark, manufacturer, or otherwise does not necessarily constitute or imply its endorsement, recommendation, or favoring by the United States Government or any agency thereof. The views and opinions of authors expressed herein do not necessarily state or reflect those of the United States Government or any agency thereof.

By acceptance of this article the publisher recognizes that the U.S. Government retains a non-exclusive, royalty-free license to publish or reproduce the published form of this contribution, or to allow others to do so, for U.S. Government purposes.

The Los Alamos National Laboratory requests that the publisher identify this article as work performed under the auspices of the U.S. Department of Energy.

**Los Alamos** Los Alamos National Laboratory  
Los Alamos, New Mexico 87545

MASTER

# FROM GROUND STATE TO FISSION FRAGMENTS: A COMPLEX, MULTI-DIMENSIONAL MULTI-PATH PROBLEM

P. MÖLLER <sup>1</sup>

*Japan Atomic Energy Research Institute, Tokai, Naka-gun, Ibaraki, 319-11 Japan*

J. R. NIX

*Theoretical Division, Los Alamos National Laboratory, Los Alamos, NM 87545*

W. J. SWIATECKI

*Nuclear Science Division, Lawrence Berkeley Laboratory, Berkeley, CA 94720*

For presentation at:

Specialists' meeting on Physics and Engineering of Fission, Kyoto University Research Reactor  
Institute, Kumatori-cho, Osaka, January 7, 1992

December 27, 1991

## Abstract

Experimental results on the fission properties of nuclei close to  $^{264}\text{Fm}$  show sudden and large changes with a change of only one or two neutrons or protons. The nucleus  $^{264}\text{Fm}$ , for instance, undergoes symmetric fission with a half-life of about 0.4 ms and a kinetic-energy distribution peaked at about 235 MeV whereas  $^{266}\text{Fm}$  undergoes asymmetric fission with a half-life of about 3 h and a kinetic-energy distribution peaked at about 200 MeV. Qualitatively, these sudden changes have been postulated to be due to the emergence of fragment shells in symmetric-fission products close to  $^{132}\text{Sn}$ . Here we present a quantitative calculation that shows where high-kinetic-energy symmetric fission occurs and why it is associated with a sudden and large decrease in fission half-lives. We base our study on calculations of potential-energy surfaces in the macroscopic-microscopic model and a semi-empirical model for the nuclear inertia. For the macroscopic part we use a Yukawa-plus-exponential (finite-range) model and for the microscopic part a folded-Yukawa (diffuse-surface) single-particle potential. We use the three-quadratic-surface parameterization to generate the shapes for which the potential-energy surfaces are calculated. The use of this parameterization and the use of the finite-range macroscopic model allows for the study of two touching spheres and similar shapes. Since these shapes are thought to correspond to the scission shapes for the high-kinetic-energy events it is of crucial importance that a continuous sequence of shapes leading from the nuclear ground state to these configurations can be studied within the framework of the model.

We present the results of the calculations in terms of potential-energy surfaces and fission half-lives for heavy even nuclei. The surfaces are displayed in the form of contour diagrams as functions of two moments of the shape. They clearly show the appearance of a second fission valley, which leads to scission configurations close to two touching spheres, for fissioning systems in the vicinity of  $^{264}\text{Fm}$ . Fission through this new valley leads to much shorter fission half-lives than fission through the old valley.

---

<sup>1</sup>Permanent Address: P. Moller Scientific Computing and Graphics, P. O. Box 1440, Los Alamos, New Mexico 87544, USA

## 1 Introduction

The advent of the macroscopic-microscopic Strutinsky shell-correction method<sup>1,2)</sup> about 20 years ago made possible detailed theoretical studies of the fission process. With this method the potential energy of a nucleus can be calculated for arbitrary shapes, within given shape parameterizations. Coupled with a wealth of new experimental results this has led to an enormous increase in our understanding of nuclear shape changes during fission and also to a better understanding of the stability of elements at the end of the periodic system. For an extensive review of some of these developments see<sup>3)</sup>. During fission the nucleus changes its shape from a usually deformed ground-state shape through saddle-point shapes and scission configurations into two separated fragments. Measurements of fragment mass asymmetries, fragment kinetic energies, fission half-lives, neutron emission, fission barrier heights and correlations between these quantities yield detailed information about the nucleus during various stages of the fission process. Here we apply our model to the  $^{264}\text{Fm}$  region for which new and somewhat unexpected experimental data are available. Our goal is to understand the nature of the fission process for the nuclei for which these new data are available and then to make predictions of properties of other nuclei in the vicinity of  $^{264}\text{Fm}$  and of fission half-lives for heavier nuclei.

### 1.1 EARLIER THEORETICAL AND EXPERIMENTAL RESULTS

The first success of the macroscopic-microscopic method was the interpretation of fission isomeric states as secondary minima in the potential-energy surface, corresponding to very deformed, approximately spheroidal shapes with a ratio of about 2/1 of the major to minor axis. This interpretation was later confirmed by experiments that measured the actual deformation of the nucleus in its fission isomeric state.

The second minimum in the potential-energy surface splits the fission-barrier saddle point into two saddles, a first and a second saddle. A next major step in the study of the fission process for heavy elements was the experimental determination of the heights of the first and second saddle points and the height of the second minimum relative to the ground state for a large number of nuclei throughout the actinide region. Calculations of these barrier heights were performed within the framework of several of the macroscopic-microscopic models. Results of the calculations usually agreed with the experimental data to within an MeV or so.

The successful theoretical description of the structure of the fission barrier involved considering axially asymmetric shapes at the first saddle point and mass-asymmetric shapes at the second saddle. The long mystery of why actinide nuclei undergo asymmetric fission was resolved. Mass-asymmetric shape degrees of freedom lowered the outer saddle by up to 3 MeV or so for the lighter actinides. The calculated value of the mass-asymmetry coordinate at the second saddle and the actually measured asymmetry of the fission fragments were found to be closely correlated for elements throughout the actinide region.

Calculated fission barriers served as a starting point for subsequent calculations of fission half-lives. Basically two types of models were used. The first type of model determines a one-dimensional fission barrier from the multi-dimensional potential-energy surface and uses a semi-empirical inertia for the motion in the fission direction. The penetrability of the barrier and the corresponding fission half-lives are then determined by use of the WKB method. The second type of model is more complicated. In this model the inertia is calculated from some microscopic model, usually a cranking model, and the problem is treated in several dimensions.

in the sense that the penetrability is calculated along several paths in a multi-dimensional deformation space. Fission is then thought to take place along the path with the highest penetrability. The simpler model has succeeded in calculating the spontaneous-fission half-life  $T_{sf}$  for even nuclei throughout the actinide region with a root-mean-square deviation of less than 2 for  $\log(T_{sf})$ . The more sophisticated models usually have larger discrepancies.

To determine the stability of heavy elements the half-lives with respect to  $\alpha$ - and  $\beta$ -decay must also be considered. These half-lives can usually be calculated with greater accuracy than the fission half-lives, since they depend only on nuclear ground-state properties. One application of models of the macroscopic-microscopic type has been to predict the properties of elements in the superheavy region, beyond the heaviest presently known elements. The predicted properties may then serve as a guide to the design of reactions leading to these elements. Another application is to do calculations of astrophysical interest. In this case one often has to make calculations for situations that are not accessible to experiment, but whose results are crucial for the understanding of astrophysical processes. It is then desirable to have available models that describe well properties of nuclei in the known regions of nuclei and which one can expect work equally well also outside the regions where the model parameters were determined.

## 1.2 THE $^{264}\text{Fm}$ REGION

We shall here not go very far from the regions of known nuclei, but instead focus most of our attention on the very interesting region in the vicinity of  $^{264}\text{Fm}$ . This nucleus, which has not been seen experimentally, is of particular interest since in symmetric fission it would divide into two doubly magic  $^{132}\text{Sn}$  nuclei. The ground-state microscopic energy for each of these  $^{132}\text{Sn}$  nuclei is  $-12$  MeV according to <sup>4)</sup>, giving a combined total microscopic energy of  $-24$  MeV. It is clear from studying tables of the ground-state microscopic energy for Sn isotopes close to  $^{132}\text{Sn}$  that the microscopic effects grow rapidly as one approaches  $^{132}\text{Sn}$ . For example, the ground-state microscopic energy for  $^{120}\text{Sn}$ , the product in the symmetric fission of  $^{252}\text{Fm}$ , is only  $-4$  MeV. For two nuclei combined it is  $-8$  MeV, which is  $16$  MeV higher than for the products in the symmetric fission of  $^{264}\text{Fm}$ . One may therefore ask how far from  $Z = 100$  and  $N = 164$  the effect of the magic or near magic fragment shells manifest themselves and also how and at what stage in the fission process the effects become important, that is, how far inside the scission point traces of the shell effects that are present in fully separated fragments remain. We shall now address these questions.

### 1.2.1 New experimental results in the $^{264}\text{Fm}$ region

First let us briefly review the experimental situation. As one sweeps through the actinide region from uranium to fermium many fission properties vary fairly smoothly. With increasing proton number there is a decrease in fission-fragment mass asymmetry, an increase in fission-fragment kinetic energies and a decrease in fission half-lives. Except for the fission half-lives these quantities vary fairly slowly with neutron number. However, at  $^{258}\text{Fm}$  there are sudden changes in all of these quantities. The first observation of the onset of symmetric fission in the region at the end of the periodic system was a study <sup>5)</sup> of  $^{257}\text{Fm}$  fission. For  $^{258}\text{Fm}$  the changes in the behavior of many fission properties are even more dramatic. Fission becomes symmetric with a very narrow mass distribution, the kinetic energy of the fragments is about  $35$  MeV higher than in the asymmetric fission of  $^{256}\text{Fm}$  and the fission half-life is  $0.38$  ms for  $^{258}\text{Fm}$  compared to  $2.86$  h for  $^{256}\text{Fm}$ . We take information about the experimental fission

half-lives from<sup>6-10</sup>). The first observation of the onset of symmetric fission in the region at the end of the periodic system was the study of <sup>257</sup>Fm fission by<sup>5</sup>). Subsequently, more observations of symmetric fission have been made in this region, for instance by<sup>11,12</sup>). Later, more extensive measurements on <sup>258</sup>Fm and other elements in this region by<sup>13</sup>) have shown that there often are two components in the kinetic-energy distribution. For <sup>258</sup>Fm most of the events are distributed around 235 MeV but a few are distributed around 200 MeV. This distribution of fission events has been characterized as "bimodal" fission. It has been suggested that in bimodal fission there are two distinct symmetric fission valleys separated by a ridge<sup>13</sup>) and that one valley leads to elongated scission shapes similar to the scission configuration for lighter actinides, with a low kinetic energy, and another valley leads to the very compact scission configuration of two touching spheres. We refer to<sup>13</sup>) for an extensive discussion of the experimental results but reproduce here as our fig. 1 the mass and kinetic-energy distributions obtained for these elements<sup>13</sup>).

### 1.2.2 Previous theoretical results for the <sup>264</sup>Fm region

One previous study of the effect of fragment shells in the <sup>264</sup>Fm region by use of a macroscopic-microscopic model is presented in the series of papers<sup>14-17</sup>). However, in all of these studies, the models used have several deficiencies when applied to the present problem. For the microscopic model the two-center oscillator model is used. This potential is spuriously high in the neck region of the nucleus<sup>16,18</sup>), which leads to fragment shell effects that manifest themselves too early during the fission process. In addition, the parameterization used is incapable of generating shapes that are crucial for the study of compact scission shapes and the accompanying high fragment kinetic energies. For instance, it cannot generate the important configuration of two touching spheres. For the macroscopic model the liquid-drop model with a modified set of constants<sup>16</sup>) is used. This model severely overestimates the energies for nuclei with pronounced necks. For a configuration of two touching spherical <sup>132</sup>Sn nuclei the resulting liquid-drop energy is 35 MeV higher<sup>19</sup>) than the energy given by the more realistic Yukawa-plus-exponential finite-range macroscopic model. Thus, we feel that many features of the symmetric high-kinetic-energy processes cannot be studied within the framework of this model.

The results of calculations by<sup>20,21</sup>) show some similarities but also large differences compared to the results we obtain below. One reason for the differences is that no independent control is exercised over the shape of the ends of the nucleus in their shape parameterization. The ends of the nucleus are not kept spherical, and therefore it is not possible to see the full effect of the fragment shells.

Some studies with the Nilsson modified-oscillator potential have also been performed for elements in this region. The focus of those calculations was mainly on fission barriers and fission half-lives<sup>22-28</sup>). In general, fission half-lives were quite well reproduced for elements throughout the actinide region. Even the complicated behaviour of the fission half-lives for the elements beyond einsteinium was quite well reproduced by the calculations. The sudden drop in fission half-life at <sup>258</sup>Fm was interpreted as due to the disappearance of the second saddle in the fission barrier below the energy of the nuclear ground state, as has also been suggested by<sup>29,30</sup>). However, in the Nilsson model the perturbed-spheroid ( $\epsilon$ ) parameterization does not permit the generation of nuclear shapes that are even close to two touching spheres. Since such shapes are expected to be of importance for at least some elements in this region one may ask why the model was so successful in this study, limited to fission barriers and half lives. The investigation below will show that the short half life of <sup>258</sup>Fm is due to the low inertia

in a new fission valley and *not* to the disappearance of the second peak in the fission barrier. We are therefore forced to conclude that the fairly good reproduction in some Nilsson-model calculations<sup>25,27)</sup> of the rapidly decreasing half-lives that occur for some heavy elements beyond  $N = 152$  was somewhat fortuitous.

We would also like to mention the static fission model of<sup>31)</sup>. In this model one assumes statistical equilibrium among the collective coordinates at the scission point. The energy is calculated for two nuclei with a fixed distance  $d$  between the ends of the nuclei. The model for the energy of the system consists of a macroscopic-microscopic model for each individual nucleus plus a macroscopic term giving the interaction energy between the two nuclei. The deformations that are studied correspond to spheroidal shapes for the two fragments. We feel that it is hard to justify many of the assumptions of this model. In addition, the model does not take into account important properties of the fissioning nucleus that influence the fission process, such as the fission-barrier structure.

The model we study below, a macroscopic-microscopic model with a Yukawa-plus-exponential macroscopic model and a folded-Yukawa single-particle potential, has also been used earlier for some studies in this region. We only mention here as one example an earlier, unpublished result, that a fission half-life of 2.7 y was obtained for  $^{258}\text{Fm}$  when the model was used in a standard way. These earlier results will be discussed below together with the results from the present calculation.

Recently, studies<sup>32,33)</sup> that were based on the Woods-Saxon single-particle model and a finite-range model for the macroscopic energy and that were designed to look for both the new and old fission valleys have been undertaken. These calculations were partly motivated by our earlier results<sup>34,35)</sup> and the results obtained are very similar to ours. We give additional comments on these results when we present our calculations. One of the calculations<sup>33)</sup> gives results only for the nucleus  $^{258}\text{Fm}$  and takes mass-asymmetric shape distortions into account both in the old and new valley. In our earlier study<sup>34)</sup> mass-asymmetric shape degrees of freedom were taken into account only in the old valley. However, here we undertake a more general investigation and also study, in a full three-dimensional grid, mass-asymmetric shape degrees of freedom in the new valley and along the path leading from the new path back to the old path.

Our primary goal in this investigation is to search for two fission valleys, one leading to elongated scission shapes, the other leading to compact scission shapes. The existence of two different valleys of this type was proposed by Hulet *et al.*<sup>13)</sup>. Their proposal was based on the observance of a high- and a low-energy component in the fission kinetic-energy spectrum of some nuclei close to  $^{264}\text{Fm}$ . A second goal is to study the implications of the presence of two valleys on quantities other than the kinetic energies, particularly on fission half-lives. To search for the new valley, we have to select a set of shapes for which to calculate the potential energy.

## 2 Nuclear shapes

Two shape parameterizations are at present implemented in the folded-Yukawa single-particle model. One is the three-quadratic-surface parameterization<sup>36)</sup> and the other is the  $\epsilon$ <sup>37)</sup> parameterization. The latter is usually the more suitable one for investigating ground-state shapes. In the calculation of potential-energy surfaces it is of considerable importance to select shapes that are related to the processes that are studied. We use the three-quadratic-surface parameterization in the calculation of potential-energy surfaces that we perform to search for

the two fission valleys, since it is the more suitable one for generating shapes beyond ground-state shapes that are of interest in fission, in particular for generating shapes close to scission configurations. However, we have also performed calculations of potential-energy surfaces as functions of  $\epsilon_2, \epsilon_4$  and mass-asymmetric  $\epsilon_3, \epsilon_5$  shape coordinates. It turns out that along the old path the lowest saddle-point energies are obtained in that parameterization partly for the reason that more shape degrees of freedom are investigated. Therefore, we use those results below in the calculation of fission half-lives along the old path. For the ground-state energy we use the lowest result obtained in the two parameterizations, after first having minimized the ground-state energy obtained in the  $\epsilon_2$ - $\epsilon_4$  parameterization with respect to  $\epsilon_6$ , for the fixed values of  $\epsilon_2$  and  $\epsilon_4$  that correspond to the nuclear ground state.

## 2.1 THREE-QUADRATIC-SURFACE PARAMETERIZATION

Since we wish to discuss fairly extensively the choices of nuclear shapes on which we base the calculation of potential-energy surfaces we give some details of the three-quadratic-surface parameterization. In it the shape of the nuclear surface is specified in terms of three smoothly joined portions of quadratic surfaces of revolution. They are completely specified<sup>36)</sup> by

$$\rho^2 = \begin{cases} a_1^2 - \frac{a_1^2}{c_1^2}(z - l_1)^2, & l_1 - c_1 \leq z \leq z_1 \\ a_2^2 - \frac{a_2^2}{c_2^2}(z - l_2)^2, & z_2 \leq z \leq l_2 + c_2 \\ a_3^2 - \frac{a_3^2}{c_3^2}(z - l_3)^2, & z_1 \leq z \leq z_2 \end{cases} \quad (1)$$

Here the left-hand surface is denoted by the subscript 1, the right-hand one by 2 and the middle one by 3. At the left and right intersections of the middle surface with the end surfaces the value of  $z$  is  $z_1$  and  $z_2$ , respectively.

There are nine numbers required to specify the expressions in eq. (1) but the conditions of constancy of the volume and continuous first derivatives at  $z_1$  and  $z_2$  eliminate three numbers. The introduction of an auxiliary unit of distance  $u$  through

$$u = \left[ \frac{1}{2} (a_1^2 + a_2^2) \right]^{\frac{1}{2}} \quad (2)$$

permits a natural definition of two sets of shape coordinates. We define three symmetric coordinates  $\sigma_i$  and three mass-asymmetric coordinates  $\alpha_i$  by

$$\begin{aligned} \sigma_1 &= \frac{(l_2 - l_1)}{u} \\ \sigma_2 &= \frac{a_3^2}{c_3^2} \\ \sigma_3 &= \frac{1}{2} \left( \frac{a_1^2}{c_1^2} + \frac{a_2^2}{c_2^2} \right) \\ \alpha_1 &= \frac{1}{2} \frac{(l_1 + l_2)}{u} \end{aligned}$$

$$\alpha_2 = \frac{(a_1^2 - a_2^2)}{u^2}$$

and

$$\alpha_3 = \frac{a_1^2}{c_1^2} - \frac{a_2^2}{c_2^2} \quad (3)$$

The coordinate  $\alpha_1$  is not varied freely but is determined by the requirement that the center of mass be at the origin.

## 2.2 SYMMETRIC MOMENTS

It is not very useful to display calculated results as functions of the shape coordinates defined in eq. (3) because their values are related in a very nonlinear way to the actual shapes. For instance, when  $z_1$  and  $z_2 \rightarrow 0$  for symmetric shapes, that is, when the middle body disappears, then  $\sigma_2 \rightarrow -\infty$ . We therefore display the calculated results as functions of moments of the shape. This has the additional advantage that results from calculations using different shape parameterizations can be displayed as functions of the same quantities. The two most important symmetric moments of the matter distribution are defined by<sup>38)</sup>

$$r = 2 \int_{z \geq 0} z \rho(r) d^3 r / \int_{z \geq 0} \rho(r) d^3 r$$

and

$$\sigma = 2 \left[ \int_{z \geq 0} (z - \frac{1}{2} r)^2 \rho(r) d^3 r / \int_{z \geq 0} \rho(r) d^3 r \right]^{\frac{1}{2}} \quad (4)$$

The following physical interpretation can be given to the definitions in eq. (4). The first moment  $r$  is the distance between the centers of mass of the two halves of the system, which is symmetric with respect to the  $z = 0$  plane. The second moment  $\sigma$  is the sum of the root-mean-square extensions along the symmetry axis of the mass of each half of the system about its center of mass. Below we display calculated total potential energies as functions of  $r$  and  $\sigma$ . Both in the figures and in the paper we use units in which the equivalent sharp radius  $R_0$  of the spherical nucleus is 1. One should note that although the coordinate  $\sigma_1$ , which is the distance between the centers of the two end bodies in units of  $u$  as defined in eqs. (2) and (3), seems similar to the coordinate  $r$ , there are large differences and the  $r$  coordinate is definitely to be preferred for displaying results of the calculations. We would also like to point out that the moments  $r$  and  $\sigma$  do not in general define the shape uniquely, but are functions of the shape. To define the shape precisely, one must define the underlying shape parameterization and either specify the values of the shape parameters or introduce higher moments so that the number of moments equals the number of shape parameters.

## 2.3 CHOICE OF NUCLEAR SHAPES

The three-quadratic-surface parameterization allows the variation of three symmetric and two asymmetric shape coordinates, according to eq. (3). Since we are primarily interested in nuclei for which fission is symmetric, we shall here not vary the asymmetric shape coordinates but limit our study to symmetric shapes. This leaves us with the three symmetric shape coordinates  $\sigma_1, \sigma_2$  and  $\sigma_3$ <sup>39)</sup>. As seen in eq. (3),  $\sigma_3$  is related to the eccentricities of the end bodies. One



realizes that only a small deviation from sphericity of the end fragments removes the influence on the shell effect by magic or near magic numbers. Consideration of shape changes for a single nucleus illustrates the extreme sensitivity of the shell correction to small shape changes. We note for instance that for  $^{208}\text{Pb}$  the shell correction for the spherical shape is  $-12.35\text{ MeV}$  (4), but already for the deformation  $\epsilon_2 = 0.20$  the shell correction is about 0.

In fig. 2 we illustrate how the shell correction evolves for two merging  $^{132}\text{Sn}$  nuclei and also the effect of deviations from sphericity of the end fragments. The overall elongation of the nucleus where we tested the effect of spherical versus deformed end bodies is best characterized by the value of the first moment, which is  $r \approx 1.3$ . In terms of  $r$  the second saddle is located in the region  $1.3 \leq r \leq 1.4$  (26). We see that for  $^{264}\text{Fm}$  the shell correction changes from  $-11.80\text{ MeV}$  to  $0.35\text{ MeV}$  when the deformation of the end fragments changes from spherical to slightly deformed. The value  $\sigma_3 = 0.60$  corresponds to approximately  $\epsilon_2 = 0.25$ . Two points are clear. First, the fragment shells have a large effect already at the second saddle, at least for  $^{264}\text{Fm}$ . Second, we note that to see the full effect of the magic fragment shells the end parts of the nuclear shape have to be kept spherical. We therefore calculate the nuclear potential energies for shapes with the end bodies kept at fixed spherical shapes, while we vary  $\sigma_1$  (separation) and  $\sigma_2$  (neck size).

We have actually also varied the third and last symmetric shape coordinate  $\sigma_3$ , but we will here, except for one or two brief references, discuss only results obtained with  $\sigma_3 = 1$ , that is, with spherical end bodies. There are several reasons for this limitation. First, let us observe that many shapes that are generated by varying  $\sigma_3$  are also approximately generated by varying  $\sigma_1$  and  $\sigma_2$  with  $\sigma_3$  fixed at 1. This is best understood by considering the pure spheroid. In our case, with the ends constrained to be spherical, it can be generated anyway, by letting the middle body grow so that the entire nuclear surface consists of just the middle body. If  $\sigma_3$  were allowed to vary, a spheroid of a certain eccentricity could be generated in an infinite number of ways, for instance by letting the middle body shrink so that the nuclear shape consists of just the two end bodies of the desired eccentricity, meeting at the middle. In a similar manner, many shapes that have  $\sigma_3 \neq 1$  can be approximated by  $\sigma_3 = 1$  and suitable values of the other two coordinates.

The above arguments also show a difficulty in interpreting the results of varying all three symmetric shape coordinates. Major problems will be caused by the fact that several points in the three-dimensional space will correspond sometimes exactly and sometimes approximately to the same shape. Thus, a spheroidal ground state corresponds in a three-dimensional deformation space to a tube or line running from one boundary surface of the calculation to another. To avoid this difficulty one can extend the definitions in eq. (4) to include one higher moment. Then one selects three-quadratic surface shapes that correspond to approximately equidistant points in moment space. However, this seemingly elegant procedure has several practical difficulties. One is that not all grid points in moment space correspond to shapes that can be generated within the three-quadratic-surface parameterization.

In some investigations that display results of multi-dimensional calculations as contour maps of only two variables the energy has been minimized with respect to the additional shape variables (16). Care must be taken in such procedures, since there may be several minima in the direction of the additional variables, in which case a minimization procedure is not sufficient to display all the features of the calculation.

Summarizing the above discussion, we have deduced that the main features in the potential energy of symmetric fission can be studied by keeping  $\sigma_3$  fixed at 1 and varying  $\sigma_1$  and  $\sigma_2$ . In our most extensive earlier study of fission potential-energy surfaces,  $\sigma_1$ ,  $\sigma_2$  and a mass-asymmetry coordinate were varied and  $\sigma_3$  depended on these three variables in a way that

was taken from liquid-drop-model calculations<sup>18,26</sup>). Thus the important class of shapes with spherical ends was never studied. The precise shapes we study here consist of a grid in  $\sigma_1$  and  $\sigma_2$ . Because  $\sigma_2$  approaches  $-\infty$  in some cases, we introduce

$$\lambda = 1 - \frac{1}{2} \frac{\sigma_1}{1 - \frac{1}{\sigma_2}} \quad (5)$$

This definition holds only for  $\sigma_3 = 1$ . In our calculation we consider the evolution of a single system from the nuclear ground state to scission configurations, but not post-scission configurations. There is a lower bound on  $\lambda$ , which for  $\sigma_1 \leq 2$  corresponds to the limit in which the middle body has disappeared, and for  $\sigma_1 \geq 2$  corresponds to the scission line. Thus for each value of  $\sigma_1$  there is a minimum value of  $\lambda$ , given by

$$\lambda_m = \begin{cases} 1 - \frac{\sigma_1}{2} & , \sigma_1 \leq 2 \\ 1 - \frac{2}{\sigma_1} & , \sigma_1 \geq 2 \end{cases} \quad (6)$$

Two touching spheres correspond to  $\sigma_1 = 2$  and  $\lambda = 0$ . The grid we choose is densely spaced for  $\sigma_1 < 2$ . Here we consider  $\sigma_1 = 0.38(0.20)1.98$ . For larger values of  $\sigma_1$  we select a less dense spacing and the corresponding  $\sigma_1$  values are  $\sigma_1 = 2.48(0.50)7.98$ . For  $\lambda$  we choose ten values that are equidistant in the interval  $(\lambda_m + 0.01)$  to 1.9, where  $\lambda_m$  depends on  $\sigma_1$  and is given by eq. (6).

The above discussion defines the shapes precisely. Our results are displayed as functions of the two moments  $r$  and  $\sigma$  given by eq. (4). We show some examples of the actual shapes considered in fig. 3a. The shapes are plotted at locations corresponding to the moment values. We note that, although in general the moments  $r$  and  $\sigma$  do not define the shapes uniquely, they do in our study here, since the shapes depend on only two variables of the underlying three-quadratic-surface shape parameterization.

In the previous study<sup>34</sup>) mass-asymmetric shapes were studied only along the old fission path. Here we also study a full three-dimensional grid that includes mass-asymmetric shape degrees of freedom in the new fission valley. We keep the ends of the fragments spherical, which means that  $\sigma_3 = 1$  and  $\alpha_3 = 0$ . Since  $\alpha_1$  is determined by the requirement that the center of mass be at the origin, this leaves three parameters, namely  $\sigma_1$ ,  $\sigma_2$  and  $\alpha_2$ , that can vary freely. These shape parameters correspond roughly to elongation, neck and mass-asymmetry degrees of freedom, respectively. For  $\alpha_2 = 0$ , that is symmetric shapes, we select a grid in  $\sigma_1$  and  $\sigma_2$  such that we in moment space obtain a regularly spaced grid in the moments  $r$  and  $\sigma$ . We make the choice such that we obtain the grid  $r = 1.3(0.1)1.7$  and  $\sigma = 0.725(0.025)0.825$ . We then keep  $\sigma_1$  and  $\sigma_2$  fixed at the values corresponding to these gridpoints and calculate the energy for  $\alpha_2 = 0.00, 0.05, 0.10, 0.20, 0.30$  and  $0.40$ .

In principle, it would be desirable to define the moments  $r$  and  $\sigma$  for asymmetric shapes and use this definition to determine new values of  $\sigma_1$  and  $\sigma_2$  for each value of  $\alpha_2$  such that  $r$  and  $\sigma$  remain constant as the asymmetry coordinate  $\alpha_2$  varies. This second, more desirable choice is technically the more difficult one to carry through, since some values of  $\alpha_2$  correspond to physically unallowed shapes. This means that the three-dimensional grid would have irregular borders. It is important to realize that the appearance of valleys and ridges in the calculations is not invariant with respect to these two choices of three-dimensional grids. However, we are mainly interested in the height of saddle points and this quantity is not affected by how the

grid is chosen. Below we in some cases present the full three-dimensional result but we usually reduce the results to a two-dimensional contour plot in the  $r$ - $\sigma$  plane by minimizing the energy with respect to  $\alpha_2$ . It is important to realize that in this two-dimensional contour map even the structure and the energy values of the saddles and minima are not invariant with respect to how the minimization is done. It is only meaningful to carry out a minimization if the function has a single minimum as a function of the coordinate that is minimized out. This is the case for the results we present below.

## 2.4 $\epsilon$ PARAMETERIZATION

The  $\epsilon$  parameterization was introduced in 1955 by Nilsson<sup>39</sup>), and was later extended to higher multipoles, for example<sup>40-43</sup>) to  $\epsilon_4$ ,  $\epsilon_3$ ,  $\epsilon_5$  and  $\gamma$ . To study the fission barrier for shapes leading to the old valley we calculate two sets of potential-energy surfaces in the  $\epsilon$  parameterization. First, we calculate potential-energy surfaces for symmetric shapes with  $\epsilon_2$  and  $\epsilon_4$  as independent variables. The potential-energy surfaces were calculated for a grid of 25 points in the  $\epsilon_2$  direction and 7 points in the  $\epsilon_4$  direction. For  $\epsilon_2$  the grid starts at  $-0.40$  and ends at  $1.00$ . The distance between gridpoints is  $0.10$  for negative  $\epsilon_2$  and  $0.05$  for positive  $\epsilon_2$ . For the other independent variable we make a transformation from  $\epsilon_4$  to  $\epsilon'_4$ , where  $\epsilon'_4$  is defined by

$$\epsilon'_4 = \begin{cases} \epsilon_4 & , \quad \epsilon_2 \leq 0.25 \\ \epsilon_4 - \frac{\epsilon_2 - 0.25}{5} & , \quad \epsilon_2 \geq 0.25 \end{cases} \quad (7)$$

This transformation has been chosen such that  $\epsilon'_4 = 0$  corresponds approximately to the bottom of the fission valley. The  $\epsilon'_4$  gridpoints are  $-0.12(0.04)0.12$ . The  $\epsilon_6$  coordinate is not varied independently, but has been determined by minimizing the macroscopic energy for  $^{240}\text{Pu}$  for each gridpoint value of  $\epsilon_2$  and  $\epsilon_4$ .

To study the effect of asymmetric shape distortions along the old fission path, we have made the following choice of shape coordinates. As the symmetric coordinate we vary  $\epsilon_2$  with  $\epsilon_4$  fixed such that  $\epsilon'_4 = 0$ . As the asymmetric coordinate we chose  $\epsilon_3$ . The  $\epsilon_3$  parameter depends on  $\epsilon_2$  and  $\epsilon_3$ <sup>24</sup>). Again we have determined  $\epsilon_6$  by minimizing the macroscopic energy for  $^{240}\text{Pu}$  with respect to  $\epsilon_6$  for fixed values of the other shape parameters. The value of  $\epsilon_6$  depends only weakly on the asymmetric shape coordinates. The surfaces are calculated for the grid  $\epsilon_2 = 0.55(0.05)1.00$  and  $\epsilon_3 = 0.00(0.04)0.28$ .

## 3 Macroscopic-microscopic model

Our model is of the macroscopic-microscopic type and has been discussed extensively in several earlier papers<sup>4,44-46</sup>). We use the model with the parameter set that was determined in a study<sup>45</sup>) that calculated ground-state masses for 4023 nuclei and fission barriers for 28 nuclei throughout the periodic system. The root-mean-square deviation between experimental and calculated ground-state masses was  $0.835$  MeV for a set of 1323 masses and  $1.331$  MeV for the 28 fission barriers. Many other properties such as ground-state deformations are also well described by the model<sup>46</sup>). The model represents a unified approach to the study of many

features of nuclear structure, fission and heavy-ion reactions. We here discuss some improvements to the model relative to the earlier study<sup>34)</sup> but refer to the previous studies<sup>4,44-46)</sup> for a more complete presentation.

In the macroscopic-microscopic model the nuclear energy, which is calculated as a function of shape, proton number  $Z$  and neutron number  $N$ , is the sum of a macroscopic term and a microscopic term. Thus the total nuclear potential energy can be written as

$$E(Z, N, \text{shape}) = E_{\text{macro}}(Z, N, \text{shape}) + E_{\text{micro}}(Z, N, \text{shape}) \quad (8)$$

There exist several different models for both the macroscopic and microscopic terms. We use a Yukawa-plus-exponential model for the macroscopic term and a folded-Yukawa single-particle potential as a starting point for calculating the microscopic term. They are briefly discussed below.

### 3.1 MACROSCOPIC MODEL

We earlier<sup>47)</sup> introduced a shape dependence for the Wigner and  $A^0$  terms for the first time. Here we discuss this shape dependence in somewhat more detail. The complete expression for the Yukawa-plus-exponential macroscopic energy has also been given earlier<sup>34)</sup>. Relative to the expression in the previous study<sup>34)</sup> the shape-dependent Wigner and  $A^0$  terms give rise to the following changes in the expression for the macroscopic energy:

$$\begin{aligned} E_{\text{macro}}(Z, N, \text{shape}) = & \dots \\ & + c_0 A^0 B_0 \\ & + W \left( |I| B_E + \begin{cases} 1/A, & Z \text{ and } N \text{ odd and equal} \\ 0, & \text{otherwise} \end{cases} \right) \\ & \dots \end{aligned} \quad (9)$$

The quantities  $B_E$  and  $B_0$  represent the shape-dependences of the Wigner and  $A^0$  terms. Paradoxically, although no shape dependences for the Wigner and  $A^0$  terms were included in a previous study, very good agreement between calculated results and experimental data was obtained<sup>34)</sup>. However, it was pointed out that shape dependences should be included for a consistent treatment of the transition from one to two systems. It was also suggested that the resolution of this paradox might be a missing term from the mass formula, with a sign such that the effects of the neglect of the missing shape dependences of the Wigner and  $A^0$  terms were approximately cancelled. Since any obvious missing term was not known and since the model seemed to agree well with data, the standard shape-independent forms of the Wigner and  $A^0$  terms were used in the earlier calculations<sup>34)</sup>.

As we discuss below we have now found not another missing term but another missing effect related to the range in the Strutinsky smoothing function. This effect does indeed approximately cancel the shape-dependent parts of the Wigner and  $A^0$  terms in the region close to  $268\text{Fm}$ .

The Wigner term, proportional to  $|I|$ , was first discussed by Wigner to account for a V-shaped trough or kink in the nuclear mass surface. It has been shown<sup>48)</sup> that a term of this unusual structure can arise from the increased overlap of particles in identical orbits. We refer to the book by Myers<sup>48)</sup> and original work referred to there for a more complete discussion of the Wigner term.

To derive an approximate shape dependence for the Wigner term we note that in an extensive discussion of the Wigner term<sup>48)</sup>, it was pointed out that if a system is broken up into  $n$  identical pieces, then the Wigner term must be evaluated separately for each piece, with the result that it simply jumps to  $n$  times its original value. For symmetric fission into two identical fragments this simple argument would imply a shape dependence corresponding to a step function at scission. In reality one would expect that the step function is washed out over some range of shapes in the scission region. Obviously, if the area of a cross section in the neck region is very small then there is hardly any communication between the two fragments and we have essentially the two-system configuration. For cylinder-like shapes and beyond, that is for shapes with  $\sigma_2 \geq 0$ , we clearly have a one-system configuration. How close we are to one or the other situation is related to the amount of communication through the neck. If the area of a cross section through the neck is  $S_3$  and the area of the maximum cross section of the smaller one of the end bodies, that is a cross section through the center of the end surface of revolution, is  $S_1$ , then we may relate the amount of communication to the dimensionless quantity  $S_3/S_1$ . As a simple ansatz we propose the shape dependence

$$B_E = \begin{cases} \left(1 - \frac{S_3}{S_1}\right)^2 a_d + 1 & , \sigma_2 \leq 0 \\ 1 & , \sigma_2 \geq 0 \end{cases} \quad (10)$$

Suppose  $a_d = 1.0$ . Then, with the above shape dependence we would find that for scission shapes we have a Wigner term that is precisely two times the Wigner term for a single system. For cylinder-like configurations and for shapes with thicker neck regions we would have a Wigner term that is equal to the term for a single shape. Thus, with the above shape dependence we obtain the desired values in the two limiting cases. However, at scission there is still *some* communication between the two fragments. This can be illustrated by considering the shell correction calculated by use of the Strutinsky method, for which we for symmetric configurations have a well-defined prescription, regardless of shape. For two touching  $^{132}\text{Sn}$  nuclei we obtain a shell correction that is about 10% lower than for two well-separated nuclei. This leads us to choose a value of  $a_d = 0.9$  for the *damping* coefficient. We have actually calculated potential-energy surfaces and investigated their structure for other choices of the parameter  $a_d$ , which also occurs in the shape dependence of the  $A^0$  term discussed below. From such studies it turns out that the above value gives results for fission half-lives and the height of the ridge between the new and old fission valleys that are in good agreement with data and with conclusions that can be drawn from experiment. The uncertainty in the estimate of  $a_d$  from these studies is about 0.1.

The origin of the  $A^0$  term may be traced to many different sources, that is, it is the sum of many different effects. For instance, in eq. (9) we could have chosen the zero reference point for the pairing energy to be the even-even nucleus. Such a change of reference point would have decreased the value of  $c_0$  by 1 or 2 MeV from its current value. As another example, we note that in the derivation of the Wigner term an  $A^0$  term occurs<sup>49)</sup>. It is not retained, since in the droplet model<sup>49)</sup> only terms through  $A^{1/3}$  are retained. Clearly there are many other such contributions to the  $A^0$  term, each with a *different* shape dependence. At this point it therefore seems an almost impossible task to derive, from fundamental arguments an exact shape dependence for the  $A^0$  term. We therefore make the simple choice

$$B_0 = B_E \quad (11)$$

that is, we choose the same shape dependence for the  $A^0$  term as for the Wigner term.

From the above discussion it is clear that there is a large contribution to the potential in the scission region from the shape-dependent Wigner and  $A^0$  terms. Below we will show that for  $^{258}\text{Fm}$  this contribution is 6 MeV at the saddle point between the old and new fission valleys compared to the case where shape-independent expressions for the Wigner and  $A^0$  terms are used. Thus, the exact appearance of the potential in the scission region is obviously influenced by the accuracy of our model for the shape dependence of the Wigner and  $A^0$  terms. In addition, it is influenced by the accuracy of the model for the Wigner term itself and by the fact that slight reformulations of the model and corresponding readjustments of its coefficients to ground-state masses give different values for the coefficients of the Wigner and  $A^0$  terms. Although it may seem from the arguments above that the coefficient  $a_d$  could be derived solely from comparing with the damping at scission of the shell correction of two touching tin nuclei compared to the shell effect in infinitely separated tin nuclei it should probably be considered, at this stage, to be an adjustable parameter. By adjusting it appropriately we compensate somewhat for whatever is lacking in our understanding of the Wigner and  $A^0$  terms and their shape dependences. It would obviously be very valuable for our understanding of the model in the scission region, to compare to Hartree-Fock calculations for shapes leading into the new fission valley, since the potentials used in Hartree-Fock models do not explicitly contain a Wigner term of the type used in models of the macroscopic-microscopic type.

The values of the constants in the macroscopic model as used here are given in our earlier study<sup>34</sup>), except for  $a_d$  for which according to our discussion above we choose the value

$$a_d = 0.9 \quad \text{scission damping constant}$$

### 3.2 MICROSCOPIC MODEL

The microscopic energy term arises because of the non-uniform distribution of single-particle levels in the nucleus. It is the sum of a shell correction term and a pairing term:

$$E_{\text{micr}}(Z, N, \text{shape}) = E_{\text{shell}}(Z, N, \text{shape}) + E_{\text{pair}}(Z, N, \text{shape}) \quad (12)$$

Both terms are evaluated from a set of calculated single-particle levels, the shell correction by use of Strutinsky's method and the pairing correction by use of the BCS approximation. Our treatment here differs from earlier studies in the choice of smoothing range in the Strutinsky shell-correction method. We have also extended the model to include the possibility of calculating odd-particle specialization energies.

#### 3.2.1 Spin-orbit force

To illustrate that our model is not excessively parameterized, we discuss briefly the spin-orbit term in our model. The spin-orbit potential is given by the expression

$$V_{s.o.} = -\lambda \left( \frac{\hbar}{2mc} \right)^2 \frac{\boldsymbol{\sigma} \cdot \nabla V_1 \times \mathbf{p}}{\hbar} \quad (13)$$

where  $\lambda$  is the spin-orbit interaction strength,  $m$  is the mass of either a neutron or a proton,  $\boldsymbol{\sigma}$  is the Pauli spin matrix and  $\mathbf{p}$  is the nucleon momentum.

The spin-orbit strength has been determined from adjustments to experimental levels in the rare-earth and actinide regions. It has been shown<sup>46)</sup> that many nuclear properties throughout the periodic system are well reproduced with  $\lambda$  given by a function linear in  $A$  through the values determined in these two regions. This gives

$$\lambda_p = 28.0 + 6.0 \left( \frac{A}{240} \right) \quad (14)$$

and

$$\lambda_n = 31.5 + 4.5 \left( \frac{A}{240} \right) \quad (15)$$

### 3.2.2 Shell correction

We calculate the shell correction by use of the Strutinsky method<sup>1,2)</sup>. Its precise implementation in our model is discussed in ref.<sup>44)</sup>. Some difficulties associated with applying the Strutinsky method for a sequence of shapes leading from a single nuclear system to two separate nuclei have been discussed earlier<sup>34,40)</sup>. In the earlier studies<sup>34)</sup> we felt that the most serious difficulties associated with applying the Strutinsky method in the scission region would occur for asymmetric configurations. Thus, in our earlier study of the new valley<sup>34)</sup>, which was limited to symmetric shapes, we applied the method exactly as specified in ref.<sup>44)</sup>.

However, as we discussed earlier<sup>40)</sup>, the smoothing range  $\gamma$  in the Strutinsky method depends on the size of the system since its magnitude is related to  $\hbar\omega_0$ , where  $\hbar\omega_0 = 41 \text{ MeV}/A^{1/3}$ . It is well-known that for the Strutinsky method to be meaningful, the shell correction has to be practically independent of the smoothing range  $\gamma$  over a range of values in the vicinity of  $\hbar\omega_0$ , the distance between two major oscillator shells. Another way of expressing this is that the shell correction has a plateau over a certain range of  $\gamma$  values. One therefore has a certain freedom of choice in selecting a  $\gamma$  value. This is illustrated by the fact that in our work we have consistently used the choice  $\gamma = 1.0 \times \hbar\omega_0$  made in 1972<sup>44)</sup>, whereas another group has consistently used the choice<sup>23)</sup>  $\gamma = 1.2 \times \hbar\omega_0$ . An inspection of fig. 20 in ref.<sup>44)</sup> shows that in our model the choice  $\gamma = 1.2 \times \hbar\omega_0$  would also have been appropriate, or in fact any choice in the range  $1.0 \times \hbar\omega_0$  to about  $1.6 \times \hbar\omega_0$ , since the shell correction exhibits a plateau in this range of energy values for the sixth-order correction that we use. The figure which shows the spherical neutron shell correction for <sup>208</sup>Pb also shows that for values of  $\gamma$  less than  $1.0 \times \hbar\omega_0$  the shell correction rises rapidly.

Now consider the shell correction for <sup>132</sup>Sn. We have confirmed that when the spherical shell correction for <sup>132</sup>Sn is calculated we obtain a plateau similar to the one present for <sup>208</sup>Pb, extending from about  $1.0 \times \hbar\omega_0$  to about  $1.6 \times \hbar\omega_0$ , with  $\hbar\omega_0 = 41 \text{ MeV}/132^{1/3}$ . As the next step let us consider what happens when we use our folded-Yukawa code in a standard way to calculate the potential-energy surface for <sup>264</sup>Fm for shapes shown in fig. 3a, that is for a choice of shapes that shows fission both into the old and into the new valleys. For the Strutinsky shell correction the code would choose a smoothing range based on the size of <sup>264</sup>Fm that is  $\gamma = 41 \text{ MeV}/264^{1/3} = 6.39 \text{ MeV}$ . This value would then be used for the calculation of all deformation points on the potential-energy surface. However, in the vicinity of the new valley we are not dealing with one <sup>264</sup>Fm nucleus but with two <sup>132</sup>Sn nuclei. Here, with the same prescription for the smoothing range as above but with the  $\hbar\omega_0$  for <sup>132</sup>Sn inserted in the expressions we see that we should really use  $\gamma = 41 \text{ MeV}/132^{1/3} = 8.05 \text{ MeV}$ . However, the code would still be using  $\gamma = 1.0 \times \hbar\omega_0^{264} = 0.79 \times \hbar\omega_0^{132}$ . This means that in the vicinity of the new valley the code would not use a smoothing range within the plateau region.

In general terms the resolution of this difficulty is to derive a shape dependence for the smoothing range  $\gamma$  or search in  $\gamma$  for the plateau region at each deformation point. To do such a search at each deformation point is not completely trivial. Some difficulties are that for some deformations there is no well-developed plateau and at other deformations there are two plateaus. It would be very difficult to derive a shape dependence that would correctly describe the size of the system or systems corresponding to the shape configuration considered. Fortunately, there is a simpler solution to the calculation of the shell corrections as the system changes from a single system to two separate nuclei. We simply observe that  $1.0 \times \hbar\omega_0^{132} = 1.26 \times \hbar\omega_0^{264}$ . Therefore, when we calculate the potential-energy surface for  $^{264}\text{Fm}$ , instead of choosing  $\gamma = 1.0 \times \hbar\omega_0^{264}$ , if instead we choose  $\gamma = 1.26 \times \hbar\omega_0^{264}$  we are in the plateau region both in the ground-state region of the potential-energy surface for  $^{264}\text{Fm}$  and in the region corresponding to two touching  $^{132}\text{Sn}$  nuclei. This means that calculations that have used the prescription  $\gamma = 1.20 \times \hbar\omega_0$  for their smoothing range can be expected to obtain more nearly correct results over the entire range of shapes considered in potential-energy surface calculations. However, it is possible that this value is slightly too small to be in the plateau region. Also, the choice  $\gamma = 1.26 \times \hbar\omega_0$  may be too close for comfort, in particular if asymmetric shapes are considered. For this reason we choose for the smoothing range in the shell correction calculation

$$\gamma = 1.4 \times \hbar\omega_0 \quad (16)$$

### 3.2.3 Odd-particle specialization energies

In the BCS theory there is an additional quasi-particle energy

$$E_{\text{qp}} = \left[ (e_\nu - \lambda)^2 + \Delta^2 \right]^{1/2} \quad (17)$$

associated with an odd particle in orbital  $\nu$  over and above the energy interpolated between neighboring even nuclei. Here  $\lambda$  and  $\Delta$  represent the Fermi energy and pairing gap, respectively, obtained in the BCS calculation. In previous calculations with the folded-Yukawa model the odd particle has always been placed in the lowest available orbit. We have previously described more precisely how the energy of such an odd system is calculated in the folded-Yukawa model (43). The method used, which for odd systems includes the quasi-particle energy associated with the ground-state orbital, is appropriate for the calculation of ground-state masses, but not for the calculation of odd-particle fission barriers.

It has been noted for a long time that there is a relative hindrance associated with the fission of odd- $A$  systems. This hindrance was first explained in 1955 (40,51) in terms of a specialization energy arising from the conservation of spin and parity of the odd particle during fission. This can give a substantial contribution to the barrier over and above a barrier obtained by interpolation between neighboring even nuclei, since far from the ground state the orbital with the required spin and parity that is closest to the Fermi surface may have a quasi-particle energy of several MeV. In general, one expects higher specialization energies to be associated with higher ground-state spins.

In our calculations here, we have accounted for the specialization energy by always choosing the orbital of given spin  $\Omega$  and parity that lies closest to the Fermi surface. For the case where there is both an odd proton and an odd neutron we have assumed that the specialization energies are additive and have not included any coupling between the two odd particles. For the case of asymmetric shapes only  $\Omega$  is conserved. Thus, in the potential energy surfaces where asymmetric shapes are studied,  $\Omega$  and parity are conserved only for the grid points



corresponding to symmetric shapes, that is on the line  $\epsilon_3 = 0$ , but at other grid points only  $\Omega$  is conserved.

It also remains to specify what spin to assign to the odd particle. One possibility is to use the experimental value for the ground-state spin. Then it would not be possible to predict fission half-lives for odd systems where the ground-state spin is not known experimentally. However, in our code we have modified the treatment of odd-particle systems in two respects. One possibility is to prescribe the spin and parity of the odd particle. This feature is used to calculate the specialization energy in fission. If no spin is specified, the code will keep track of the spin of the lowest state of the odd particle. Thus, we were able to run the code for a set of ground-state shapes determined in a mass calculation<sup>52,53</sup>) and obtain predicted spins for the odd particles at the ground state. In our studies here, we use these predicted spins to calculate potential-energy surfaces for odd systems.

It is of interest to compare the predictions with experiment. In the actinide region the agreement is usually very good. For instance, the calculated ground-state odd-neutron spins agree with experimental data for uranium isotopes ranging from  $^{229}\text{U}$  to  $^{239}\text{U}$  and for plutonium isotopes ranging from  $^{239}\text{Pu}$  to  $^{245}\text{Pu}$ . However, for neutron numbers above  $N = 152$  there is some disagreement. In this region there are several neutron levels very close together in the calculated level diagrams as can be seen in several figures in ref.<sup>37</sup>). This makes it difficult to predict the correct level order. At present we feel the current situation is close to the best possible with a model of this type. Because the spins are not always predicted correctly the calculated potential-energy surfaces for odd systems should be interpreted with some care.

## 4 Calculated results

We now present calculated results for nuclei in the vicinity of  $^{264}\text{Fm}$ . We have learned that it is extremely useful to consider fission half-lives in the interpretation of the calculated potential-energy surfaces. However, it is instructive to first discuss solely the structure of the potential-energy surfaces. We therefore start with a discussion of potential energies for Fm isotopes and then proceed to discuss the significance of fission half-lives, making additional comments in that context about the Fm isotopes. Then we present and discuss potential-energy surfaces for additional elements.

### 4.1 CALCULATED POTENTIAL-ENERGY SURFACES FOR Fm ISOTOPES

We display the calculated energies in the form of contour diagrams. First we show the smooth trends of the underlying macroscopic energy. As a representative nucleus we show  $^{252}\text{Fm}$  in fig. 3b. The spherical shape is not included in the set of shapes studied, but is located at  $r = 0.75$ ,  $\sigma = 0.4873$  (cf.<sup>38</sup>). The saddle point energy is about 2 MeV and is located at  $r = 1.07$ ,  $\sigma = 0.68$ . A prominent structure in the diagram is a mountain, centered around the configuration of two touching spheres, at  $r = 1.5874$ ,  $\sigma = 0.7099$ . One should, as we have pointed out above, realize the importance of using a finite-range model for the macroscopic energy to get a realistic value for the energy of this configuration. In the investigation by<sup>18</sup>), using the liquid-drop model, which is *not* of the finite-range type, the calculated energy obtained for this shape configuration, for a nucleus with approximately the fissility of  $^{252}\text{Fm}$ , is about 50 MeV above the energy of the spherical shape. After passing over the saddle point, the dynamical path of the nucleus depends strongly on dissipation. A dynamical calculation shows that with no dissipation the nucleus follows approximately the valley that can be seen beyond

the saddle point and reaches the scission line at about  $r = 3.5^{64}$ ). We now show how these features and conclusions are modified by taking into account the microscopic part in the model for the total potential energy.

In figs. 3c and 3d we show calculated total potential-energy surfaces for  $^{252}\text{Fm}$  and  $^{264}\text{Fm}$ . The contour map for  $^{252}\text{Fm}$  in fig. 3c is quite different from the one for the macroscopic energy displayed in fig. 3b. In fig. 3c we can see the deformed ground-state at  $r = 0.87$ ,  $\sigma = 0.57$ , a first saddle at  $r = 0.99$ ,  $\sigma = 0.63$  and a second minimum at  $r = 1.15$ ,  $\sigma = 0.69$ . The area beyond the second minimum shows interesting structure. There are two mountains, one centered at the two-touching-sphere configuration, the other at  $r = 1.33$ ,  $\sigma = 0.77$ . The latter mountain is surrounded by two saddle points that are of equal height to within 0.5 MeV. The energy of the peak of the mountain separating these two saddle points is about 2 MeV higher than the saddle-point energies. A nucleus passing over either of the two saddles would seem to evolve into shapes leading into a valley that is similar to the one that is present in the macroscopic case in fig. 3b, which in this case reaches the scission line at between  $r = 3.75$  and  $r = 4.25$ . Access to the scission configuration of two touching spheres is blocked by the other mountain, which is about 3 MeV higher than the saddle points.

In the study by <sup>20)</sup> limited to the two nuclei  $^{258}\text{Fm}$  and  $^{259}\text{Md}$  part of this structure is seen, namely the mountain at  $r = 1.33$ ,  $\sigma = 0.77$  with the two surrounding saddle points. In a later study by the same group <sup>21)</sup> a "super-short" valley towards scission is seen for  $^{252}\text{Cf}$ . This is contrary to our results below. In <sup>21)</sup> fig. 2 shows that the shapes of the fragments at the end of this valley are far from spherical. The results of <sup>21)</sup> may therefore be somewhat spurious and may occur because of the particular constraints imposed by their shape parameterization on the shape of the end of the nucleus or because a liquid-drop model with a standard surface-energy term is used instead of a more appropriate finite-range model for the surface energy. In fig. 3a in <sup>21)</sup> some point outside the figure and somewhat below the lower left corner corresponds to two touching spheres. This important shape is inaccessible to the shape parameterization used. In addition one can see the unphysical rise in energy at this location, which is due to the choice of an inadequate macroscopic model. The contour maps are displayed in terms of geometrical parameters of the shape, whereas we display the contour maps as functions of moments of the shape, which is a more appropriate method. This difference may also lead to differences in the appearance of valleys and ridges, since these structures are not invariant under coordinate transformations.

Also in other, earlier studies that featured more limited shape parameterizations and models for the macroscopic energy that did not allow for the study of shapes in the vicinity of the two-touching-sphere configuration, very little of the type of structure which we see here has been present. Examples of such results are fig. 1c in <sup>24)</sup>, which presented a general survey of heavy-element fission barriers, and fig. 9 of <sup>14)</sup>, which was directed specifically towards the study of the influence of fragment shells.

Fig. 3d shows a corresponding potential energy surface for  $^{264}\text{Fm}$ . There are major differences in structure between this nucleus and  $^{252}\text{Fm}$  shown in the previous figure. Here there is no second minimum. Instead, a short but deep valley starts at the first saddle and leads directly to the two touching-sphere configuration. The mountain that is present at this configuration in the  $^{252}\text{Fm}$  case has completely disappeared here. This short, deep valley is separated by a high ridge from another valley in the upper part of the diagram.

On the ridge there is a mountain at  $r = 1.41$ ,  $\sigma = 0.83$  and above this mountain there is a slightly lower saddle leading into the upper valley. The upper valley is similar to the one found in the plot of the macroscopic energy only, in fig. 3b. The lower valley has clearly been created by fragment shell effects. Using terminology from <sup>13)</sup>, the lower valley is fragment

shell-directed and the upper one is liquid-drop-like. The upper valley is the old valley and the lower valley is the new valley. In a pure macroscopic model there is for separated, spherical fragments a valley called the fusion valley. The results of<sup>38)</sup> show that the fusion valley ends at about  $r = 2.0$ . In our discussions here we mean by new valley the valley carved out by shell corrections beyond the end of the conventional fusion valley. Since it is only very recently that experimental studies have probed the manifestations of this valley, we feel the designation "new" is appropriate.

The results of<sup>14)</sup> for  $^{264}\text{Fm}$  also show, in their fig. 10 a deep valley extending to the first saddle. However, by comparing figs. 9 and 10 of<sup>14)</sup> it is clear that their results are quite different from ours. The figures show that the initial part of the new valley in fig. 10 corresponds to the same shape as the second saddle for  $^{252}\text{Fm}$  in fig. 9. We find, in contrast, that a key feature of our results is that the old and new paths correspond to *different* shapes, as early in the fission process as the second saddle. Another difference is that our results show that the scission configuration for  $^{264}\text{Fm}$  is reached already at  $-6$  MeV in the new valley. This is just 4 MeV below the ground state. In the results of<sup>14)</sup> the energy 4 MeV below the ground state in the new valley for  $^{264}\text{Fm}$  corresponds to a shape with a fairly large neck,  $d \approx 0.35$ .

We have displayed results for  $^{264}\text{Fm}$  because it is the nucleus for which one would expect the fragment shell effects to be maximum and it is of value to see the theoretical results for this case. However, this nucleus has not been observed experimentally. Were the fission of this nucleus ever to be observed experimentally, one would expect all fission to follow the lower valley, since it is separated from the valley higher in the diagram by a high ridge. The cases that have been experimentally observed<sup>13)</sup> often seem to lie in a transition region between fission in one valley or the other. In particular, for  $^{258}\text{Fm}$  most of the events have a kinetic energy peaked around 235 MeV, but the skewed kinetic-energy distribution indicates the presence of a second smaller peak at 200 MeV.

It would be desirable to deduce the dynamical evolution of nuclear shapes from the last saddle from a dynamical model. Since shell effects are important in the region we study, such a model should also incorporate shell effects. A survey of a large number of nuclei with such a model would require an enormous effort. We therefore base some simple arguments about the dynamical evolution from saddle to scission mostly on the structure of the static potential-energy surfaces we present here. However, we relate the results of our arguments to experimental data. This will show if our approach is a useful one. The choice of coordinates in terms of which the potential energy is displayed is suitable for arguments of this type, since the mass and dissipation tensors for separated fragments are diagonal in  $r$  and  $\sigma$ <sup>34)</sup>. It should therefore be close to diagonal also for connected shapes close to scission, the region in which we are most interested.

## 4.2 POTENTIAL-ENERGY SURFACES FOR EVEN Fm ISOTOPES

As a first example we show in fig. 4 the result obtained previously<sup>34)</sup> for  $^{258}\text{Fm}$  in the current formulation of the model in which the shape dependences of the Wigner and  $A^0$  terms are included. Here the structure of the surface is such that it provides a consistent interpretation of the experimental results, in particular since we show below that the saddle along the long dashed - it switchback path is lowered by mass asymmetric shape degrees of freedom. The mass-asymmetric shape degrees of freedom will be studied in the shaded region of the contour diagram. Most of the fission events will follow the short dashed path leading into the new valley. Just as in the calculation with the old version of the model<sup>34)</sup> there is a *switchback* path leading from a point along the new path across a saddle at about  $r = 1.50$  and  $\sigma = 0.85$ .

back to the old valley. This switchback path according to our interpretation is responsible for the few low-kinetic-energy events that are observed for this nucleus. The *old* fission path, shown as a dot-dashed line, is not involved at all in the fission process according to our current interpretation. Shapes along the three paths are shown in fig. 5.

In fig. 6 we show the result obtained for  $^{258}\text{Fm}$  with the new range  $\gamma = 1.4 \times \hbar\omega_0$  in the Strutinsky method, but *without* the new shape dependences for the Wigner and  $A^0$  terms included. For  $^{258}\text{Fm}$  there is now no second barrier in the new valley, which would agree with the old interpretation for the short half-life for this nucleus. However, the ridge between the old and new valley is much too high to allow any branching into the old valley as is indicated by experiment. The fission barrier along a path corresponding the bottom of the new valley in fig. 6 is very similar to a corresponding barrier obtained by another group<sup>33</sup>). That calculation uses a Woods-Saxon single-particle potential, the Yukawa-plus-exponential macroscopic model and a choice of shapes that includes shapes close to two touching spheres. As in our fig. 6, their Wigner and  $A^0$  terms are shape-independent.

In figs. 7, 8a-8c and 9a-9b we present additional potential-energy surfaces for symmetric shapes. However, before commenting on these results we discuss the effect of mass-asymmetric shapes in the new valley. The saddle along the switchback path in fig. 4 is about 3 MeV higher than the saddle leading to compact scission shapes. To calculate the branching ratio between fission along the switchback path and fission into compact shapes one needs to consider the penetrabilities through the barriers in a dynamical calculation. However, since the saddle along the switchback path in fig. 4 is 3 MeV higher than the outer saddle in the new valley one may feel justified to conclude that access to the old valley is almost completely blocked by the ridge. On the other hand, one may suspect that mass-asymmetric shape degrees of freedom may lower the saddle along the switchback path.

To investigate this possibility we have calculated the potential energy for a full three-dimensional grid for a choice of shapes that include the switchback saddle and the outer saddle along the new fission valley. The exact choice of shape coordinates has been discussed earlier. Some results for  $^{258}\text{Fm}$  are shown in figs. 10a and 10b. Each surface shows the potential energy for a fixed value of  $\tau$  as a function of  $\sigma$  and the mass-asymmetry coordinate  $\alpha_2$  of the three-quadratic-surface parameterization. For  $\alpha_2 = 0.0$  the results should be identical to those plotted in fig. 4. However, there are some minor differences. These have arisen because the two types of surfaces are based on different sets of grid points and the fact that the potential energy varies very rapidly in some regions of deformation space. The two surfaces in figs. 10a and 10b give results for the two values of  $\tau = 1.4$ , and 1.6. To obtain a more three-dimensional picture of the results we may pretend that we are standing at about  $\tau = 2.0$  and  $\sigma = 0.775$  in fig. 4, that we look in the negative  $\tau$  direction and that energy values have been calculated vertically out of the plane as a function of the third coordinate  $\alpha_2$ . The surfaces in figs. 10a and 10b represent  $\sigma$ - $\alpha_2$  planes rising above the  $\tau$ - $\sigma$  plane in fig. 4, as we would see them from our vantage point. Parts of the new and old fission valleys are seen in figs. 10a and 10b to the lower left and to the upper right, respectively. The bottoms of the two valleys are usually not present in the two figs. 10a and 10b, but the saddle between the two valleys stands out very clearly in these figures. This saddle corresponds to the ridge between the old and new fission valleys in fig. 4 but with the effect of mass asymmetry on the height of this ridge taken into account. The lowest point on the sequence of saddle points in cuts of the type shown in figs. 10a and 10b corresponds to the height of the saddle on the switchback path between the old and new valleys, now with mass asymmetry taken into account.

To make our three dimensional results easier to interpret, we reduce the results in figs. 10a and 10b to a two dimensional contour plot. This we accomplish by plotting the minimum in

the  $\alpha_2$  direction, minimized for fixed values of  $\sigma_1$ ,  $\sigma_2$  and  $\sigma_3$ , as a function of  $r$  and  $\sigma$  in the form of a contour diagram. In fig. 11b we present such a contour diagram for  $^{258}\text{Fm}$ . The plot is based on figs. 10a and 10b and similar results at  $r = 1.3, 1.5, \text{ and } 1.7$  that we have not shown. A minimization procedure, such as the one we use here is most meaningful and most simple to interpret if there is only one minimum in the direction of the variable that is eliminated by minimization, as is the case for the results we present here. Were there several minima one would obtain several contour-map sheets and the results would be more difficult to interpret.

Figure 11b shows the influence of mass asymmetry on the small shaded region of fig. 4. From an inspection of figs. 10a and 10b it is clear that the outer saddle along the new fission path at about  $r = 1.6$  and  $\sigma = 0.75$  is not lowered by mass asymmetry. The fact that the energy of this saddle is at about 0.75 MeV in fig. 11b and at about 1.5 MeV in fig. 4 only reflects the different sets of grid points used to plot the two figures. Figure 11b is the more accurate one. In most regions of the contour diagrams the difference between the two figures is much smaller. In fig. 4 the energy decreases very rapidly at  $r = 1.6$  as a function of  $\sigma$ , starting from the lower border of the contour diagram and proceeding in the direction of the saddle. This property is somewhat difficult to reproduce by interpolation and is the reason why a somewhat inexact value is obtained for the saddle-point energy in fig. 4. In fig. 11b one grid point is located at  $r = 1.6$  and  $\sigma = 0.75$  and another at  $r = 1.6$  and  $\sigma = 0.725$ . This results in an excellent accuracy for the saddle-point energy.

A further comparison of figs. 4 and 11b shows that the saddle on the switchback path is indeed lowered by mass asymmetry. In fig. 11b it is equal in height to the outer saddle in the new valley. It is also of interest to note that it has moved from  $r = 1.5$  and  $\sigma = 0.825$  in fig. 4 to  $r = 1.4$  and  $\sigma = 0.75$ , although we expect that the movement would have been smaller if  $r$  and  $\sigma$  had been conserved when  $\alpha_2$  was varied.

We mentioned earlier that a study<sup>33)</sup> with a Woods-Saxon single-particle model and a Yukawa-plus-exponential macroscopic model had obtained very similar results to ours for  $^{258}\text{Fm}$ . However, that calculation did not use shape-dependent Wigner and  $A^0$  terms. To be able to make a more relevant comparison between those results and the results obtained with our model, we show in fig. 11c a contour diagram for  $^{258}\text{Fm}$  obtained exactly as in fig. 11b but without any shape dependence for the Wigner and  $A^0$  terms. We see that in this case there is a fairly high ridge separating the new and old fission valleys. In addition, there is no outer saddle in the new valley. A comparison of figs. 6 and 11c shows that the energy along the new fission valley is not lowered by mass asymmetric shape degrees of freedom, but that the ridge separating the new and old fission valleys becomes somewhat lower when mass-asymmetric shape degrees of freedom are considered.

When we compare our results for the case with shape-independent Wigner and  $A^0$  terms to the results obtained in the study by the Polish group<sup>33)</sup> with the Woods-Saxon model it is clear that the results for symmetric shapes are very similar, in fact almost identical along the new valley. However, for the case with mass-asymmetric shape degrees of freedom taken into account the Polish group finds that the ridge between the old and new valleys disappears at about  $r = 1.5$ . This is in contrast to our results, for which fig. 11c shows that there remains a ridge at least out to  $r = 1.7$ , which is the last point shown in fig. 11c. The Polish group concludes from their results that whether the nucleus ends up in the old or new valley is decided by dynamics after the barrier has been penetrated and not by different penetrabilities through different barriers. We feel that their calculational results do not prove this point. An inspection of the figure of the shapes on which the potential energy surface for  $^{258}\text{Fm}$  in the Polish study is based shows that as the asymmetry of the shape increases there is a strong increase in

the overall elongation of the nucleus, especially at larger values of  $r$ . Since there is a strong decrease in the Coulomb energy of the system when the elongation of the nucleus increases, this coupling between elongation and asymmetry in the Polish calculation is the mechanism behind the disappearance of the ridge between the two valleys. Thus, the disappearance of the ridge in their calculations is *not* caused by the effect of mass-asymmetric shape degrees of freedom, but by the coupling between the mass-asymmetry and elongation shape degrees of freedom in their parameterization.

We also feel that in addition to selecting an orthogonal set of shape degrees of freedom, it is necessary to consider the shape dependences of the Wigner and  $A^0$  terms, as we have done in figs. 4 and 11b. The shapes corresponding to the contour map of fig. 11b are shown in fig. 11a. We mentioned in earlier that for  $\alpha_2 \neq 0$ , we do not exactly conserve  $r$  and  $\sigma$ . In fact, there is some ambiguity in how to define these concepts for asymmetric shapes. We have investigated a number of possible extensions of the definitions of  $r$  and  $\sigma$  to asymmetric shapes. The point where the ambiguity arises is when we specify how to define the two parts of the system. We have several possibilities, including dividing the nucleus at a point midway between the ends or at the minimum neck radius. The effect of conserving  $r$  and  $\sigma$  by use of these and other prescriptions is to *increase* the height of the ridge between the new and old valleys in fig. 11c, thus only reinforcing our conclusion above that there is a ridge between the new and old valleys. However, in contrast to the case in figs. 3c, 3d, 6 and 11c, we elsewhere use a model with shape-dependent Wigner and  $A^0$  terms, as shown in fig. 11b, for example. In such cases there is often a saddle on the ridge between the old and new fission valleys and then a prescription for conserving  $r$  and  $\sigma$  would not change the most important features of the potential-energy contour map, namely the height of this saddle point, since saddle-point heights are invariant under coordinate transformations.

From the above discussion we find that the mechanism behind the bimodal fission process remains the one proposed in our earlier study<sup>34)</sup>: For  $^{258}\text{Fm}$  fission initially proceeds along the new fission valley, with most events penetrating the outer saddle along this path. However, a small number of events branch off from the new valley to under the saddle along the switchback path and penetrate into the old fission valley. An important point made in our earlier study<sup>34)</sup> is that because the barriers leading into the new and old valleys are the same from the ground state to the exit point at the end of the barrier, *except for a tiny portion at the end of the barrier*, it is possible for the branching ratio to be about unity, as is also observed experimentally.

To show the structure of the potential-energy surface for nuclei at some distance away from where the transition point between fission into the old valley and fission into the new valley occurs, we display a potential-energy contour map for symmetric shapes for  $^{252}\text{Fm}$  in fig. 7. From fig. 7 for  $^{252}\text{Fm}$  it is clear that access to the new valley is blocked by a mountain ridge. Experimentally it is known that  $^{252}\text{Fm}$  fission properties exhibit characteristics associated with fission in the old valley. The contour map in fig. 7 shows that there are two saddles leading into the old valley, one saddle on the old fission path at  $r = 1.4$  and  $\sigma = 0.85$  and another saddle on the switchback path at  $r = 1.5$  and  $\sigma = 0.80$ . Both of these saddles are lowered by mass-asymmetric shape degrees of freedom. The mountain ridge is unaffected by mass asymmetry at  $\sigma$  values below  $\sigma = 0.75$ . Consideration of fission half-lives below shows that it is likely that during fission this nucleus follows the switchback path. The effect on the potential energy of the new valley should be maximum for  $^{204}\text{Fm}$ . Our calculations show that there is a very deep new valley, with a ridge approximately 10 MeV high separating the new and old valleys in a potential-energy surface based on symmetric shapes only. We will later show a potential energy contour map for this nucleus with mass asymmetric shape degrees of freedom taken into account.

Mass-asymmetric shape degrees of freedom lower the switchback saddle somewhat. In figs. 12a-12b we show for  $^{256}\text{Fm}$  and  $^{260}\text{Fm}$ , respectively, the effect of mass-asymmetric shape degrees of freedom on the structure of the potential-energy surface in the outer region of the new valley. For  $^{252}\text{Fm}$  (not shown) our calculations show that mass asymmetry lowers the switchback saddle by about 1 MeV and that a high mountain blocks access to compact scission shapes and pushes the fission path over the switchback saddle into the old fission valley. For  $^{256}\text{Fm}$  fig. 12a shows that the ridge blocking the outer part of the new valley is only about 1 MeV higher than the saddle on the switchback path. However, since the ridge is also very wide in the direction of compact scission shapes the structure of the surface suggests that fission almost totally branches into the old fission valley. For  $^{260}\text{Fm}$ , shown in fig. 12b, the saddle along the switchback path is 2 MeV higher than the outer saddle in the new valley.

Since the widths of the barriers and the inertia associated with fission along the two paths also influence the branching ratios, one cannot conclude solely from a comparison of barrier heights whether fission into the old or new valleys will dominate. However, the surfaces in figs. 12a, 12b and 11b interpreted together with the experimental data available for  $^{256}\text{Fm}$  and  $^{258}\text{Fm}$  indicate that for  $^{260}\text{Fm}$  all fission will be in the new valley. We draw this conclusion by considering the effect of the small change in the structure of the potential-energy surface between  $^{256}\text{Fm}$  and  $^{258}\text{Fm}$  in figs. 12a and 11b on the fission properties of these two elements. For  $^{256}\text{Fm}$  the saddle in the new valley is about 1 MeV higher than the switchback saddle and for  $^{258}\text{Fm}$  it is of the same height as the switchback saddle. This gives a change in fission properties from fission almost entirely into the old valley to fission almost entirely into the new valley. Thus, for  $^{260}\text{Fm}$ , where the saddle into the new valley is now 2 MeV lower than the switchback saddle, we expect no fission into the old valley.

### 4.3 ADDITIONAL POTENTIAL-ENERGY SURFACES

We have also calculated potential-energy surfaces for other heavy elements. We present and discuss some results of these calculations in this subsection, but postpone part of the discussion until the section on fission half-lives.

For even nuclei some additional potential-energy surfaces are shown as functions of  $r$  and  $\sigma$  in figs. 8a-8c. In fig. 8a the results for  $^{240}\text{Pu}$  are exhibited. This nucleus is far removed from neutron and proton numbers favoring the new valley. As expected, there is also no trace of a new valley in the calculated potential-energy surface. Instead, there is a mountain some 30 MeV high at the location of two touching spheres. For  $^{272}\text{110}$  in fig. 8b there is a structure corresponding to the new valley in the potential-energy surfaces. The implications of its presence will be considered in the subsection on fission half-lives below. Somewhat surprisingly there is also a second lower valley present in the potential-energy surface for  $^{260}\text{110}$  displayed in fig. 8c.

In figs. 9a-9b we show potential-energy surfaces for symmetric shapes for two odd systems. Since the effects of mass-asymmetric shape distortions are not considered in these figures, the heights of the saddles on the ridge between the new and old valleys are overestimated. The reductions of the height of the ridge if mass-asymmetric shape degrees of freedom were taken into account obviously depends both on the particular proton and neutron numbers of the nucleus, and on the specialization energy associated with the odd particle. For the even fermium isotopes we have above seen an effect of about 2 MeV on the height of the ridge and will in our discussion below consider this to be the reduction, on the average, also in the odd case. One should, however, always keep in mind that this number is only a very rough estimate.

The most notable feature in the potential-energy surfaces for the odd nuclei is the large effect of the  $\Omega$  spin value on the specialization energy. This is most clearly seen for a sequence of Lr isotopes discussed in ref.<sup>55</sup>). Although the neutron number for  $^{266}\text{Lr}$  is  $N = 163$ , which is only one unit away from the most favorable neutron number  $N = 164$  for the new valley, the barrier in the new valley is much higher for  $^{266}\text{Lr}$  than for  $^{262}\text{Lr}$ . This is of course due to the very high specialization energy associated with the  $N = 163$  orbital with  $\Omega_n = 13/2$ . In addition, the calculated spin for the odd  $Z = 103$  proton is  $\Omega_p = 9/2$  for many Lr isotopes. At the bottom of the new valley at  $r = 1.50$  the specialization energy is more than 8 MeV for  $^{266}\text{Lr}$ .

The prediction that the ground-state spin of the  $N = 163$  orbital is  $\Omega_n = 13/2$  is subject to some uncertainty. An inspection of calculated Nilsson diagrams for the folded-Yukawa model, for instance figs. 1b and 2b in ref.<sup>37</sup>), shows that the orbital in question is  $[716_{13/2}^{15}]$  coming from the  $j_{15/2}^{15}$  spherical shell. The position in the region of the deformed ground states of the  $\Omega_n = 13/2$  level is right above the  $N = 162$  deformed gap. This gap has long been present<sup>4,37</sup>) in calculations with single-particle potentials that go to zero at infinity. However, it is only more recently after new experimental results were obtained<sup>56-58</sup>) for elements in this region that the consequences of this deformed gap for the stability of the heaviest elements were realized. The experiments themselves and recent calculations<sup>59-61</sup>) show that the importance of this gap for the stability of the heaviest elements is considerable. Since the calculations reproduce some experimental results in this region fairly well, the predicted level spectrum should be fairly reliable. Of course, the prediction that it is precisely the  $N = 163$  orbital that has spin  $\Omega_n = 13/2$  is subject to the uncertainties of the theoretical model. However, from an inspection of the calculated level diagrams it is clear that several high- $\Omega$  levels should be present in the vicinity of  $N = 162$  and from these rather general arguments we see that for some odd- $N$  nuclei in this region we should expect very high ground-state spins and, correspondingly, very long fission half-lives. Another factor that has to be considered is that in some cases the very highest  $\Omega$  values associated with the top Nilsson orbitals emanating from very highly degenerate spherical shells may not occur as ground-state orbitals in a deformed nucleus<sup>62</sup>), because of the effect of residual interactions not taken into account here.

Figures 13a-13b, and 14a-14b show calculated potential-energy surfaces, minimized with respect to a mass-asymmetry coordinate, in the vicinity of the outer part of the new valley and the switchback path from the new to the old valley. Our calculated results presented in these figures together with other calculated contour maps that are not exhibited, show that for Cf, No, Rf and  $Z = 106$  the new valley emerges as the more dominant one approximately at  $^{282}\text{Cf}$ , at  $^{282}\text{No}$ , at  $^{264}\text{Rf}$  and at  $^{260}106$ , respectively. When considering the implications of the valleys and saddle points in the calculated potential-energy surfaces it is very useful to simultaneously consider calculated fission half-lives corresponding to various paths from ground state to scission in the potential-energy surface. The results presented in this section will therefore be further discussed in the next section on fission half-lives.

In a study<sup>63</sup>) of  $^{240}\text{Pu}$  fission properties based on a density-dependent Hartree-Fock Bogolyubov approach a potential-energy surface with two different valleys is also obtained. There are some considerable differences between this potential-energy surface and the dynamical calculations based on it and the results we have obtained in the Fm region. This does not necessarily constitute a contradiction, because the fission properties in these two regions are considerably different. In the potential-energy surface calculated in<sup>63</sup>) the valley corresponding to compact shapes starts outside the last saddle point and is very similar to the fusion valley seen in calculations based on pure macroscopic models, for instance by<sup>34</sup>). Thus, it is different from the new valley we see in our calculations. As we discussed above, by new



valley we mean the valley carved out by shell corrections inside the end of the usual fusion valley as given by macroscopic calculations. However, an interesting feature in the structure of the potential-energy surface obtained by <sup>63)</sup> is the ridge separating the two fission valleys. In the dynamical study by <sup>63)</sup> transitions from the fission valley to the fusion valley occur along the entire extension of this ridge and provide a mechanism for generating a kinetic-energy distribution extending from cold fission to the more probable events with internally excited fragments. Our results for the Fm region indicate a different mechanism for the cold fission in that region. In our picture we reach the old and new fission valleys by starting from the same second minimum and following paths that lead under two different second saddle points. However, our picture and that of <sup>63)</sup> are not necessarily contradictory, since our trajectories correspond to the mean of high and low kinetic-energy distributions, whereas the results of <sup>63)</sup> represent a first step in a calculation of an entire kinetic-energy distribution with a single peak. The two approaches emphasize slightly different aspects of the fission process.

#### 4.4 FISSION HALF-LIVES

It has been proposed that the rapid change in half-life when going from <sup>256</sup>Fm to <sup>258</sup>Fm is due to the disappearance of the second saddle in the barrier below the ground-state energy. Fission through only one barrier, the first, gives very good agreement with the observed short half-life of <sup>258</sup>Fm <sup>25,27)</sup>. However, one may ask if and how the fission half-life is connected to the change in the other fission properties at this transition point, namely to the change to symmetric fission and to high kinetic energies. We show that the old interpretation that the barrier of <sup>258</sup>Fm has disappeared below the ground state is inconsistent with results from the present calculation and propose a new mechanism for the short half-life. In addition, we show that the connection between quantities like kinetic energies, fission half-lives and old and new fission valleys is complex, but that there is an interpretation that is consistent with the experimental data observed up to now.

To calculate fission half-lives it is necessary to know the potential energy, the inertia associated with the motion through the barrier and the path from the ground state through the barrier. As we mentioned in the introduction, mainly two models have been used for studies of this type. The first type is a microscopic model for the inertia, and the second type is a semi-empirical model. Since we base the calculation of the nuclear potential energy on a microscopic model it would seem desirable and consistent to base also the calculation of the inertia on some type of microscopic model. However, the microscopic models for the inertia seem more uncertain than the macroscopic-microscopic model for the potential energy. Different microscopic models yield very different results for the inertia, as can be seen from fig. 3 in <sup>25)</sup>, for instance. Usually the calculated inertia varies in a somewhat periodic manner with a peak-to-valley ratio of about two in some typical cases. One should also note that the peak-to-valley ratio and the magnitude of the calculated inertia are extremely sensitive to small changes in the model assumptions. However, we may observe from fig. 2 in <sup>64)</sup> that in some recent results from microscopic models, the calculated inertia shows a rapidly fluctuating behaviour around a mean which is approximately equal to the more simple semi-empirical model for the inertia. We may argue that the effect of the fluctuations averages out, since one evaluates an integral over the product of the fission-barrier height and the inertia. It is also clear that when more effects are taken into account in the determination of the microscopic inertia the fluctuations become smaller. Because of the uncertainties in and the complexities of the microscopic models for the inertia, we here use the semi-empirical approach.

As a first step in the semi-empirical approach we select a one-dimensional path through

the multi-dimensional potential-energy surface. This path starts at the nuclear ground state and includes saddle points and minima in the fission direction and a few points beyond the last saddle. Obviously, the choice of path between the saddle points and minima is open to some ambiguity. However, selecting somewhat different paths affects the calculated half-lives by less than an order of magnitude. But to remove the small ambiguity, we only use the energies and values of the position coordinate  $r$  at the saddle points and minima in the construction of the one-dimensional fission barrier. We then construct the fission barrier by connecting the ground state to the first saddle with a third-degree polynomial whose derivatives are zero at the ground state and at the saddle. This completely defines the third-degree polynomial. The rest of the barrier is constructed in a corresponding manner, by connecting neighbouring extremum points with third-degree polynomials. If there are no extrema beyond the exit point, which is the point where the barrier energy becomes lower than the ground-state energy, we construct the last part of the barrier by a straight line from the saddle point through a point somewhat beyond the exit point at the bottom of the valley that leads towards scission. An inspection of contour diagrams published in this paper shows that the contour lines are fairly equidistant in this valley, which means that it is much better to use a straight line in this region than a polynomial.

In a one-dimensional WKB spontaneous-fission model the fission half-life is connected to the penetrability by<sup>23,65)</sup>

$$T_{sf} = 10^{-28.04} \gamma/P \quad (18)$$

where the value  $\omega_0 = 1 \text{ MeV}/\hbar$  is used for the frequency of assaults on the barrier. The probability  $P$  of penetrating the barrier  $V(r)$  at the energy  $E_0$  is given by<sup>66)</sup>

$$P = \frac{1}{1 + e^K} \quad (19)$$

where

$$K = 2 \int_{r_1}^{r_2} \left\{ \frac{2B_r(r)}{\hbar^2} [V(r) - E_0] \right\}^{1/2} dr \quad (20)$$

Here  $V(r)$  is the barrier energy along the selected path. The penetration energy  $E_0$  is the ground-state energy plus the zero-point energy in the fission direction at the ground state.

The function  $B_r(r)$  is the inertia with respect to  $r$  associated with motion in the fission direction. An important aspect of the semi-empirical approach is to deduce asymptotic properties of the semi-empirical inertia from arguments about the expected general properties of the inertia at small and large  $r$  values. Thus, at large distances we expect  $B_r(r)$  to approach the value  $\frac{1}{4}M$  appropriate to separated symmetric fragments. At small  $r$  values the inertia is expected to be considerably higher than what is given by a hydrodynamical irrotational-flow model, due to microscopic quantum-mechanical effects. In the semi-empirical model these asymptotic constraints are taken into account by relating the inertia  $B_r$  to the inertia  $B_r^{irr}$  corresponding to irrotational flow by<sup>65)</sup>

$$B_r - \mu = k(B_r^{irr} - \mu) \quad (21)$$

where  $k$  is a semi-empirical constant and  $\mu$  is the reduced mass of the final symmetric fragments. The  $k$  parameter accounts for the increase of the inertia above the hydrodynamical value due to quantum-mechanical effects.

The irrotational inertia has been numerically calculated for  $\gamma$ -family shapes, which are defined in terms of the saddle-point shapes for an idealized uniformly charged liquid drop<sup>65)</sup>.

We approximate the numerical results by<sup>67)</sup>

$$B_r^{ir} - \mu = \frac{17}{15} \mu \exp \left[ -\frac{128}{51} \left( r - \frac{3}{4} \right) \right] \quad (22)$$

In another study Randrup *et al.*<sup>27)</sup> varied the coefficient in the exponential term, which affected the rate at which the semi-empirical inertia approached the asymptotic limit  $\mu = \frac{1}{4}M$ . However, for the old fission valley this variation did not significantly decrease the root-mean-square deviation between the calculated and experimental fission half-lives. They therefore chose a value close to  $\frac{128}{51}$  and determined  $k = 11.5$  from an adjustment to experimental data. The approach<sup>25,65)</sup> was referred to as semi-empirical with one adjustable parameter.

In our case, we use the value  $k = 16$ , which was determined in<sup>67)</sup> from an adjustment to five actinide fission half-lives. In that adjustment the root-mean-square deviation between the logarithms of the calculated and experimental half-lives was 2.5. If this method of calculating fission half-lives does not diverge outside the region of adjustment we may consequently expect a deviation between calculated and experimental fission half-lives of two to three orders of magnitude. We therefore call the agreement between calculated and experimental results *good* if the deviation is less than about three orders of magnitude.

The value  $k = 16$  obtained in<sup>67)</sup> is larger than the value  $k = 11.5$  used in ref.<sup>27)</sup>. The reason is that fission barriers calculated with the folded-Yukawa single-particle microscopic model are systematically thinner than those obtained with the Nilsson modified-oscillator single-particle potential.

In our study here we have calculated fission barriers also in the  $\epsilon$  parameterization. We use those results to determine the barrier along the old valley. We have calculated two-dimensional symmetric potential-energy surfaces as functions of  $\epsilon_2$  and  $\epsilon_4$ , with single-particle parameters for <sup>272</sup>110. These calculations yield slightly lower values for the saddle on the top side of the mountain around  $r = 1.35$  than the results of the calculation in the three-quadratic-surface parameterization, which are presented in the form of contour diagrams in this paper. We also take mass asymmetry into account when we determine this saddle-point height. The effects of mass asymmetry we take from unpublished old calculations in terms of  $\epsilon_3$  and  $\epsilon_5$  at the second saddle. The shape coordinates for that study were exactly as in<sup>24)</sup>, and the calculation used a slightly different set of parameters compared to the present calculation for the folded-Yukawa single-particle potential. It used the droplet model for the macroscopic energy, with a parameter set given by<sup>26)</sup>. Although a slightly different model was used, which results in different barriers, we only take the *reduction* in the barrier height due to mass asymmetry from that calculation. The error in the value for the *reduction* in barrier height, in the old valley, that results from using the different model is very low, less than 200 KeV out of a total reduction of 1 to 2 MeV. We take the value for the zero-point energy from unpublished results from our 1981 ground-state mass calculation<sup>4,45)</sup>.

Investigation in refs.<sup>34,55)</sup> show that the short spontaneous-fission half-life for <sup>258</sup>Fm is *not* due to a non-existent second peak in the fission barrier. Instead it is due to a much lower inertia associated with fission in the new valley. We have investigated the single-particle level structures in the old and new valleys. In figs. 15a and 15b we show proton single-particle levels for shapes evolving from a spherical shape into the two valleys. Figure 15a shows proton levels for liquid-drop saddle-point shapes or  $y$ -family shapes<sup>44)</sup>, which are shapes corresponding to fission-barrier shapes along the old fission path. Figure 15b shows proton levels for intersecting spheres. These shapes correspond to shapes at the lower limit of  $\sigma$  in the contour diagrams exhibited in fig. 4. This limit is slightly lower than the new valley for <sup>258</sup>Fm, but we have also calculated the levels in the new valley for <sup>258</sup>Fm and they are practically indistinguishable

from the levels for intersecting spheres. Since the new valley is slightly different for different nuclei and also because a valley is a slightly less well-defined concept than intersecting spheres we display here only the levels corresponding to the intersecting-spheres family of shapes.

It is immediately clear from inspecting figs. 15a and 15b that the level structures in the two valleys are radically different. In the old valley the level crossings continue through the entire deformation range studied, which for the heavy elements studied here corresponds to penetrating the entire fission barrier. Although gaps corresponding to ground-state and isomeric minima are present no truly large-scale structures are present. The level structure appears fairly random. Figure 15a together with the microscopic calculations discussed above explain the success of fission half-life calculations based on a smooth semi-empirical inertia<sup>26,27</sup>).

For the new valley it is clear that our current form of the semi-empirical inertia is inadequate. In its present form the inertia reaches the limiting value  $\frac{1}{4}M$  at infinity. However, since in the new valley the fragments separate already at  $r = 1.59$  the asymptotic limit  $\frac{1}{4}M$  should be reached already here. In addition we see by inspecting fig. 15b that the magic gap  $Z = 50$  extends far inside the point of two touching spherical nuclei. The gap extends into such compact shapes as  $r = 1.20$ . To a somewhat lesser extent the presence of the gap is seen as far as  $r = 1.07$ , which is the deformation corresponding to the *first* saddle. Over this entire region the levels are parallel and there are very few level crossings compared to the situation in the old valley. We have found that also for neutrons the  $N = 82$  gap extends far inside the point of touching at  $r = 1.59$ . Thus, in this region, already before separation, the inertia should have reached or be very close to its limiting value of  $\frac{1}{4}M$ .

Since we have, from general arguments been able to set some limits on the inertia in the new valley, we will investigate a generalization of the semi-empirical inertia for the old valley given by eq. (21), which allows for a natural and simple way of fulfilling the limiting conditions for the new valley. For the new valley we propose

$$B_r - \mu = f(r, r_{sc})k(B_r^{int} - \mu) \quad (23)$$

where

$$f(r, r_{sc}) = \begin{cases} \left( \frac{r_{sc} - r}{r_{sc} - 0.75} \right)^m & , \quad r \leq r_{sc} \\ 0 & , \quad r \geq r_{sc} \end{cases} \quad (24)$$

and  $r_{sc}$  is the  $r$  value where the new valley reaches scission, which in our investigation here is set equal to the  $r$  value for two touching spheres, which is  $r_{sc} = 1.59$ . The inertia in eq. (23) has the property that it is equal to the old inertia at the spherical shape and equal to  $\frac{1}{4}M$  at the scission point, two limiting conditions we want to fulfill. In addition, it approaches the limiting value horizontally for  $m \geq 2$ . That is, the derivative at this point is continuous, which is also a reasonable requirement. By varying  $m$  we change how fast the inertia approaches its limiting value of  $\frac{1}{4}M$ . The level structure indicates that the inertia is close to this value far inside the point of touching.

Also at the ground state one can expect the inertia to be lower for shape changes that evolve towards the new valley, compared to shape changes that lead to the old valley. This can occur because the inertia is not related to the values of the shape coordinates themselves but instead to their derivatives, or more precisely, to the direction of change of the shape coordinates. Quantitative support for this can be found in the level diagrams in figs. 15a and 15b. Often the distance between levels at level crossings is larger in fig. 15b than in fig. 15a. As a specific example we compare the level crossing of the proton states  $\left\{ 642 \frac{1}{2} \right\}$  originating

from the  $i_{\frac{1}{2}}^{11}$  spherical state at  $-0.8$  MeV and  $[402\frac{3}{2}]$  originating from the spherical state  $d_{\frac{3}{2}}^3$  at  $-11.0$  MeV. In fig. 15a, which corresponds to a path leading into the old valley, the crossing occurs at  $r \approx 1.0$  and at an energy of about  $-6.0$  MeV, with a splitting at the crossing of about  $0.3$  MeV. In fig. 15b, which corresponds to a path that leads to the new valley, this crossing occurs at about the same location but the splitting at the level crossing is now  $1.5$  MeV. Thus, the contribution to the inertia from this level crossing should be considerably smaller in the latter case than in the former. The situation is similar at many other level crossings.

We have calculated the fission half-life for  $^{258}\text{Fm}$  along the new valley with the inertia given by eqs. (23) and (24) and  $m = 2$ , the simplest choice. The calculated fission half-life under these assumptions is  $9\text{s}$ , or about 4 orders of magnitude larger than the experimental value. It is still nevertheless fairly close to the experimentally observed value of  $10^{-11}$  y. One should also note that in the macroscopic-microscopic model it is often difficult to reproduce over a small range of neutron numbers the entire magnitude of an effect that experimentally occurs over a range of 2 neutron numbers. In the theoretical model these changes often develop over a slightly larger range of neutron number. Thus, it is not surprising that in this particular case we do not reach the ms range of half-lives until  $^{260}\text{Fm}$ , as is seen in table 1. We also observe in table 1 that the calculations in the old valley completely fail to reproduce the experimental half-lives for the heavier Fm isotopes. Based on the above discussion and on the results obtained below we choose  $m = 2$  for the inertia in the new valley. The semi-empirical inertias for the old and new valleys are plotted in fig. 16.

Our discussion above leads to a new proposal for the mechanism behind the short half-life for  $^{258}\text{Fm}$ . The mechanism is *not*, as previously proposed, the disappearance of the second peak in the barrier below the energy of the nuclear ground state. Instead, it is the lower inertia associated with the new path to compact scission shapes. Thus, we find that it is not an accident that there is a sudden drop in fission half-life at the same time as highly energetic asymmetric fission fragments appear, but instead that the two events are intimately connected.

The proposed inertia for the new valley is most appropriate for  $Z$  near 100 and  $N$  near 164. Below we see that in the potential-energy surfaces the new valley remains for  $Z$  and  $N$  values rather far from these values. For such nuclei we expect that the inertia is higher than the one proposed here. Since we have shown that a consistent explanation of fission-barrier heights and fission half-lives requires radically different inertias for different nuclei, it is clearly desirable to develop a model for the microscopic inertia in the different valleys. Such a project is a major undertaking and outside the scope of this investigation, and for the new valley we consistently use the simple prescription given by eqs. (23) and (24). We expect that this leads to some underestimate of the fission half lives of nuclei far from  $^{264}\text{Fm}$ .

We give calculated spontaneous fission half lives for nuclei ranging from Cf to  $Z = 109$  in table 1. For even nuclei some of the calculated half lives are plotted and compared to experimental data in figs. 17a-17e. Some half lives along the old path are much longer in this calculation than those obtained earlier<sup>34</sup>). This occurs because we have here also included the effect of  $\epsilon_0$  deformations on the ground-state energy. This additional degree of freedom lowers the ground state by up to about 1 MeV around  $^{252}\text{Fm}$ , which explains the 6 order of magnitude increase in half lives we obtain in this region relative to those in the previous study.

Figure 17a shows calculated and experimental fission half lives for Cf isotopes. Solid circles represent experimental data, open triangles calculated half lives for fission along the new path and open squares calculated half lives for fission along the old path. The dominating path is the path that for a particular  $N$  value gives the lowest calculated fission half life. The symbols corresponding to the dominating path are connected by a dashed line and represent the results

that are to be compared with experimental data. Fission half-lives for the new path cannot be calculated until this path is clearly present in the calculated potential-energy surfaces. This usually occurs at  $N = 156$  or  $N = 158$ . Usually we see in figs. 17a-17e that for low  $N$  values the half-life along the new path is longer than the experimental value. In most of these cases the saddle along the switchback path is lower than the outer saddle in the new valley and it is likely that if the half-life along the switchback path could be calculated the results would show that the switchback path is the dominating path and the calculations would probably be in better agreement with experimental fission half-lives.

There is a large discrepancy between calculated and experimental data in the vicinity of  $N = 152$ . When analyzing the deviations between data and calculations one must be aware of the sensitivity of the calculated results to changes in the various quantities that enter the fission half-life calculation. We find that an increase of the ground-state energy of  $^{250}\text{Cf}$  by 1 MeV decreases the calculated fission half-life from  $10^{12.47}$  y to  $10^{6.49}$  y. Since the error in the mass model used to calculate the nuclear ground-state energy is 0.8 MeV<sup>45</sup>), it is therefore not unreasonable to expect errors of this magnitude in calculated fission half-lives. However, in many calculations<sup>27,30,64</sup>) the average deviation between calculated results and experiment is, surprisingly, much smaller than the above observation would lead one to expect. Typically, the deviation is only about 2 orders of magnitude. This good agreement may have been fortuitous, in which case it is of course wrong to try to explain the large discrepancies we here obtain between calculated and experimental data for Cf as due to some other effect rather than to the known average model error for the nuclear ground-state energies.

One may, on the other hand, try to make a more detailed argument to investigate if one can expect the errors in the calculated fission half-lives to be smaller. The error in the mass model is somewhat larger in the region of light nuclei than in the actinide region, where in contrast the error is smaller than average and fairly slowly varying<sup>45</sup>). In addition, some of the error in the actinide region is removed by the  $\epsilon_6$  shape degree of freedom, which we consider here. Apart from errors in the calculated ground-state energy, other factors that we expect to give rise to errors in the calculated fission half-lives are our simple model for the nuclear inertia and the fact that we do not calculate fission half-lives along the switch-back path. We find that an overall decrease in the inertia by 5% decreases the calculated half-life of  $^{250}\text{Cf}$  from  $10^{12.47}$  y to  $10^{11.44}$  y. An explanation for the largest discrepancies between calculated and experimental fission half-lives may be that we do not calculate the penetrability along the switchback path. We will make some additional comments on the effect of the switchback path in the discussion of Fm below.

Figure 17b shows fission half-lives for fermium isotopes. For the heaviest Fm isotopes the half-lives calculated for the new valley are considerably lower than the half-lives for the old valley. For  $^{256}\text{Fm}$  the results seem to indicate that fission occurs into the new valley, contrary to what is suggested by experimental results on fission-fragment mass and kinetic-energy distributions<sup>13</sup>). However, an inspection of the calculated potential-energy surface for  $^{256}\text{Fm}$  in fig. 12a shows that there is a saddle between the new and old valley at  $r = 1.38$  and  $\sigma = 0.74$ . This is a saddle on the so called switchback path, which has been extensively discussed in our previous study<sup>34</sup>). It is clear from this figure that the half life for  $^{256}\text{Fm}$  along the switchback path may be shorter than the half life into the new valley. Also, for lighter Fm isotopes, fission may proceed initially along the new path to exploit the low inertia along this path and later switchback to the old valley. An inspection of fig. 7 for  $^{252}\text{Fm}$ , for example, indicates that it is a very realistic possibility for this nucleus. It is therefore our view that a consideration of half lives along the switchback path would remove some of the discrepancies between calculated and experimental fission half lives in the region close to  $N = 152$  for Fm.

Cf and possibly elements beyond Fm. However, if the sensitivity of fission half-life calculations to small changes in the barrier energies is considered, as discussed above for Cf, one must consider the agreement between calculated and experimental half-lives in fig. 17b, as it stands, to be commensurate with expectations.

Figure 17c shows fission half-lives for No. For  $N = 156$ , and slightly beyond, figs. 13a and 13b show that it is plausible that the switchback path is the dominating path. This may also be the case for lower  $N$  values and thus provides a mechanism for removing some of the discrepancy between calculated and experimental values. For  $N = 156$  and beyond, the experimental fission half-lives remain fairly constant. This tendency is present, but somewhat less pronounced, in the calculated results. Again, we expect this particular feature to be more clearly present in the calculations if the switchback path is taken into account. For Rf, shown in fig. 17d, the peak in the experimental fission half-lives that is present at  $N = 152$  for Fm and No has disappeared, but it is still present in the calculations. This peak is also present in the calculated results for element  $Z = 106$  shown in fig. 17e.

The properties of the calculated potential-energy surfaces for  $^{259}\text{Md}$  and  $^{260}\text{Md}$  and the calculated spontaneous fission half-lives shown in table 1 provide an explanation of the measured half-lives of these two nuclei. The fission half-life for  $^{260}\text{Md}$  is  $32 \text{ d}^{13}$ ). This is 10 orders of magnitude higher than the fission half-life of  $^{258}\text{Fm}$ , which has one proton and one neutron less than  $^{260}\text{Md}$ , even though in the absence of single-particle effects the addition of protons should lower the fission half-life. However, it is entirely reasonable to expect such a huge specialization effect from the addition of one odd neutron and one odd proton in this region, since our calculations show that the odd proton has the fairly high spin  $\frac{7}{2}$ , with negative parity.

It is now possible to interpret the experimental data obtained by  $^{13)}$  for  $^{259}\text{Md}$  and  $^{260}\text{Md}$  in terms of our model. We expect high-kinetic-energy fission to occur when the spherical fragment shell effects due to the approach of  $^{264}\text{Fm}$  have reached a certain magnitude. The symmetric fission products of  $^{258}\text{Fm}$  are  $^{129}\text{Sn}$ . A study of calculated ground-state shell corrections  $^{4)}$  shows that the effect on the shell correction of adding protons or subtracting neutrons from  $^{129}\text{Sn}$  is similar. The reason is that in both cases the distance from the doubly magic  $^{132}\text{Sn}$  is changed by the same number of nucleons, and in this region the neutron and proton shell corrections behave in a similar way when particles are added or subtracted. Thus, we expect that adding protons to  $^{258}\text{Fm}$  will have roughly the same effect on the kinetic-energy distributions as subtracting neutrons, apart from charge effects. The kinetic-energy distributions for  $^{257}\text{Fm}$  and  $^{260}\text{Md}$  should therefore be similar, which is the case. Adding another neutron to  $^{259}\text{Md}$  yields  $^{260}\text{Md}$ , which according to our above arguments should have a kinetic-energy distribution similar to that for  $^{258}\text{Fm}$ , which is also the case. The rapid change in the appearance of the kinetic energy distribution when going from  $^{259}\text{Md}$  to  $^{260}\text{Md}$  is not an odd-particle effect but is instead just a reflection of the rapidly changing fission properties as  $^{264}\text{Fm}$  is approached. Our calculated half-lives are in rough agreement with data, in particular if one assumes that fission for  $^{259}\text{No}$  occurs along the switchback path, exploiting the lower inertia in the lower valley. Mass asymmetric shape degrees of freedom which were only calculated for even systems would also be expected to lower the ridge on the switchback path considerably.

Our argument for interpreting the bimodal fission as fission along a new valley followed by a switchback into the old valley is based partly on the fact that the fission half-lives calculated along the old path for  $^{260}\text{No}$ ,  $^{258}\text{No}$  and  $^{258}\text{Fm}$  are 6, 6 and 11 orders of magnitude larger than the experimental half-lives, respectively. Since we feel it is a reasonable assumption that the error in the model is smaller than this magnitude, it follows that it is fission along the switchback path that leads to scission in the old valley in most cases where bimodal fission is

observed.

However, there is an additional argument for interpreting the switchback as the mechanism for bimodal fission that is independent of the accuracy of the theoretical fission half-life model. Experimentally, the fission half-lives change extremely rapidly from nucleus to nucleus in this region. For instance, from  $^{256}\text{Fm}$  to  $^{258}\text{Fm}$  the half-life changes by seven orders of magnitude. At a transition point one might expect the half-lives for fission through the two different barriers to be similar, as a general rule. However, when the change across the transition point is seven orders of magnitude it is unlikely that the two half-lives are equal to within two orders of magnitude. It might perhaps occur in one case but experimentally there are four cases of observed bimodality and it is extremely unlikely that the two barriers have approximately the same half-life in all four cases with such violent changes in half-lives across the transition points.

Table 1 shows additional half-lives. Again, the agreement between calculated and experimental half-lives is commensurate with expectations despite a few large deviations. We expect that fission half-lives on the rock of stability around  $^{272}110$  are strongly affected by the presence of the magic-fragment neutron number  $N = 2 \times 82$  and by the deformed magic ground-state neutron number  $N = 162$ . The magic-fragment neutron number  $N = 2 \times 82$  has a destabilizing effect, whereas the deformed magic ground-state number  $N = 162$  has a stabilizing effect. In our model these two effects approximately cancel each other, as can be seen from the half-lives calculated for the new valley for  $Z = 106$ . The calculated half-lives vary by only one order of magnitude from  $N = 156$  to  $N = 164$ . For  $Z = 108$  there is an increase by three orders of magnitude in the calculated fission half-life from  $N = 156$  to  $N = 162$ . Most earlier calculations that consider only the old valley overestimate the fission half-lives of elements on the rock of stability.

#### 4.5 KINETIC ENERGIES

Experimentally <sup>13)</sup> it is observed that for  $^{258}\text{Fm}$  the low-energy and high-energy peaks in the kinetic-energy distributions are centered at 200 and 235 MeV, respectively. These experimental observations can be understood qualitatively in terms of our calculated potential-energy surface for  $^{258}\text{Fm}$ . The final fission-fragment kinetic energy is approximately equal to the precession contribution plus the Coulomb energy of two spheres separated by a distance  $r_{sc}$ . Because the value of  $r_{sc}$  is smaller in the new, lower fission valley than in the old, upper fission valley, the kinetic energy will be correspondingly higher in the new valley than in the old valley. However, a precise calculation of the fission fragment kinetic energy requires a consideration of dynamical effects, which is outside the scope of the present investigation.

#### 4.6 ADDITIONAL IMPLICATIONS OF THE NEW VALLEY

##### 4.6.1 Effect of magic numbers on heavy-ion fusion

The potential-energy surfaces for those nuclei where the fragment shell effects lead to a new valley illustrate the anticipated beneficial influence of magic target-projectile combinations on fusion and evaporation residue cross sections in heavy ion reactions.

First, the magicity of the fragments lowers the energy of the two touching sphere configuration relative to what it would be in the absence of shell effects. It follows that in cases where a compound nucleus is formed by a dynamical descent from the two touching sphere configuration, the compound nucleus will be formed with less excitation energy than if fragment shell



effects were absent. The resulting relatively cold compound nucleus has then a better chance of surviving, without fissioning, the subsequent stage of de-excitation by particle emission. The result is an enhancement of evaporation-residue cross sections.

The second, more subtle, effect has to do specifically with the appearance of a *valley* in the potential-energy surface and the effect this has on minimizing the need for an extra push to fuse heavy nuclei<sup>68,69</sup>). Roughly speaking, this extra push, or additional collision energy in excess of the energy of the two-touching-sphere configuration, is needed when, roughly speaking, the electric repulsion after contact exceeds the nuclear attraction between the two fusing nuclei. As will be argued presently, this attraction is considerably greater for nuclei that manage to preserve approximately their spherical shapes than for nuclei that allow a neck to form between them. As a result, magic nuclei that resist as far as possible the growth of a neck, beyond the minimum defined by the geometry of overlapping spheres, experience a stronger compactifying force and can evolve towards fusion in the face of a stronger electric repulsion than if shell effects were absent.

The semi-quantitative argument for this mechanism is as follows. According to the proximity force theorem<sup>70</sup>) the force between two nuclei in the form of portions of slightly intersecting spheres is approximately  $4\pi\bar{R}\gamma$ , where  $\gamma$  is the specific surface energy and  $\bar{R}$  is the reduced radius of the two spheres, equal to  $R_1R_2/(R_1 + R_2)$ . On the other hand, the attraction that is provided by a cylindrical neck of radius  $r$  is only  $2\pi r\gamma$ , the rate of increase of the cylinder's surface energy with the cylinder's length. Now the condition that the stronger attraction  $4\pi\bar{R}\gamma$  should persist is that the configuration of the fusing system should stay as close as possible to that of portions of intersecting spheres, corresponding to the lower boundary, to the left of  $r = 1.5874$ , of the contour maps in this paper. This means that there should be a force resisting the growth of the neck. In other words, there should be a valley running close to that boundary. So long as such a valley is present, the attractive nuclear force will remain relatively large and the need for an extra push in fusion will be minimized or avoided entirely. The new valley in a potential-energy surface such as in fig. 3d demonstrates that fragment shell effects such as those in  $^{132}\text{Sn}$  can survive in configurations with even a fairly large window between the two halves, thus providing a mechanism for mitigating the extra-push hindrance in reactions between near magic nuclei. We believe it is quite likely that this mechanism is responsible for the anomalously low hindrance factors in fusion reactions such as  $^{48}\text{Ca} + ^{208}\text{Pb}$ <sup>54,71,72</sup>).

#### 4.0.2 The new valley and nuclear molecules

So long as fragment shell effects can be counted on to confine the nuclear configuration to the vicinity of portions of overlapping spheres, the possibility arises of a straightforward balancing of the forces acting in the separation degree of freedom in such a way that a nuclear molecule would result. Roughly speaking, this requires that the electric repulsion should balance the nuclear force, resulting in a potential energy with a meta stable minimum. That such a minimum can, in fact, be formed under suitable conditions is illustrated in fig. 4 for  $^{258}\text{Fm}$ . Here the solid circle at  $r = 1.30$ ,  $\sigma = 0.70$  can reasonably be described as corresponding to a molecular configuration of two  $^{129}\text{Sn}$  nuclei in fairly intimate contact, stabilized against neck growth by the fragment shell effects and against fusion or reseparation by a balance between nuclear and electric forces.

In cases where angular momentum is present, a similar situation may result if the charge on the system is reduced, so that the sum of electric and centrifugal forces continues to balance the nuclear forces. Molecules consisting of more than two magic or near magic nuclei might also prove meta stable when their sizes and the amount of angular momentum are similarly

adjusted.

## 5 Summary

Our most important results are

- Shape dependences have to be considered for the Wigner and  $A^0$  terms.
- An appropriate, fairly large smoothing range has to be used in the Strutinsky shell-correction method.
- For elements close to  $^{264}\text{Fm}$  a deep valley leading to compact scission shapes is a very prominent feature in the calculated potential-energy surfaces.
- From a study of single-particle level diagrams and a calculation of fission barriers and fission half-lives we conclude that there is a much lower inertia associated with fission in the new valley than in the old valley.
- There are three paths in the calculated potential-energy surfaces, namely the old path, the new path to compact scission shapes and a switchback path from the new path to the old path.
- Fission may initially proceed along the new valley and *switchback* to the old valley at a later stage during the process.
- The short half-life of  $^{258}\text{Fm}$  is due to the low inertia in the new valley and *not* to the disappearance of the second peak in the fission barrier.
- The new valley is present at least up to  $Z = 110$  for neutron numbers close to  $N = 2 \times 82$ . Its existence lowers the fission half-lives of some of these elements relative to predictions that do not consider the new valley.
- Odd-particle specialization effects substantially increase the calculated fission half-lives also in the new valley.
- Fission half-lives have been calculated for more than 60 nuclei. Because of the extreme sensitivity of the calculated fission half-lives to small changes in the ground-state potential energy, calculated and experimental half-lives agree with each other to within our expectations. Some remaining deviations suggest that fission along the switchback path has to be considered and also that a microscopic model for how the inertia changes as one moves away from magic-fragment neutron and proton numbers should be developed.

We would like to acknowledge valuable discussions with R. Bengtsson, D. C. Hoffman, E. K. Hulet, W. D. Myers and P. Somerville. Peter Möller would like to thank the Los Alamos National Laboratory, the Lawrence Livermore National Laboratory and the Lawrence Berkeley Laboratory for their hospitality and support during the course of this investigation.

## References

- 1) V. M. Strutinsky, Nucl. Phys. **A06** (1967) 420.

- 2) V. M. Strutinsky, Nucl. Phys. A122 (1968) 1.
- 3) S. Bjørnholm and J. E. Lynn, Rev. Mod. Phys. 52 (1980) 725.
- 4) P. Möller and J. R. Nix, Atomic Data Nucl. Data Tables 26 (1981) 165.
- 5) J. P. Balagna, G. P. Ford, D. C. Hoffman, and J. D. Knight, Phys. Rev. Lett. 26 (1971) 145.
- 6) Table of Isotopes, 7th edition, edited by C. M. Lederer and V. S. Shirley (Wiley, New York, 1978).
- 7) J. K. Tuli, Nuclear Wallet Cards, National Nuclear Data Center, Brookhaven National Laboratory (1985).
- 8) L. P. Somerville, M. J. Nurmi, J. M. Nitschke, A. Ghiorso, E. K. Hulet, and R. W. Lougheed, Phys. Rev. C31 (1985) 1801.
- 9) G. Münzenberg, S. Hofmann, H. Folger, F. P. Heßberger, J. Keller, K. Poppensieker, B. Quint, W. Reisdorf, K.-H. Schmidt, H. J. Schött, P. Armbruster, M. E. Leino, and R. Hingmann, Z. Phys. A322 (1985) 227.
- 10) G. Münzenberg, P. Armbruster, G. Derthes, H. Folger, F. P. Heßberger, S. Hofmann, K. Poppensieker, W. Reisdorf, B. Quint, K.-H. Schmidt, H. J. Schött, K. Sümmerer, I. Zychor, M. E. Leino, U. Gollerthan, and E. Hanelt, Z. Phys., A324 (1986) 489.
- 11) E. K. Hulet, R. W. Lougheed, J. H. Landrum, J. F. Wild, D. C. Hoffman, J. Weber, and J. B. Wilhelmy, Phys. Rev. C21 (1980) 966.
- 12) D. C. Hoffman, J. B. Wilhelmy, J. Weber, W. R. Daniels, E. K. Hulet, R. W. Lougheed, J. H. Landrum, J. F. Wild, and R. J. Dupzyk, Phys. Rev. C21 (1980) 972.
- 13) E. K. Hulet, J. F. Wild, R. J. Dougan, R. W. Lougheed, J. H. Landrum, A. D. Dougan, M. Schädel, R. L. Hahn, P. A. Baisden, C. M. Henderson, R. J. Dupzyk, K. Sümmerer, and G. R. Bethune, Phys. Rev. Lett. 56 (1986) 313.
- 14) U. Mosel and H. W. Schmitt, Phys. Rev. C4 (1971) 2185.
- 15) M. G. Mustafa, U. Mosel, and H. W. Schmitt, Phys. Rev. Lett. 28 (1972) 1535.
- 16) M. G. Mustafa, U. Mosel, and H. W. Schmitt, Phys. Rev. C7 (1973) 1519.
- 17) M. G. Mustafa, Phys. Rev. C11 (1975) 1059.
- 18) P. Möller and J. R. Nix, Proc. Third IAEA Symp. on the physics and chemistry of fission, Rochester, 1973, vol. I (IAEA, Vienna, 1974) p. 103.
- 19) J. Blocki and W. J. Swiatecki, Lawrence Berkeley Laboratory Report LBL 12811 (1982).
- 20) A. Müller, S. Großmann, and U. Brosa, Scientific Report 1985, Gesellschaft für Schwerionenforschung Report GSI 86 1 (1986) p. 153.
- 21) U. Brosa, S. Großmann, and A. Müller, Z. Phys. A325 (1986) 241.

- 22) S. G. Nilsson, J. R. Nix, A. Sobiczewski, Z. Szymański, S. Wycech, C. Gustafson, and P. Möller, Nucl. Phys. **A115** (1968) 545.
- 23) S. G. Nilsson, C. F. Tsang, A. Sobiczewski, Z. Szymański, S. Wycech, C. Gustafson, I.-L. Lamm, P. Möller, and B. Nilsson, Nucl. Phys. **A131** (1969) 1.
- 24) P. Möller, Nucl. Phys. **A192** (1972) 529.
- 25) J. Randrup, C. F. Tsang, P. Möller, S. G. Nilsson, and S. E. Larsson, Nucl. Phys. **A217** (1973) 221.
- 26) P. Möller and J. R. Nix, Nucl. Phys. **A229** (1974) 269.
- 27) J. Randrup, S. E. Larsson, P. Möller, S. G. Nilsson, K. Pomorski, and A. Sobiczewski, Phys. Rev. **C13** (1976) 229.
- 28) W. M. Howard and P. Möller, Atomic Data and Nuclear Data Tables **25** (1980) 219.
- 29) Yu. Ts. Oganessian, Lect. Notes Phys. **33** (1974) 221.
- 30) A. Baran, K. Pomorski, A. Lukasiak, and A. Sobiczewski, Nucl. Phys. **A361** (1981) 83.
- 31) B. D. Wilkins, E. P. Steinberg, and R. R. Chasman, Phys. Rev. **C14** (1976) 1832.
- 32) A. Sobiczewski, Proc. 22nd School on nuclear physics, Zakopane, 1987, to be published.
- 33) S. Ćwiok, P. Rozmej, and A. Sobiczewski, Proc. 5th Int. Conf. on nuclei far from stability, 1987, Rosseau Lake, Ontario, Canada, AIP Conf. Proc. **164** (AIP, New York, 1988) p. 821.
- 34) P. Möller, J. R. Nix, and W. J. Swiatecki, Nucl. Phys. **A409** (1987) 1.
- 35) P. Möller, J. R. Nix, and W. J. Swiatecki, Proc. Int. School-Seminar on heavy ion physics, Dubna, USSR, 1986, JINR Report JINR-D7-87-68 (1987) p. 167.
- 36) J. R. Nix, Nucl. Phys. **A130** (1970) 241.
- 37) P. Möller, S. G. Nilsson, and J. R. Nix, Nucl. Phys. **A220** (1974) 292.
- 38) P. Möller and J. R. Nix, Nucl. Phys. **A272** (1976) 502.
- 39) S. G. Nilsson, Kgl. Danske Videnskab. Selskab. Mat.-Fys. Medd. **20**:No. 16 (1955).
- 40) B. S. Nilsson, Nucl. Phys. **A129** (1969) 445.
- 41) P. Möller, S. G. Nilsson, A. Sobiczewski, Z. Szymański, and S. Wycech, Phys. Lett. **30B** (1969) 223.
- 42) P. Möller and S. G. Nilsson, Phys. Lett. **31B** (1970) 283.
- 43) S. E. Larsson, S. G. Nilsson, and I. Ragnarsson, Phys. Lett. **38B** (1972) 269.
- 44) M. Holsterli, E. O. Fiset, J. R. Nix, and J. L. Norton, Phys. Rev. **C6** (1972) 1050.
- 45) P. Möller and J. R. Nix, Nucl. Phys. **A301** (1981) 117.

- 46) R. Bengtsson, P. Möller, J. R. Nix, and Jing-ye Zhang, *Phys. Scr.* **29** (1984) 402.
- 47) P. Möller, J. R. Nix, and W. J. Swiatecki, *Proc. Winter Workshop on nuclear dynamics V, Sun Valley, Idaho, (1988)*.
- 48) W. D. Myers, *Droplet model of atomic nuclei (IFI/Plenum, New York, 1977)*.
- 49) P. Möller and J. R. Nix, *Nucl. Phys. A* **281** (1977) 354.
- 50) J. O. Newton, *Prog. Nucl. Phys.* **4** (1955) 234.
- 51) J. A. Wheeler, *Nuclear fission and nuclear stability, in Niels Bohr and the development of physics: Essays dedicated to Niels Bohr on the occasion of his seventieth birthday (Pergamon, London, 1955) p. 163*.
- 52) P. Möller and J. R. Nix, *LANL Preprint LA-UR-86-3983 (1986)*.
- 53) P. Möller and J. R. Nix, *Atomic Data and Nuclear Data Tables* **39** (1988) 213.
- 54) A. J. Sierk, *private communication (1986)*.
- 55) P. Möller, J. R. Nix, and W. J. Swiatecki, *Nucl. Phys. A* **492** (1989) 349.
- 56) G. Münzenberg, S. Hofmann, Y. K. Argarwal, F. P. Heßberger, K. Poppensieker, J. R. H. Schneider, W. F. W. Schneider, K.-H. Schmidt, H. J. Schött, P. Armbruster, C.-C. Sahm, and D. Vermeulen, *Z. Phys. A* **315** (1983) 145.
- 57) G. Münzenberg, P. Armbruster, H. Folger, F. P. Heßberger, S. Hofmann, J. Keller, K. Poppensieker, W. Reisdorf, K.-H. Schmidt, H. J. Schött, M. E. Leino, and R. Hingmann, *Z. Phys. A* **317** (1984) 235.
- 58) P. Armbruster, *Ann. Rev. Nucl. Part. Sci.* **35** (1985) 135.
- 59) S. Ćwiok, V. V. Pashkevich, J. Dudek, and W. Nazarewicz, *Nucl Phys. A* **410** (1983) 254.
- 60) P. Möller, G. A. Leander, and J. R. Nix, *Z. Phys. A* **323** (1986) 41.
- 61) K. Böning, Z. Patyk, A. Sobiczewski, and S. Ćwiok, *Z. Phys. A* **325** (1986) 479.
- 62) W. Ogle, S. Wahlborn, R. Piepenbring, and S. Fredriksson, *Rev. Mod. Phys.* **43** (1971) 424.
- 63) J. F. Berger, M. Girod, and D. Gogny, *Nucl. Phys. A* **428** (1984) 23c.
- 64) A. Baran, K. Pomorski, S. E. Larsson, P. Möller, S. G. Nilsson, J. Randrup, A. Lukaslak, and A. Sobiczewski, *Proc. 4th IAEA Symp. on physics and chemistry of fission, Jülich, 1979, vol. 1 (IAEA, Vienna, 1980) p. 143*.
- 65) E. O. Fiiset and J. R. Nix, *Nucl. Phys. A* **103** (1972) 647.
- 66) N. Fröman and P. O. Fröman, *JWKB Approximation (North Holland, Amsterdam, 1965) chap. 9, sect. 1, pp. 92-97*.
- 67) P. Möller and J. R. Nix, *Phys. Rev. Lett.* **37** (1976) 1461.

- 68) J. R. Nix and A. J. Sierk, *Phys. Rev. C* **15** (1977) 2072.
- 69) S. Bjørnholm and W. J. Swiatecki, *Nucl. Phys.* **A391** (1982) 471.
- 70) J. Blocki, J. Randrup, W. J. Swiatecki, and C. F. Tsang, *Ann. Phys. (N. Y.)* **105** (1977) 427.
- 71) F. P. Heßberger, S. Hofmann, W. Reisdorf, K.-H. Schmidt, H. J. Schött, P. Armbruster, R. Hingmann, B. Thuma, and D. Vermeulen, *Z. Phys.* **A321** (1985) 317.
- 72) J. P. Blocki, H. Feldmeier, and W. J. Swiatecki, *Nucl. Phys.*, to be published.
- 73) D. C. Hoffman and L. P. Somerville, *Charged particle emission from nuclei*, ed. D. N. Poenaru and M. S. Ivaşcu, Vol. III (CRC, Boca Raton, 1989) p. 1.
- 74) E. K. Hulet, private communication (1988).

Z	N	A	Calc. old path	Calc. new path	Exp.
98	146	244	12000 y		
98	148	246	$10^{6.72}$ y		2000 y
98	150	248	$10^{9.61}$ y		32000 y
98	152	250	$10^{11.67}$ y		17000 y
98	154	252	$10^{9.16}$ y		86 y
98	156	254	35000 y		61 d
98	158	256	24 y	4.2 d	12 m
98	160	258	630 y	1.7 d	
98	162	260	22000 y	19 s	
98	164	262	170 d	1.3 $\mu$ s	
100	142	242	6.0 $\mu$ s		0.8 ms
100	144	244	2.2 ms		3.7 ms
100	146	246	2.3 m		14 s
100	148	248	93 y		11 h
100	150	250	$10^{5.62}$ y		6.9 y
100	152	252	$10^{6.73}$ y		150 y
100	154	254	11000 y		0.62 y
100	155	255	$10^{7.59}$ y	2500 y	10000 y
100	156	256	13 y	49 d	2.86 h
100	157	257	$10^{5.98}$ y	320 y	131 y
100	158	258	130 d	8.7 s	0.38 ms
100	159	259	63 y	15 s	1.5 s
100	160	260	730 y	5.9 ms	
100	162	262	18 y	53 $\mu$ s	
100	164	264	37 d	5.7 $\mu$ s	
101	158	259	51000 y	28 d	100 m
101	159	260	$10^{6.70}$ y	1.1 y	32 d
102	146	248	130 $\mu$ s		
102	148	250	1.4 s		0.25 ms
102	150	252	3.2 d		8.6 s
102	152	254	21 y		6 h
102	154	256	31 d		18 m
102	156	258	13 h	5.9 s	1.2 ms
102	158	260	5.5 d	630 ms	100 ms

TABLE 1 (continued)

Z	N	A	Calc. old path	Calc. new path	Exp.
102	160	262	79 d	33 $\mu$ s	5 ms
102	162	264	3.6 y	13 $\mu$ s	
102	164	266	13 d	15 $\mu$ s	
103	158	261	23 y	5.0 h	39 m
103	159	262	4200 y	1.5 d	216 m
104	148	252	35 $\mu$ s		
104	150	254	430 ms		0.5 ms?
104	152	256	2.9 h		6.9 ms
104	154	258	18 s		14 ms
104	156	260	5.9 s	9.4 ms	21 ms??
104	158	262	15 m	10 ms	47 ms
104	160	264	4.2 h	17 $\mu$ s	
104	162	266	12 d	69 $\mu$ s	
104	164	268	11 h	22 $\mu$ s	
105	157	262	1.9 d	71 d	46 s
106	150	256	26 ms		
106	152	258	16 m		
106	154	260	3.0 m		7.2 ms
106	156	262	3.1 m	1.1 ms	
106	158	264	3.4 m	150 $\mu$ s	
106	160	266	52 m	100 $\mu$ s	
106	162	268	140 d	3.7 ms	
106	164	270	22 d	240 $\mu$ s	
107	161	268		11 m	
108	156	264	220 ms	10 $\mu$ s	$\geq 0.1$ ms
108	162	270	110 d	72 ms	
109	161	270	$10^{17.61}$ y	210 y	
109	162	271	$10^{16.40}$ y	150 d	
109	163	272	$10^{36.51}$ y	$10^{15.58}$ y	



- Fig. 6 Potential energy surface with  $\gamma = 1.4 \times \hbar\omega_0$  in the Strutinsky method, but without inclusion of the shape dependences of the Wigner and  $A^0$  terms. The ridge between the new and old valleys seems too high to allow any branching into the old valley, as indicated by experiment.
- Fig. 7 Potential-energy surface corresponding to symmetric shapes, showing a ridge blocking the new valley and two saddles at the beginning of the old valley. One saddle is located at  $r = 1.38$  and  $\sigma = 0.85$  and the other at  $r = 1.48$  and  $\sigma = 0.78$ . Our interpretation is that fission initially proceeds along the new valley but later along the switchback path across the lower saddle into the old valley. The switchback saddle is lowered by mass-asymmetric shape degrees of freedom.
- Fig. 8a Potential-energy surface for a nucleus far from nucleon numbers that favor the existence of the new fission valley. Only every fifth contour line is plotted for energies above +25 MeV. The mountain at the location of two touching spheres is more than 30 MeV high. Only the old fission valley is present in this contour map.
- Fig. 8b Also for this high proton number we find a fairly prominent new valley close to the doubly magic neutron number  $2 \times 82$ . The fission half-life is lowered relative to earlier expectations, because of the presence of the new valley. In this figure and some of our later figures, only every fifth contour line is plotted for energies below -25 MeV.
- Fig. 8c Potential-energy surface for a conventional superheavy nucleus. Surprisingly there is a second, lower valley present in this contour map, relatively far from doubly magic fragment nucleon numbers.
- Fig. 9a Effect of specialization energy on the structure of the calculated potential energy surface. The high- $\Omega$  value of the ground-state spin substantially increases the fission half-life compared to a value interpolated between neighboring even nuclei. There is a low ridge separating the new fission valley from the old fission valley. Experimental results<sup>13)</sup> show that most fission-fragment kinetic energies are low.
- Fig. 9b Ridge that is 4 MeV high separating the new fission valley from the old fission valley. Experimental results<sup>13)</sup> show that most fission-fragment kinetic energies are high, but that a second smaller component with low kinetic energies is also present.
- Fig. 10a Saddle region between the new and old fission valleys. The line  $\alpha = 0$  corresponds to the line  $r = 1.4$  in fig. 4. The new valley is to the lower left and the old valley to the upper right.
- Fig. 10b The potential energy in the  $\alpha - \alpha_2$  plane at  $r = 1.6$ . The saddle separating the two valleys is clearly lowered by mass asymmetric shape degrees of freedom. The minimum at the lower left corresponds to the outer saddle in the new valley seen in fig. 4. As discussed in the text, the energy at the saddle in this figure is about 0.75 MeV compared to 1.5 MeV in fig. 4. The difference is due to

interpolation inaccuracies in fig. 4, which are particularly large near the outer saddle because of the steep rise in the energy with decreasing  $\sigma$ .

- Fig. 11a Shapes corresponding to the contour map in fig. 11b. Shapes corresponding to the new valley are in the lower part of the figure and remain symmetric. As the switchback path from the new valley crosses over the saddle at  $r = 1.4$  and  $\sigma = 0.75$  into the old valley, asymmetry becomes more and more developed. As we discussed in the text, we have not conserved  $r$  and  $\sigma$  exactly as mass asymmetry develops. Nevertheless, it is clear from an inspection of this figure that as the asymmetry develops the overall extension remains approximately constant for fixed values of  $r$ . This is a desirable property for a more straightforward interpretation of the calculated potential-energy contour maps.
- Fig. 11b Contour map showing the vicinity of the outer saddle along the new valley and the saddle along the switchback path between the new valley and the old valley. The energy has been minimized with respect to the mass-asymmetry coordinate  $\alpha_2$  for fixed values of the other symmetric three-quadratic-surface shape parameters. As discussed in the text, this means that  $r$  and  $\sigma$  are not exactly conserved as  $\alpha_2$  varies. However, this does not influence the heights of the saddle points that are obtained from the calculation. The new valley enters in the extreme lower left of this figure and fission may either evolve into the old valley across the saddle at  $r = 1.4$  and  $\sigma = 0.75$  or proceed in the direction of compact scission shapes across the saddle at  $r = 1.6$  and  $\sigma = 0.74$ . These two saddles are of about equal height.
- Fig. 11c Outer part of the new valley in a calculation that does not include shape dependences for the Wigner and  $A^0$  terms. Here there is no outer saddle in the new valley. Access to the old valley is blocked by prominent ridge. As discussed in the text, these results contrast somewhat with those obtained by a Polish group<sup>34)</sup>, where there is no ridge between the old and new valleys at large values of  $r$ .
- Fig. 12a Nucleus close to the point of transition from fission into the old valley to fission into the new valley. Here a low ridge with a saddle that is about 1 MeV higher than the switchback saddle blocks access to compact scission shapes.
- Fig. 12b Well developed new valley. The switchback saddle is 2 MeV higher than the outer saddle along the path to compact scission shapes and should block access to the old fission valley.
- Fig. 13a Outer new valley region for  $^{258}\text{Cf}$ . The potential energy has been minimized with respect to mass asymmetric shape degrees of freedom at each grid point. The end of the new valley is blocked by a saddle that is about 2 MeV higher than the saddle on the switchback path and the fission path is deflected across the saddle on the switchback path into the old valley.
- Fig. 13b Potential energy surface for a neutron rich Cf isotope. At this high neutron number the saddle on the switchback path is about the same height as the outer saddle in the new valley. Thus, this nucleus may be at the transition between low kinetic energy and high kinetic energy fission.

- Fig. 14a For this nobelium isotope a low ridge sits at the end of the new valley. Experimentally<sup>13)</sup> it is found that this isotope primarily fissions into fragments with low kinetic energies.
- Fig. 14b At this neutron number,  $N = 160$ , the outer saddle in the new valley is about 2 MeV lower than the saddle on the switchback path, which suggests that fission of this isotope is mostly of the high-kinetic-energy type.
- Fig. 15a Proton single-particle levels corresponding to fission along the old valley. The spherical  $Z = 82$  gap is centered at  $-9.2$  MeV. No truly large-scale structure is seen. On a smaller scale there are gaps in the level spectra that for actinide nuclei give rise to deformed ground states and secondary minima.
- Fig. 15b Proton single-particle levels corresponding approximately to fission along the new valley. The  $Z = 2 \times 50$  gap is very prominent and is not completely damped out until slightly outside the *first* peak in the barrier. The structure suggests that the inertia is close to the reduced mass early during the barrier-penetration process. We also note the additional feature that already close to the ground state the inertia along the new path can be expected to be lower than along the old path, since the splittings at level crossings are often substantially larger here than along the old path.
- Fig. 16 Comparison between the semi-empirical inertia along the old path, the semi-empirical inertias along the new path for  $m = 2$  and  $m = 4$ , the irrotational inertia along the old path and the reduced mass  $\mu$ . The inertia along the new path for the parameter choice we select here ( $m = 2$ ) is represented by a solid line. This choice yields a somewhat higher inertia than  $m = 4$ , which was the choice made in our previous<sup>14)</sup> study.
- Fig. 17a Experimental fission half-lives compared to calculated half-lives for fission along the old and new valleys. A new valley is present in the calculated potential-energy surface only for  $N \geq 158$ . When half-lives have been calculated for both valleys for a particular neutron number, the shorter (dominating) calculated half-lives should be compared with experimental values. The discrepancy between calculated and experimental results in the vicinity of  $N = 152$  may arise from either an error in the calculated ground state energy or the neglect of fission along the third, switchback path, as discussed in the text.
- Fig. 17b Rapidly changing experimental and calculated fission half lives. The discrepancy around  $N = 152$  may be partially removed through the calculation of fission half-lives along the switchback path.
- Fig. 17c New experimental feature of fairly constant half life from  $N = 156$  and beyond. This feature is moderately well reproduced by the calculations.
- Fig. 17d Nearly constant experimental fission half life as a function of  $N$ . The theoretical half lives are too high near  $N = 152$ . However, the discrepancy corresponds only to an error of about 1 MeV in the calculated ground state energy.
- Fig. 17e Fairly constant calculated fission half life in the new valley beyond  $N = 156$ . This shows that the destabilizing effect of the spherical magic fragment neutron

number  $N = 2 \times 82$  approximately cancels the effect of the deformed magic-ground-state neutron number  $N = 162$ .

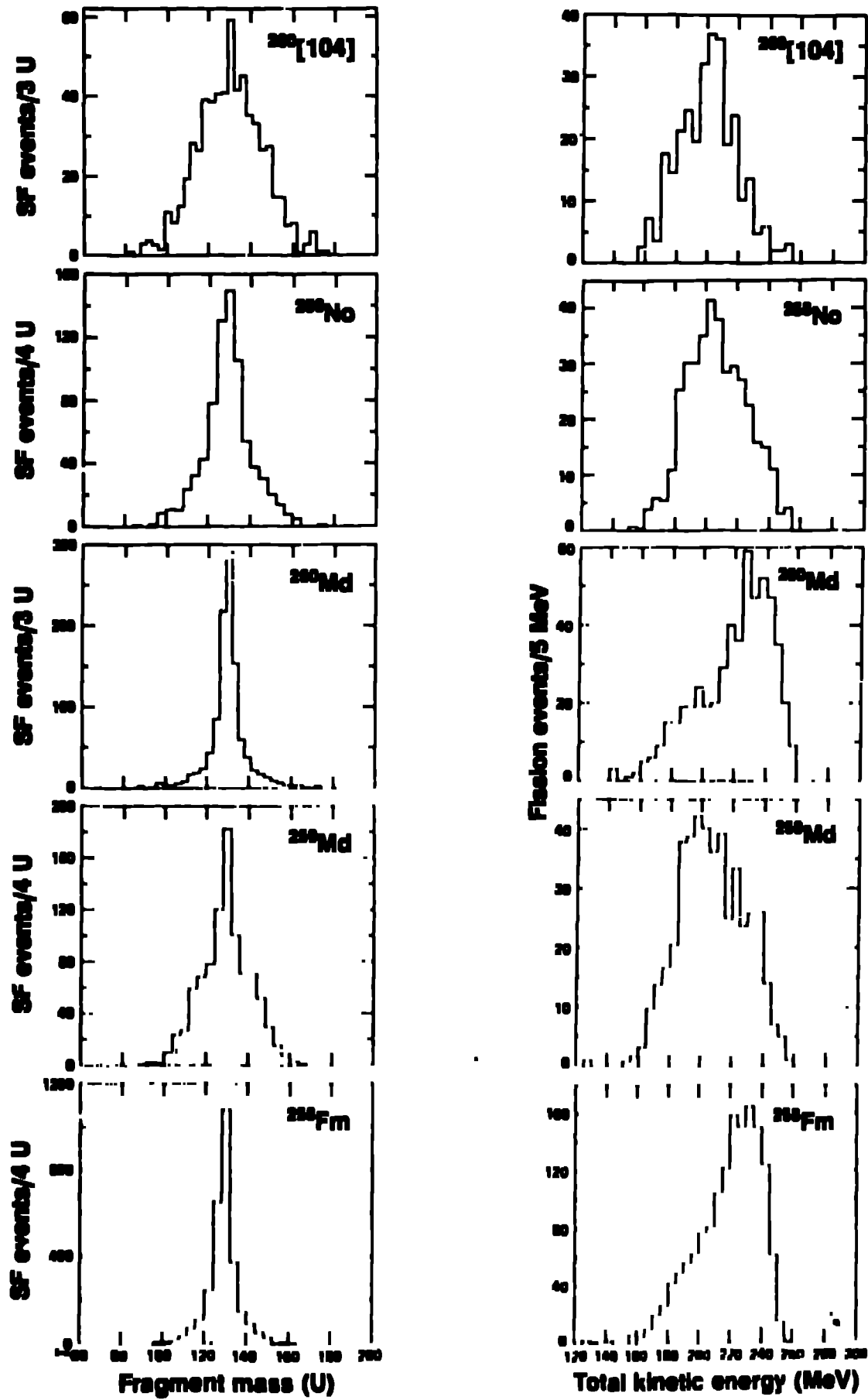


Figure 1

## Fragment shell effects

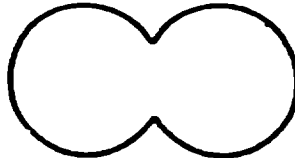
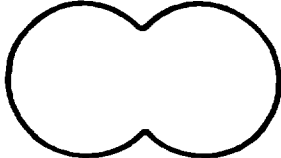
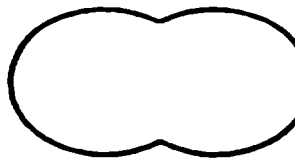
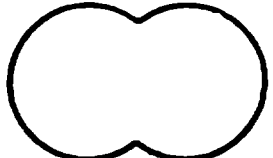
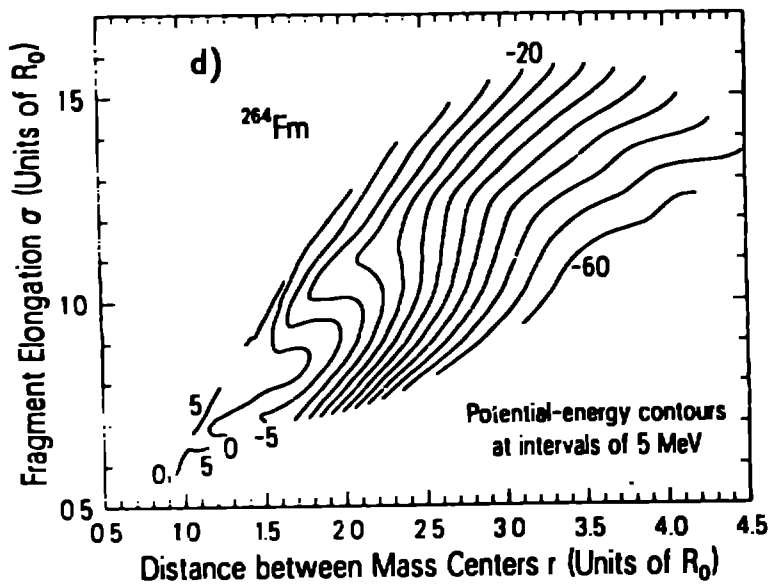
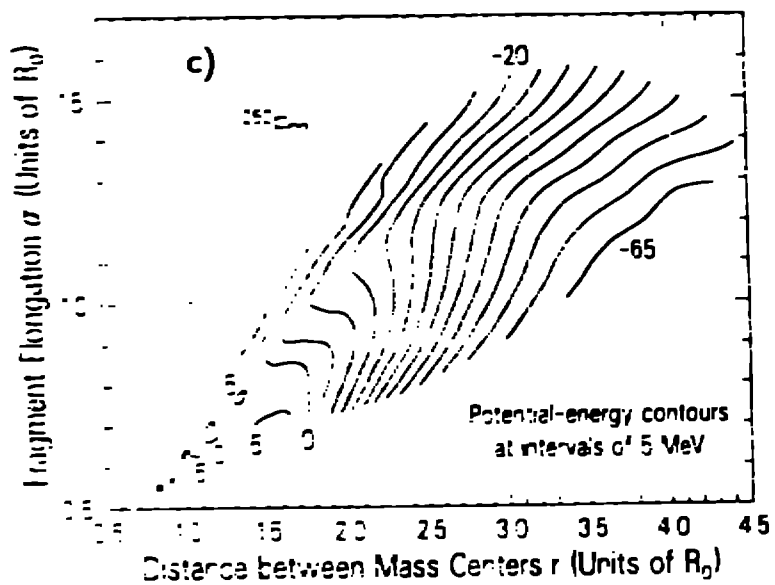
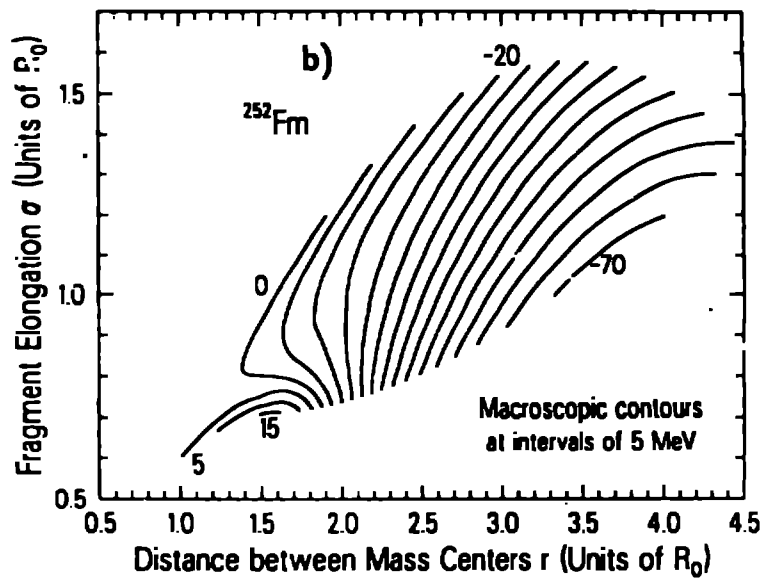
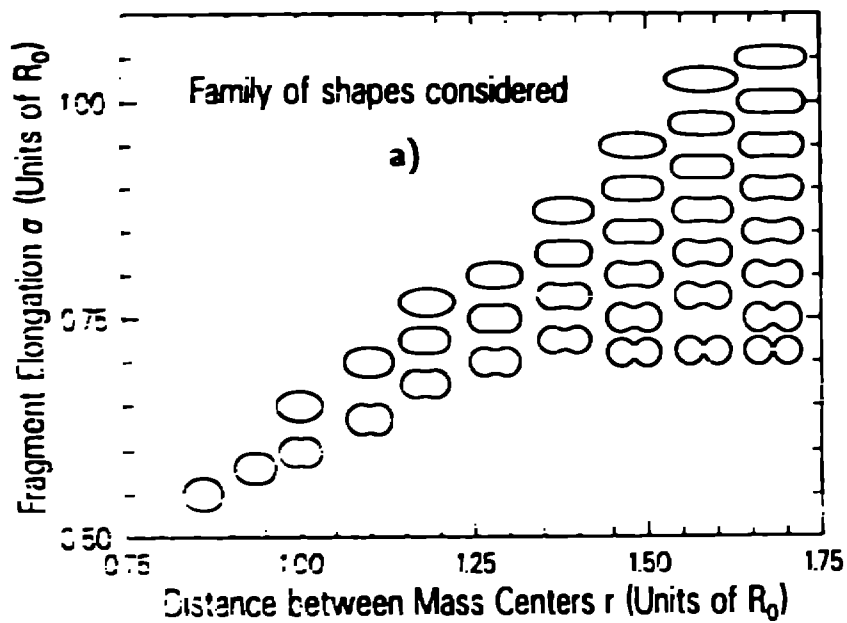
Energy (MeV)		Shape		
$^{254}\text{Fm}$	$^{264}\text{Fm}$	$r$	$\sigma_3$	
-10.47	-18.24	1.41	1.00	
-10.33	-11.80	1.27	1.00	
-3.69	0.35	1.31	0.60	
-6.60	-3.66	1.15	1.00	

Figure 2



**Figure 3**

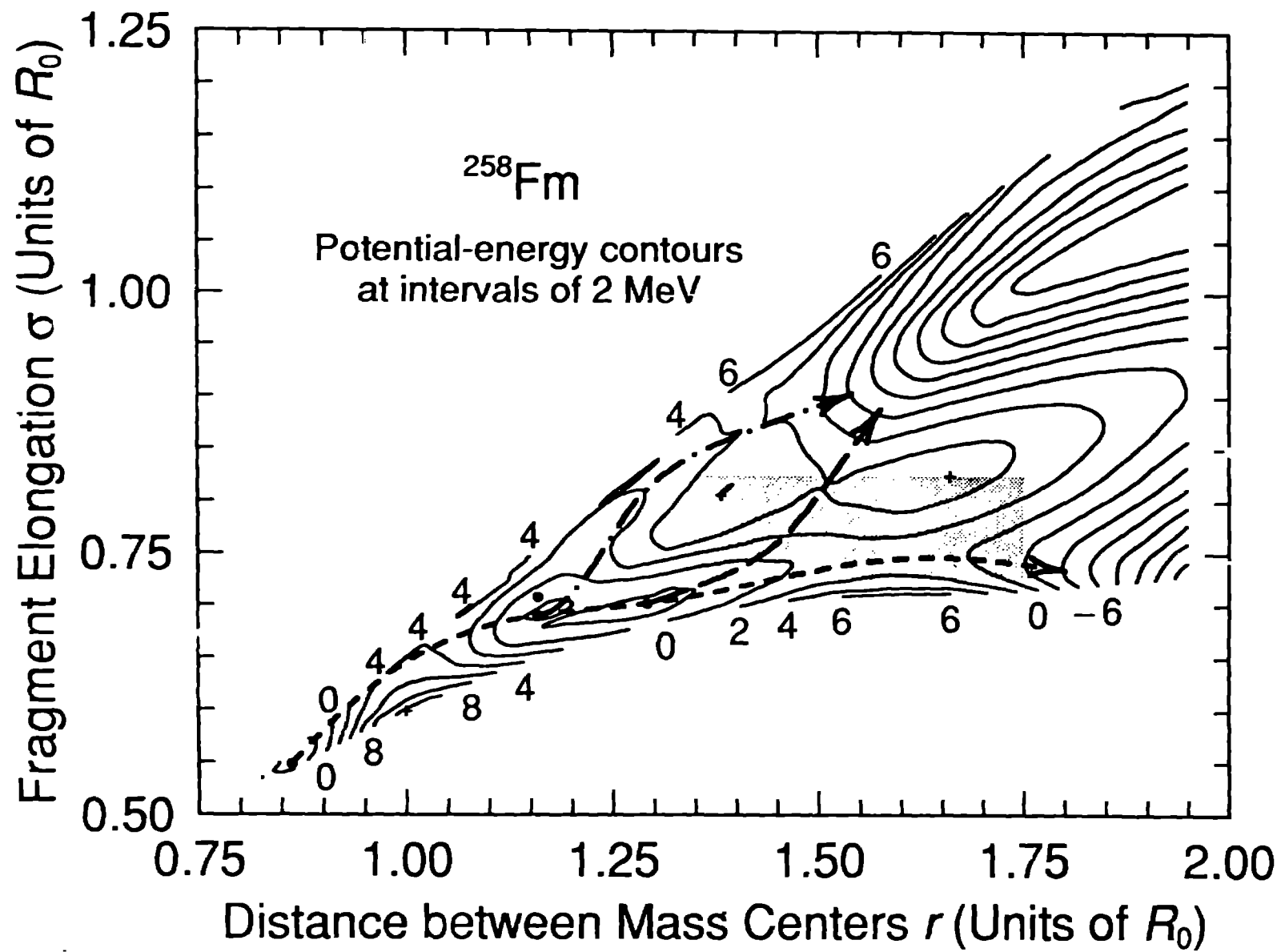


Figure 4



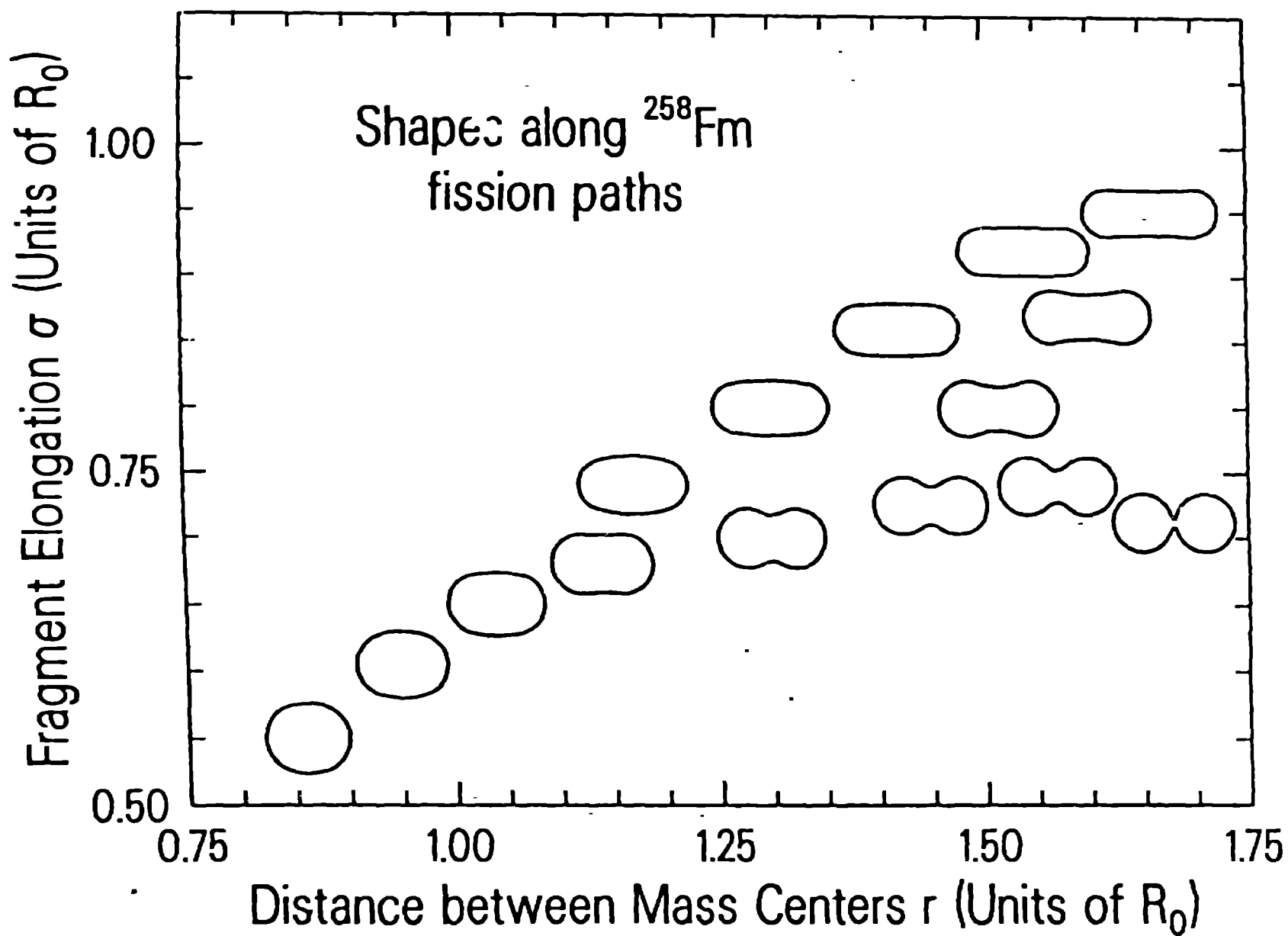


Figure 5

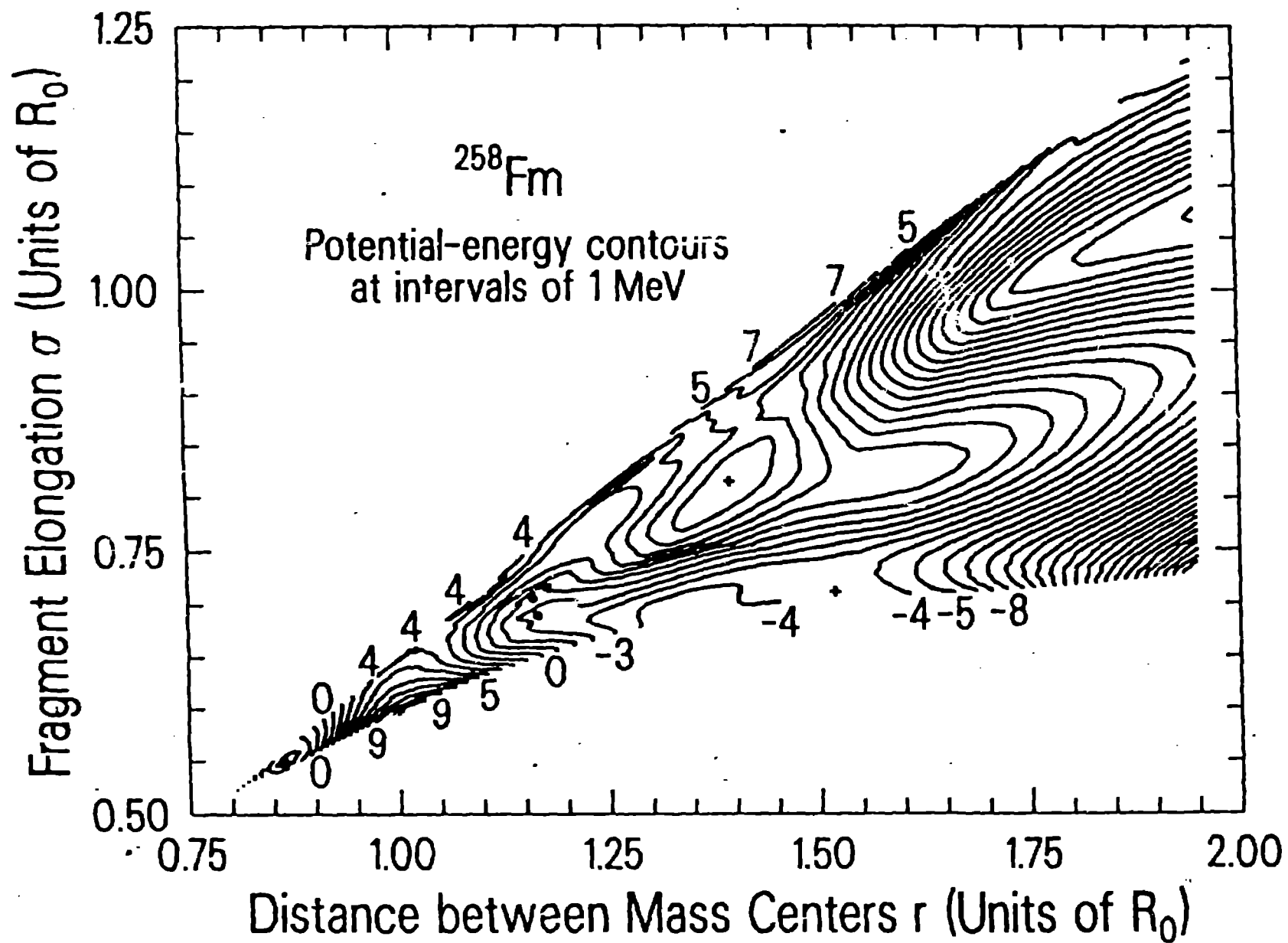


Figure 6

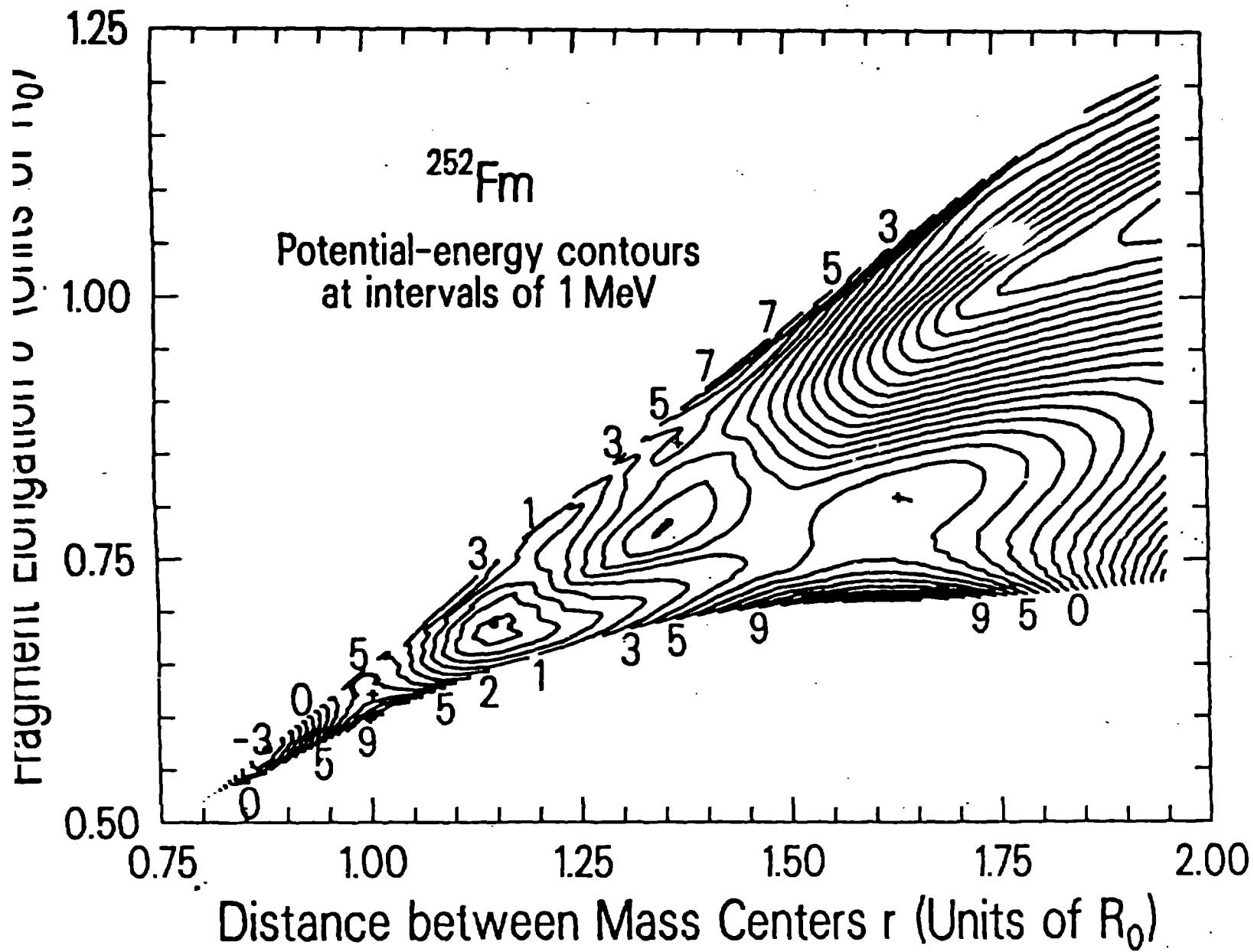


Figure 7

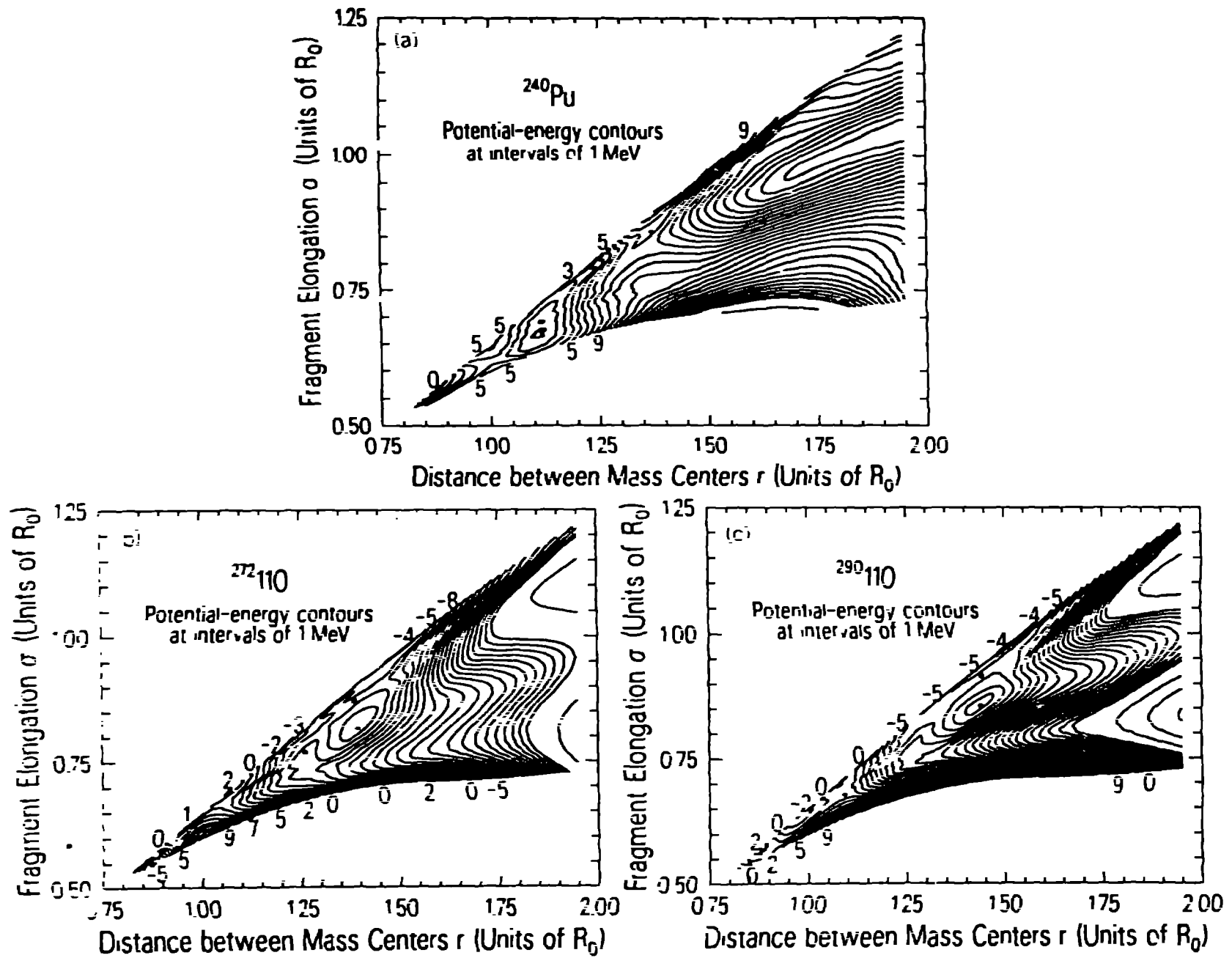


Figure 8

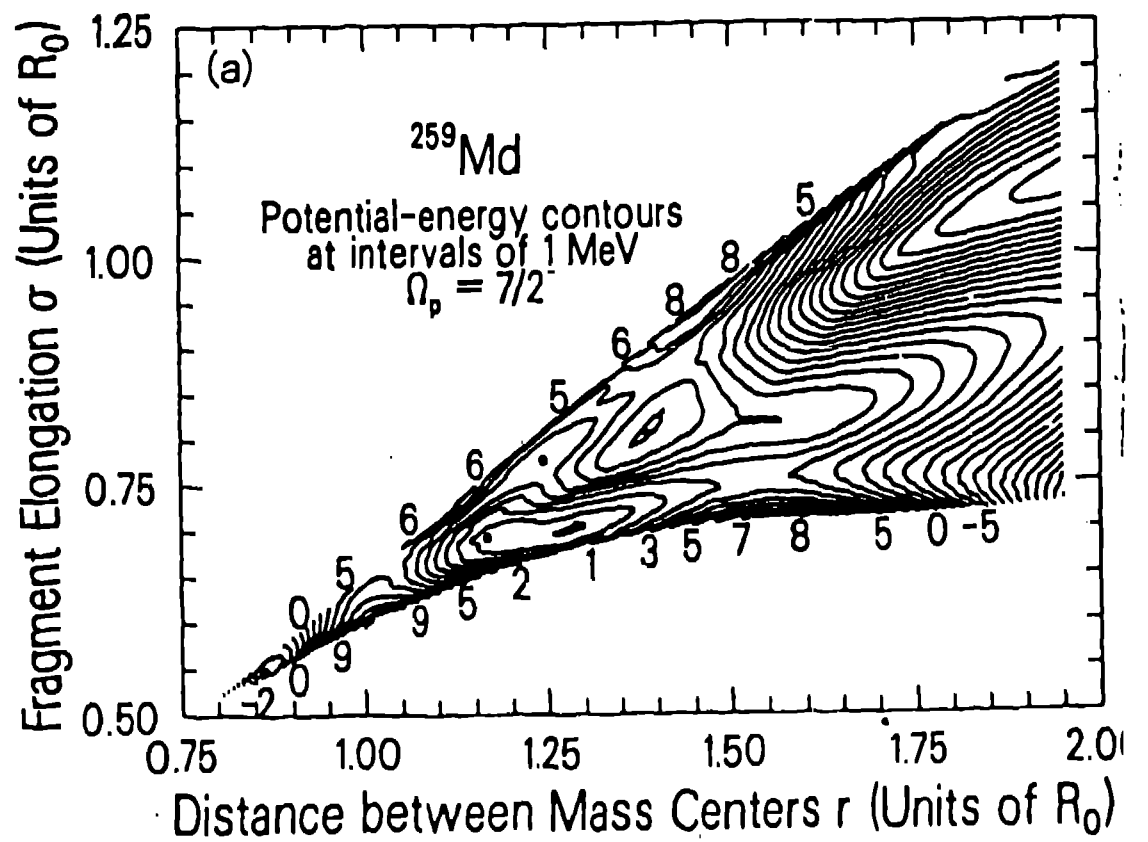
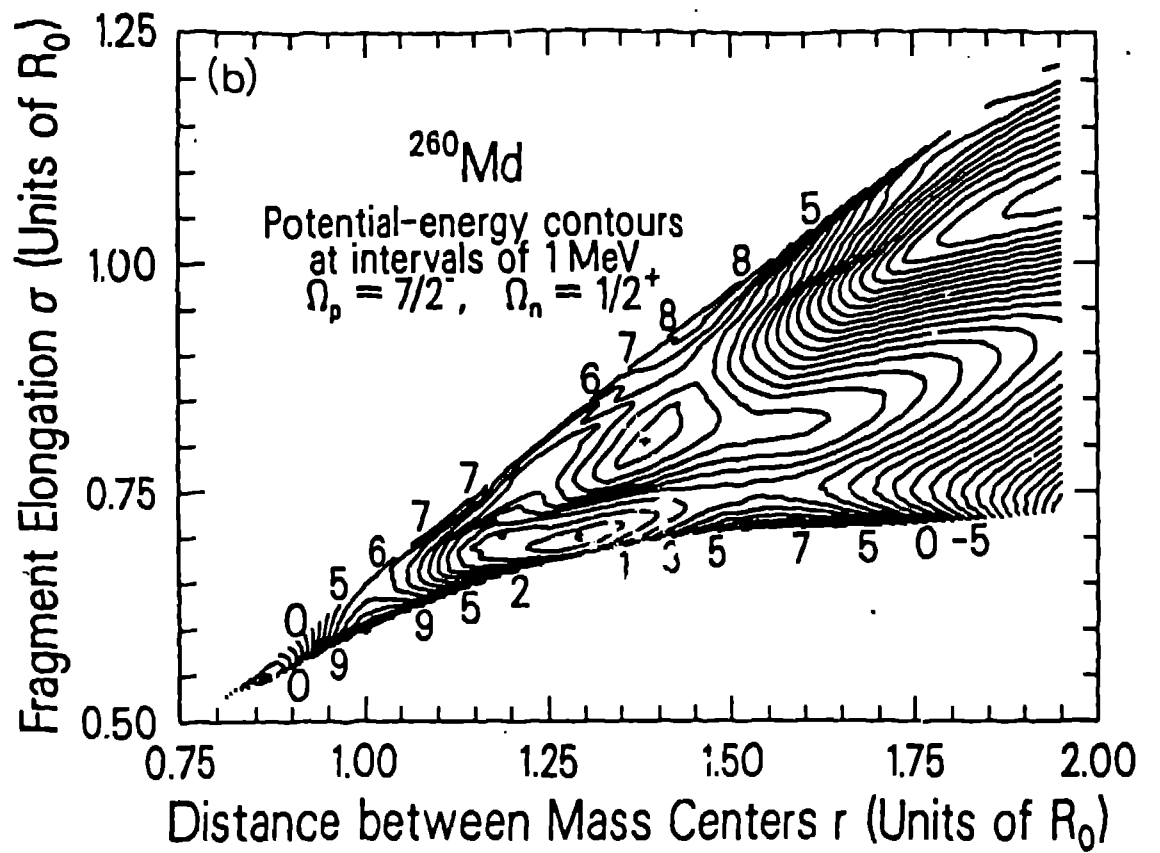


Figure 9

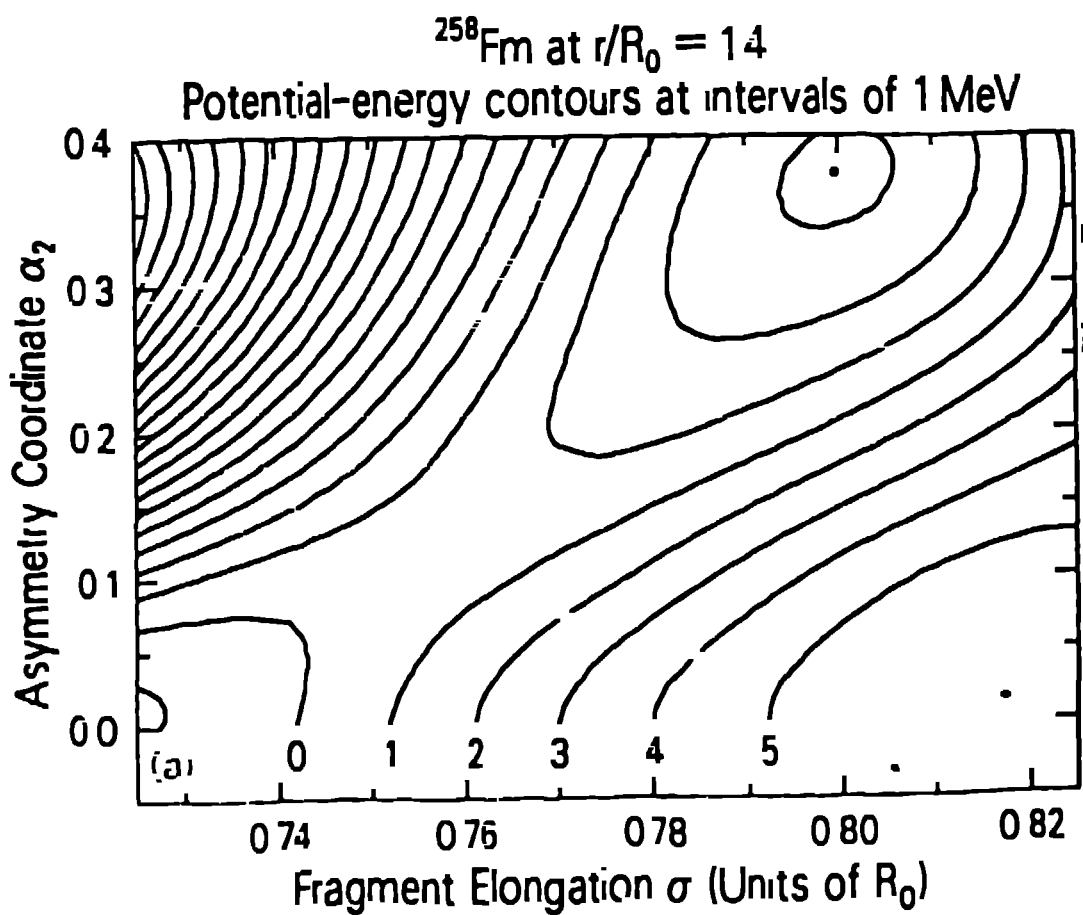
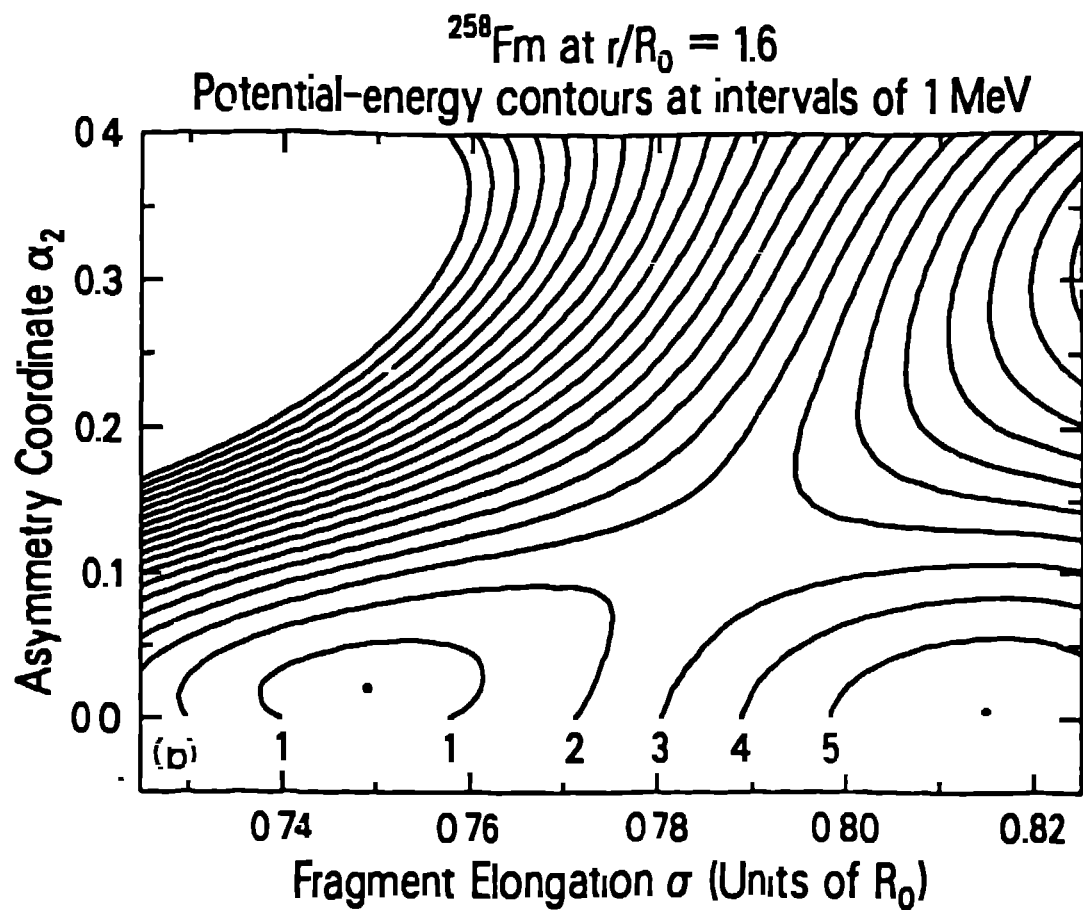


Figure 10

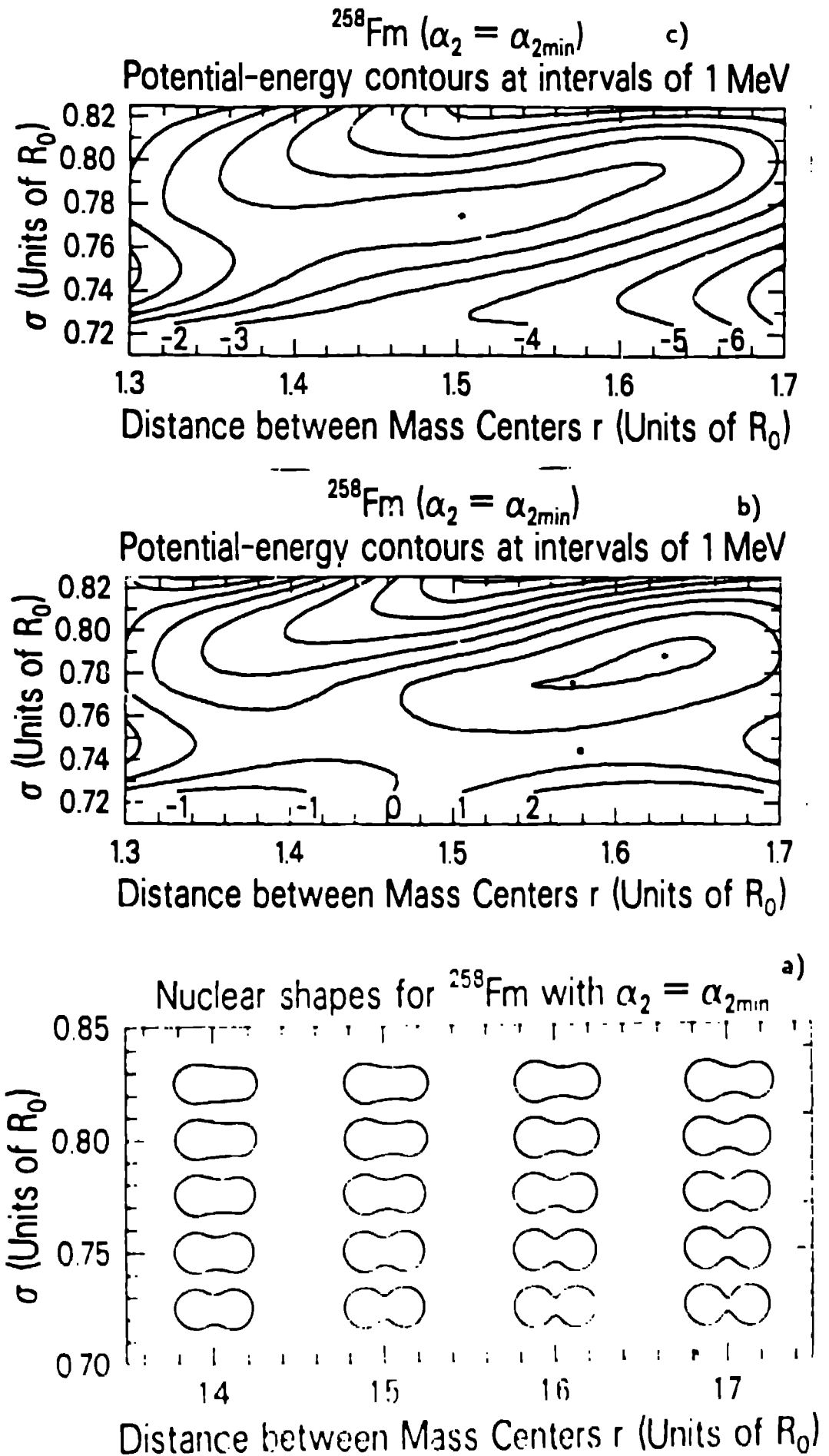


Figure 11

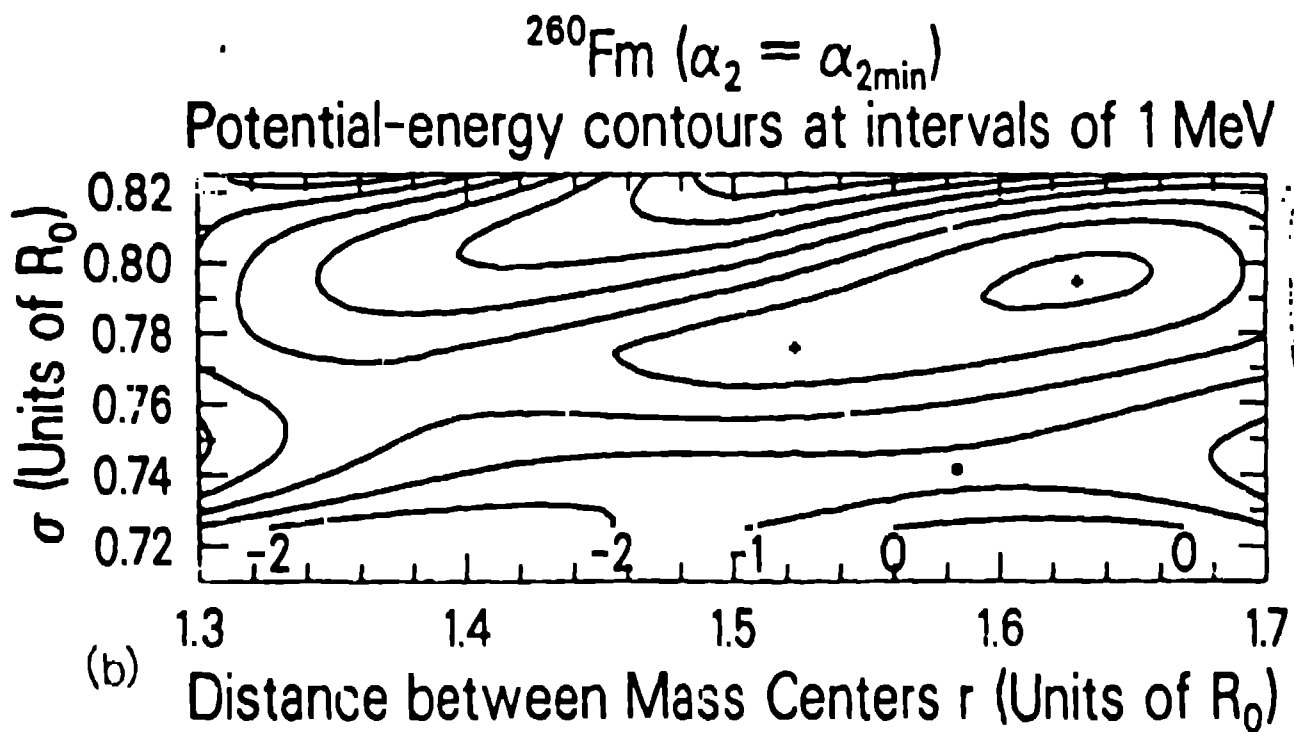
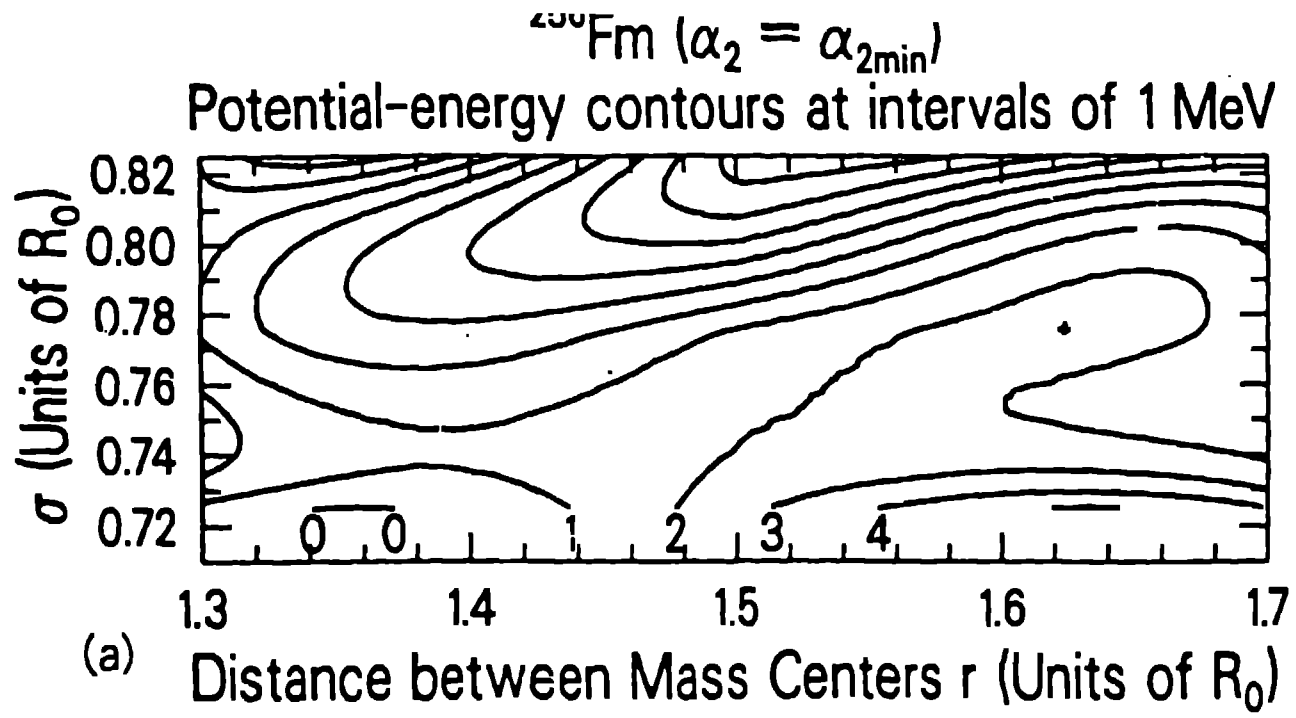
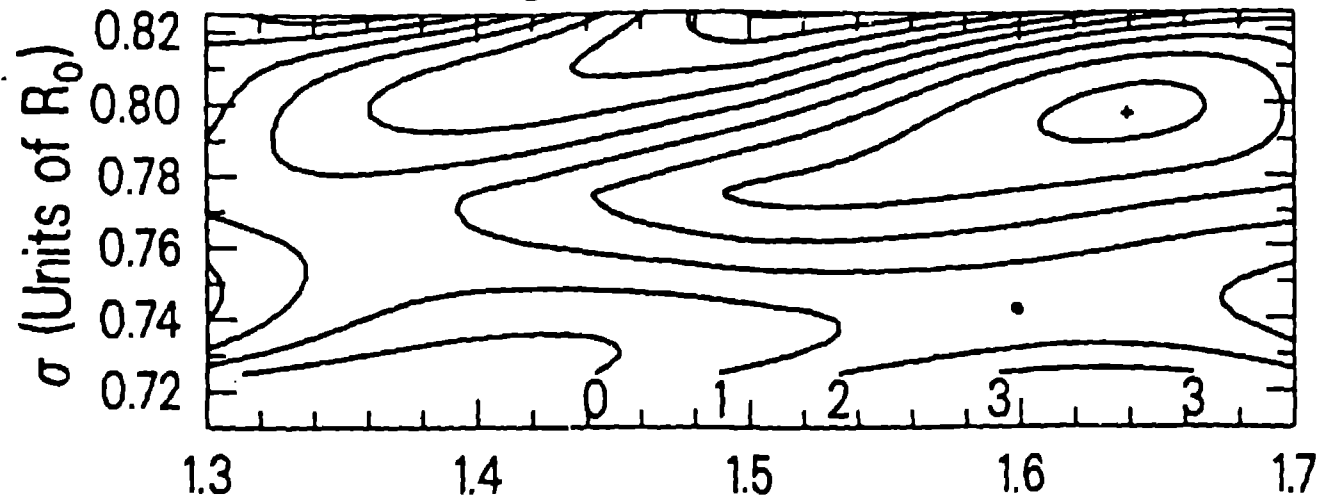


Figure 12



$^{260}\text{Cf} (\alpha_2 = \alpha_{2\text{min}})$

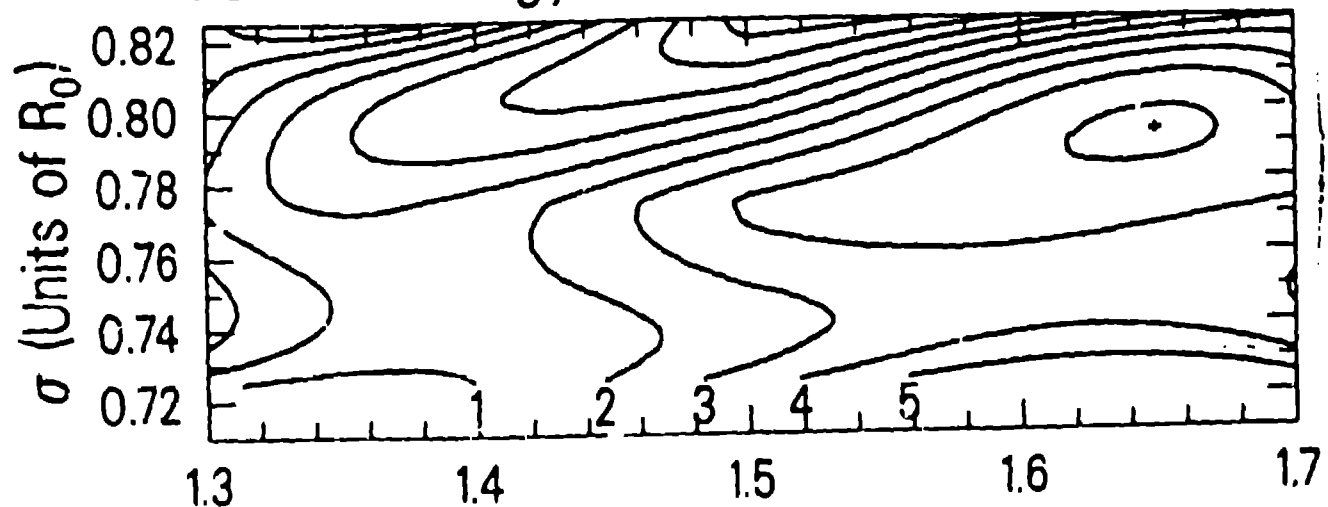
Potential-energy contours at intervals of 1 MeV



(b) Distance between Mass Centers  $r$  (Units of  $R_0$ )

$^{258}\text{Cf} (\alpha_2 = \alpha_{2\text{min}})$

Potential-energy contours at intervals of 1 MeV



(a) Distance between Mass Centers  $r$  (Units of  $R_0$ )

Figure 13

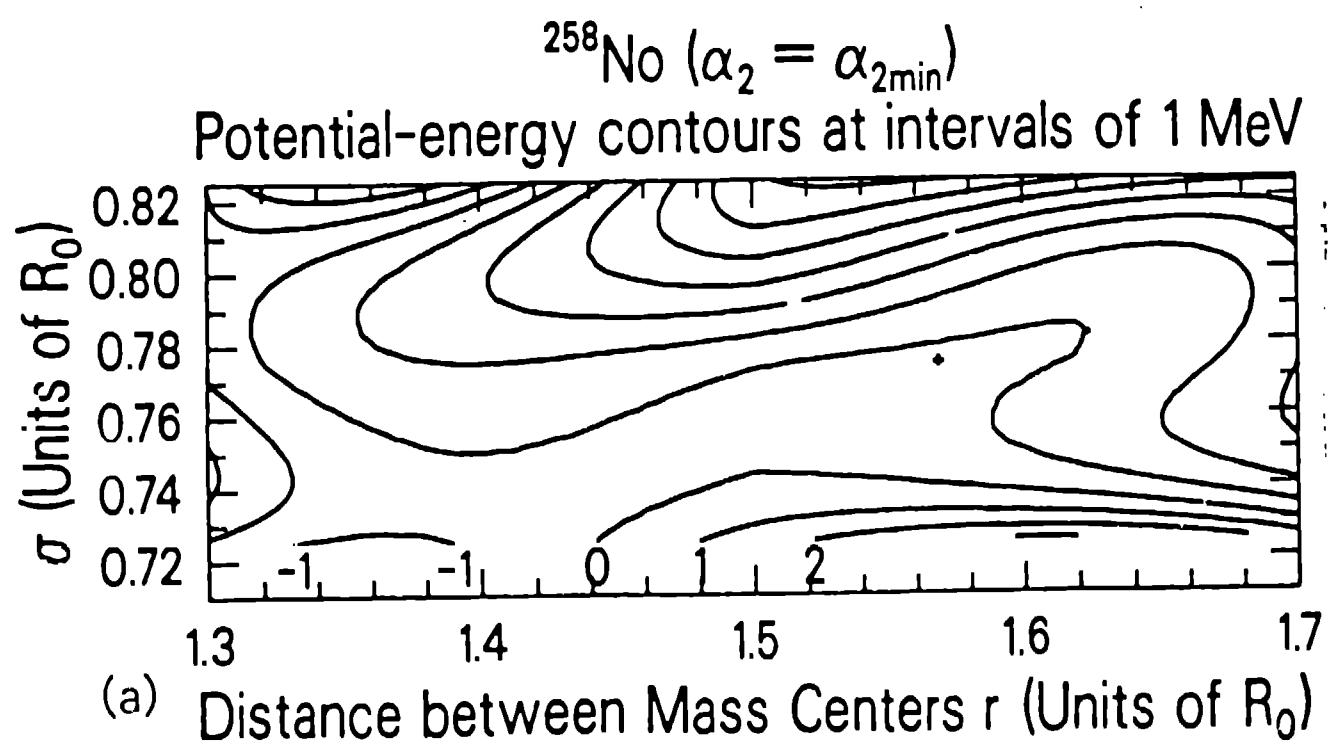
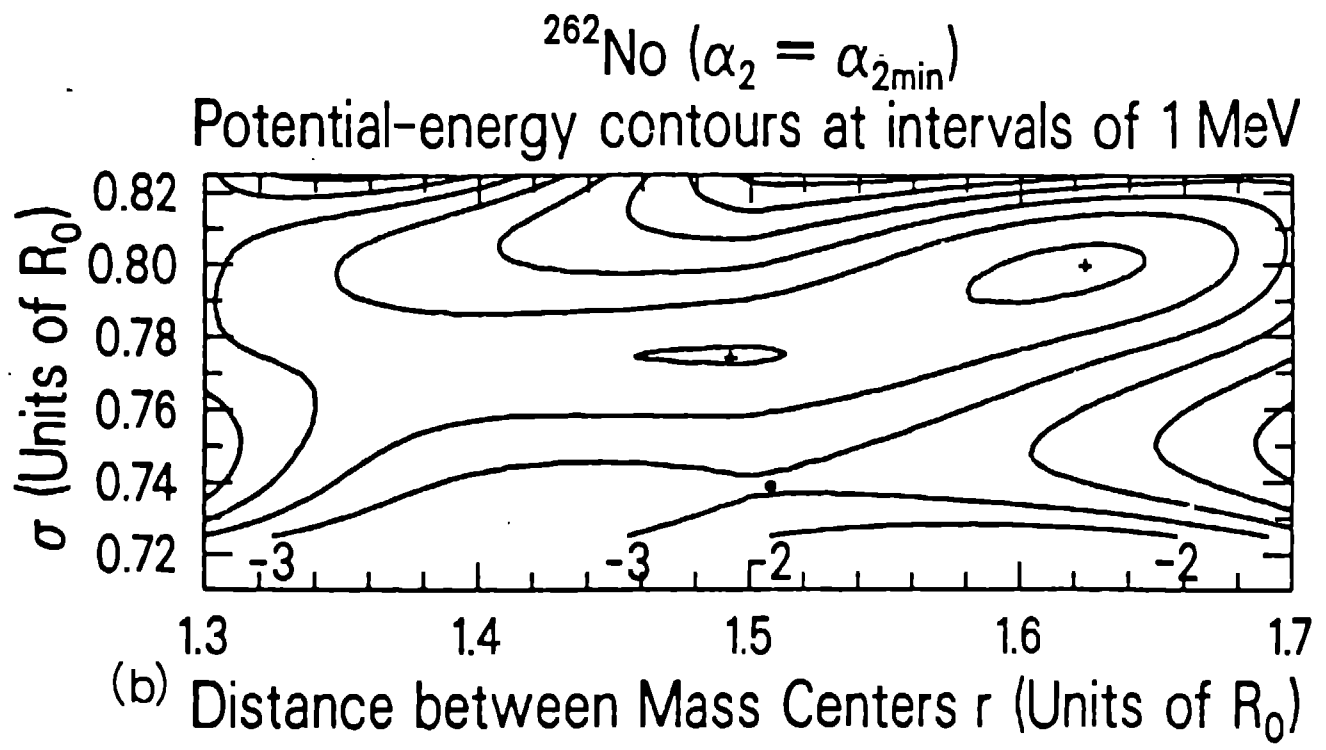


Figure 14

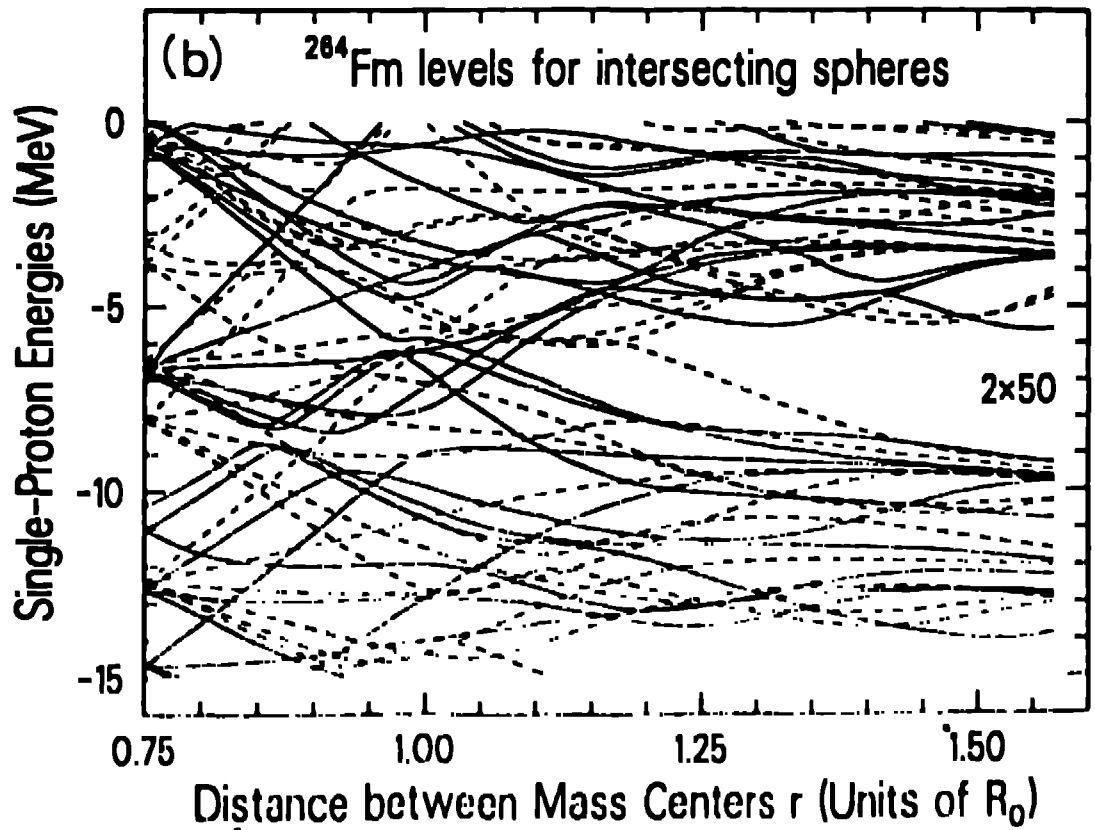
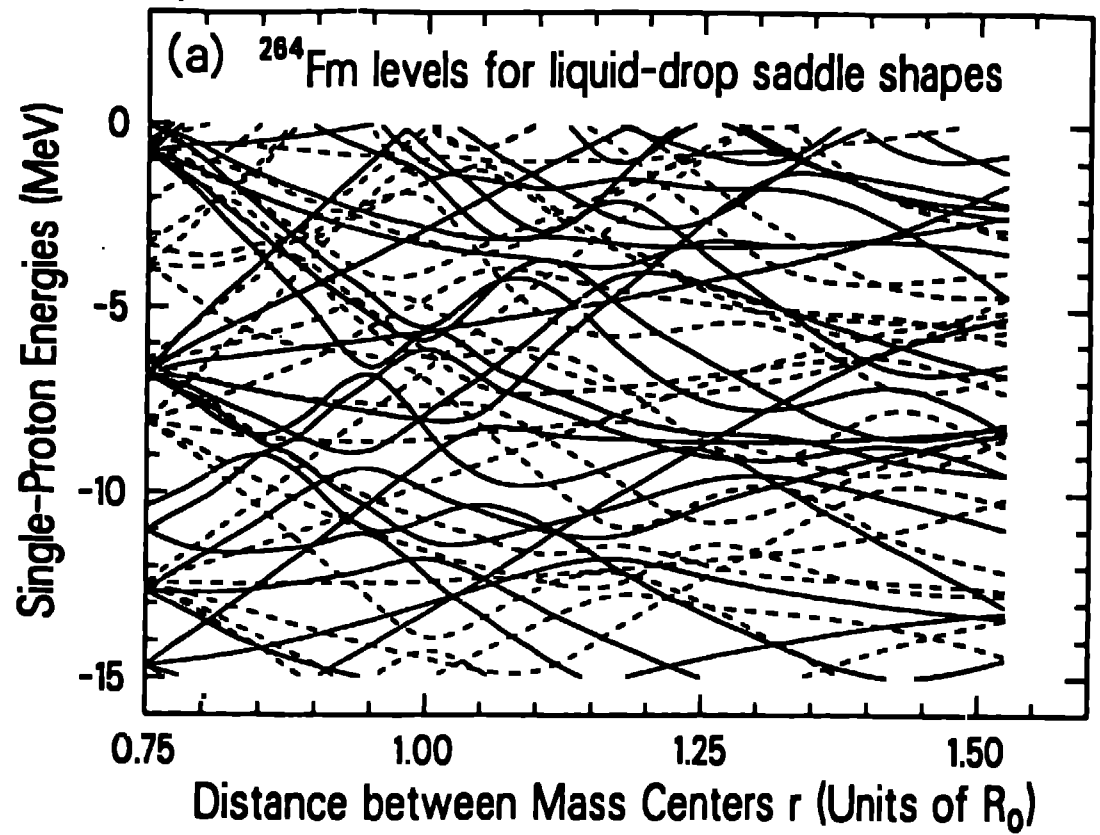


Figure 15

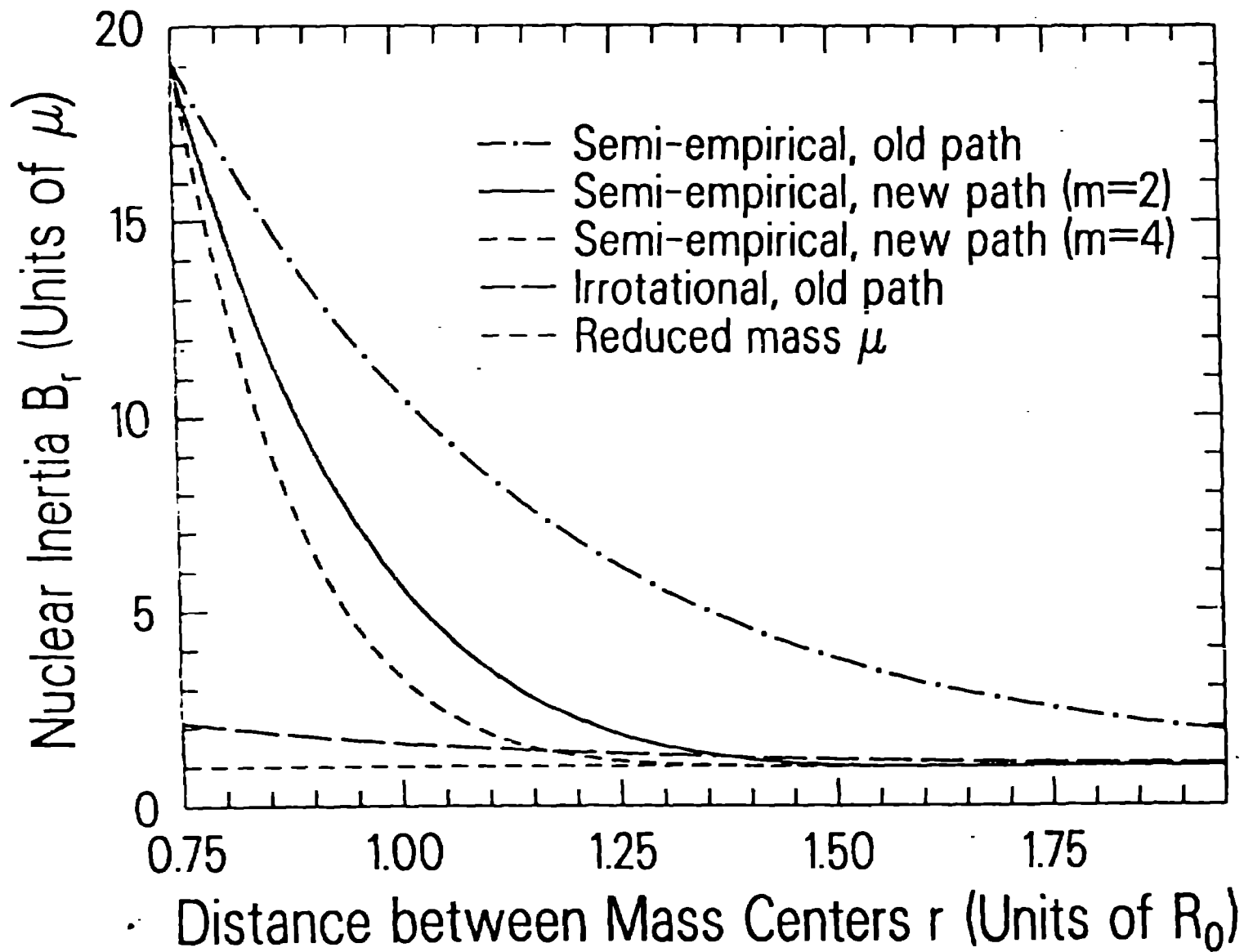


Figure 16

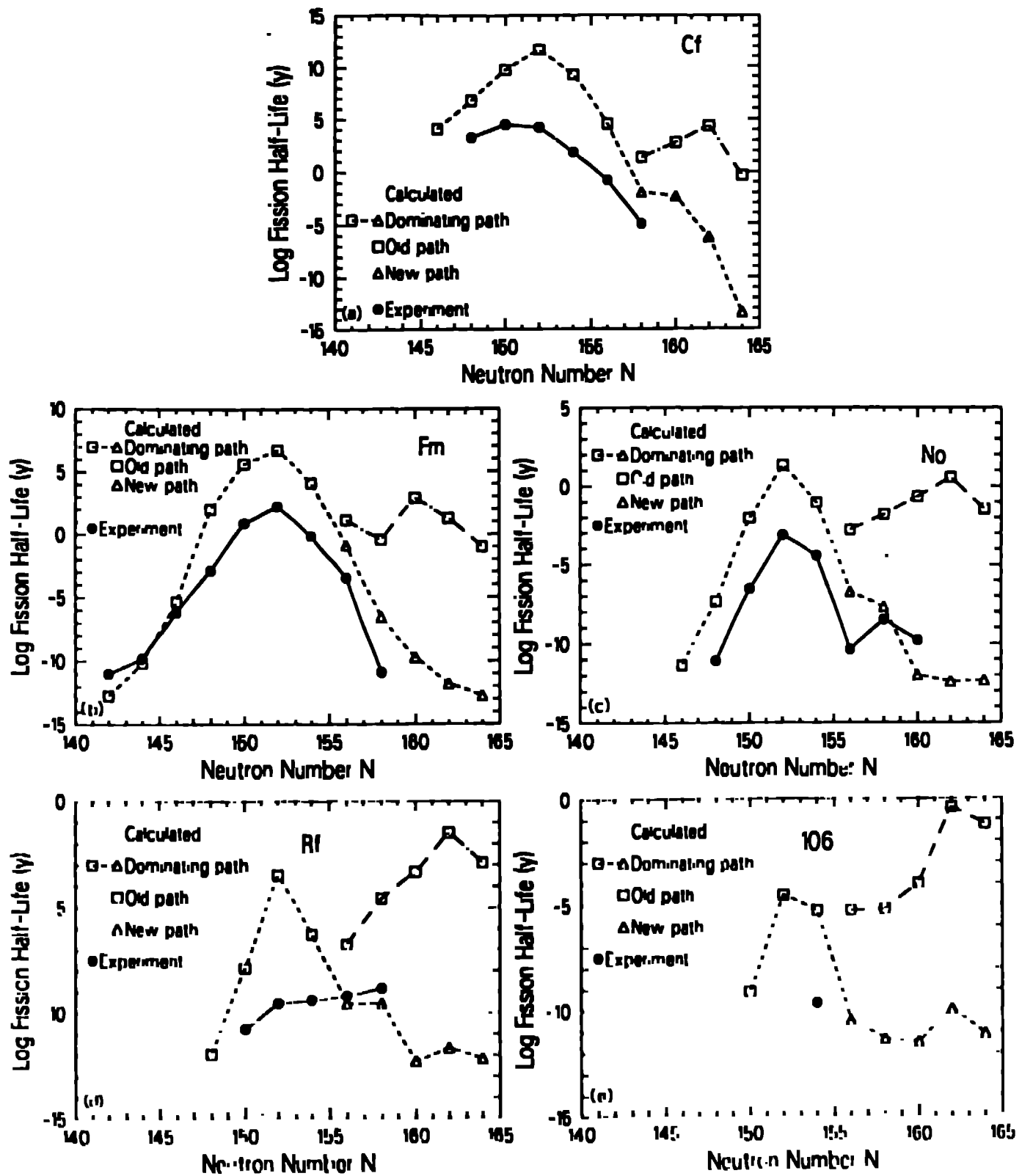


Figure 17